Making Sense of Rare Earth Electronic Structure. A Tutorial.

Mike Reid
University of Canterbury
Christchurch
New Zealand
mike.reid@canterbury.ac.nz

UNIVERSITY OF CANTERBURY
Te Whare Wānanga o Waitaha
CHRISTCHURCH NEW ZEALAND

DODD-WALLS CENTRE
for Photonic and Quantum Technologies

Sergey Feofilov. 1958-2020

Marek Grinberg. 1952-2020

UNIVERSITY OF CANTERBURY
Te Whare Wānanga o Waitaha
CHRISTCHURCH NEW ZEALAND

The Dodd-Walls Centre
for Photonic and Quantum Technologies

~~Yashar Alizadeh~~
~~Nick Jobbitt~~
Pratik Solanki
~~Kieran Smith~~
Jamin Martin
~~Dian Zou~~
~~Sangeetha Balabhadra~~
Mike Reid
Jon Wells
Sagar Mothkuri

Bulk (YSO etc.)
Nanoparticles
Ring Lasers

Lily Williams
Michael Moull
Ben Haenraets
Emma Johnson
Rezvan Anvari

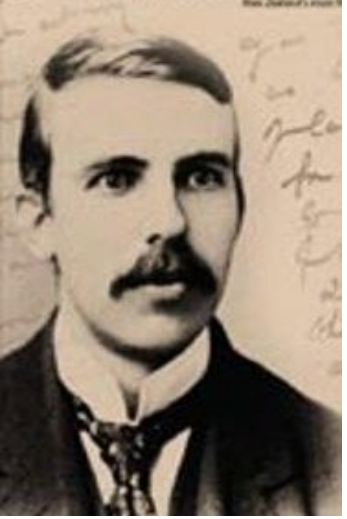

Art. LIX.—*Magnetization of Iron by High-frequency Discharges.*

By E. Rutherford, M.A.

[*Read before the Philosophical Institute of Canterbury, 7th November, 1894.*]

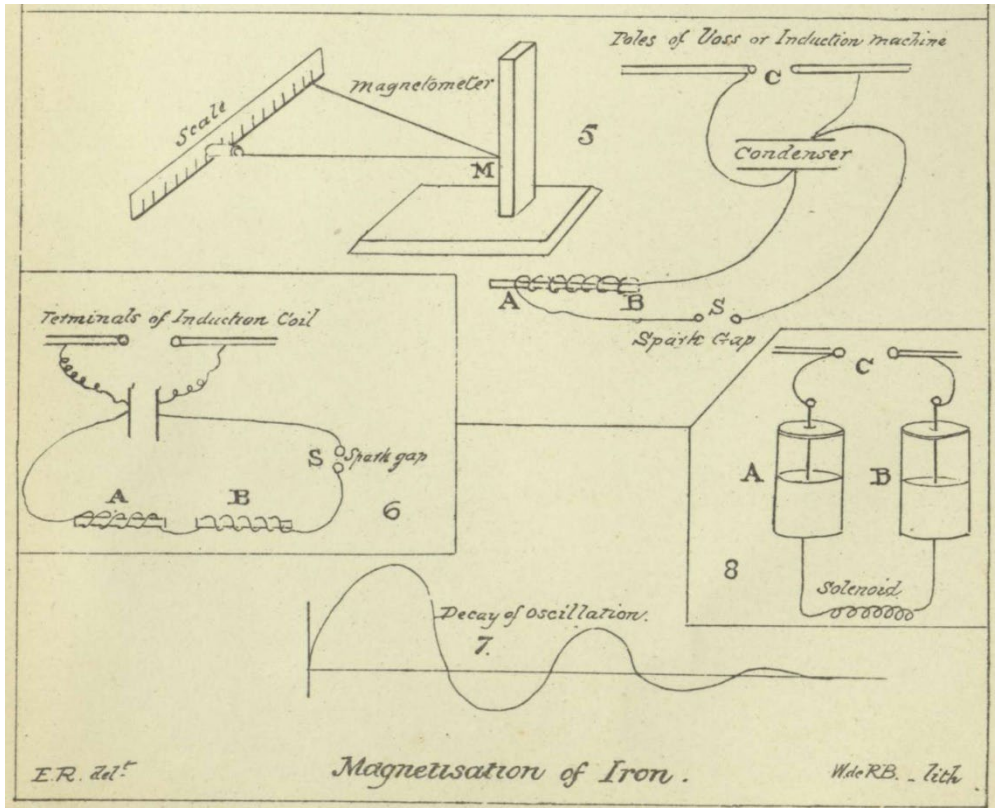

It has been shown that iron still exhibits magnetic properties in fields of over 100,000,000 oscillations per second. A needle may be magnetized or demagnetized in open circuit by the oscillations set up in the wire.

Brian Wybourne. PhD 1960.
Later Professor of Physics

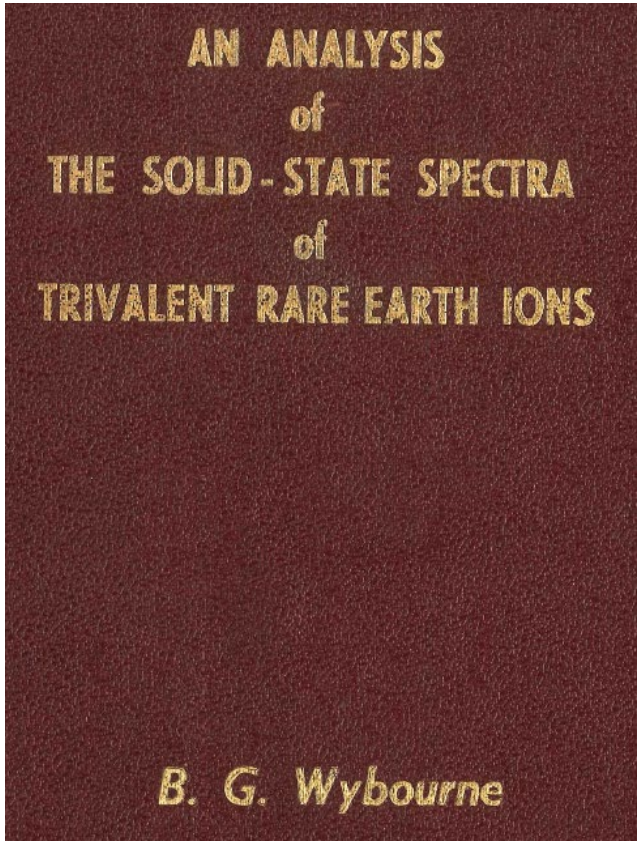

Judd Ofelt Wybourne

Optical and Magnetic Properties of some Transition Ion Complexes. PhD 1963

R.M. Macfarlane

Physics Department

University of Canterbury.

R.M. Macfarlane.

SUB-KILOHERTZ OPTICAL LINEWIDTHS OF THE $^7F_0 \leftrightarrow {}^5D_0$ TRANSITION IN $Y_2O_3:Eu^{3+}$

R.M. MACFARLANE and R.M. SHELBY

IBM Research Laboratory, San Jose, CA 95193, USA

Received 17 June 1981

Homogeneous optical linewidths as small as 760 Hz (fwhm) have been observed in $Y_2O_3:Eu^{3+}$ using delayed heterodyne photon echoes. Hyperfine and lifetime contributions to dephasing are estimated to contribute < 300 Hz to this width, and the remainder is attributed to quasi-resonant energy transfer.

Lanthanide (Rare Earth) 3+ ground state: $5s^2\ 5p^6\ 4f^N\ 5d^0$

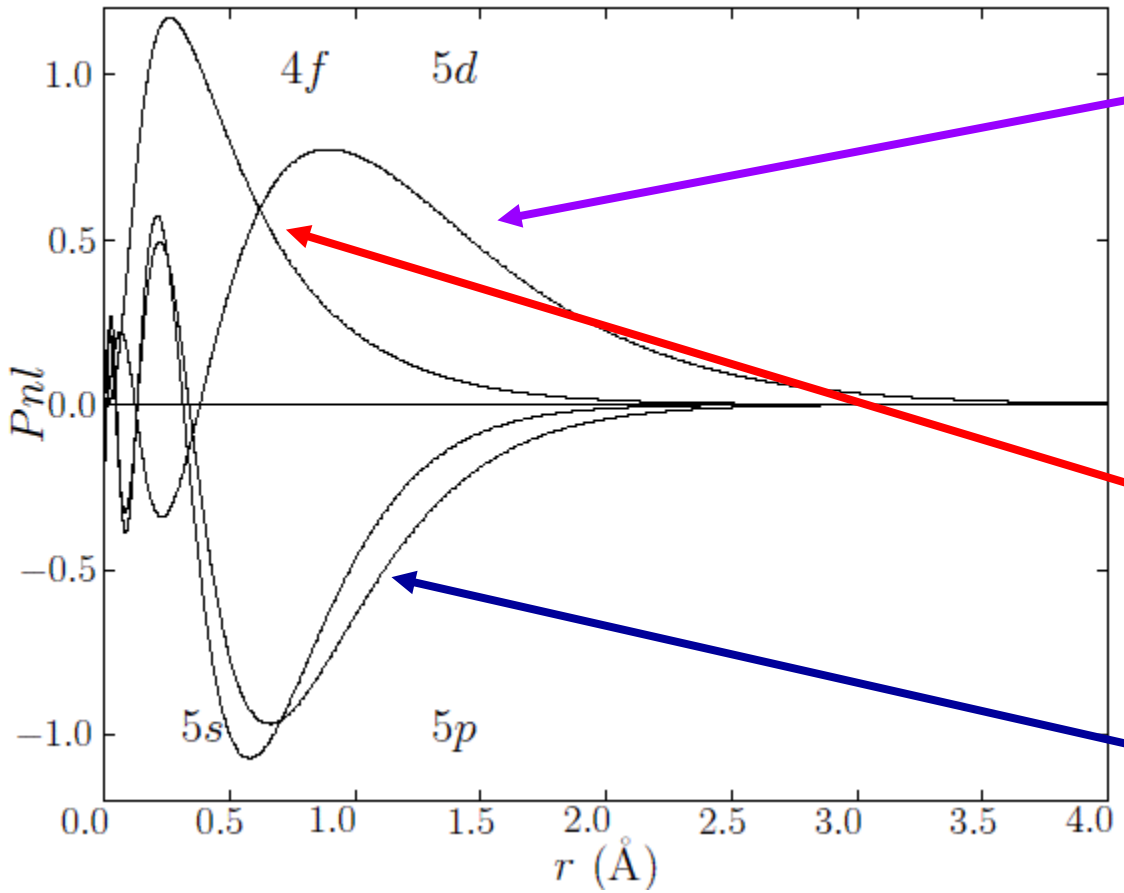

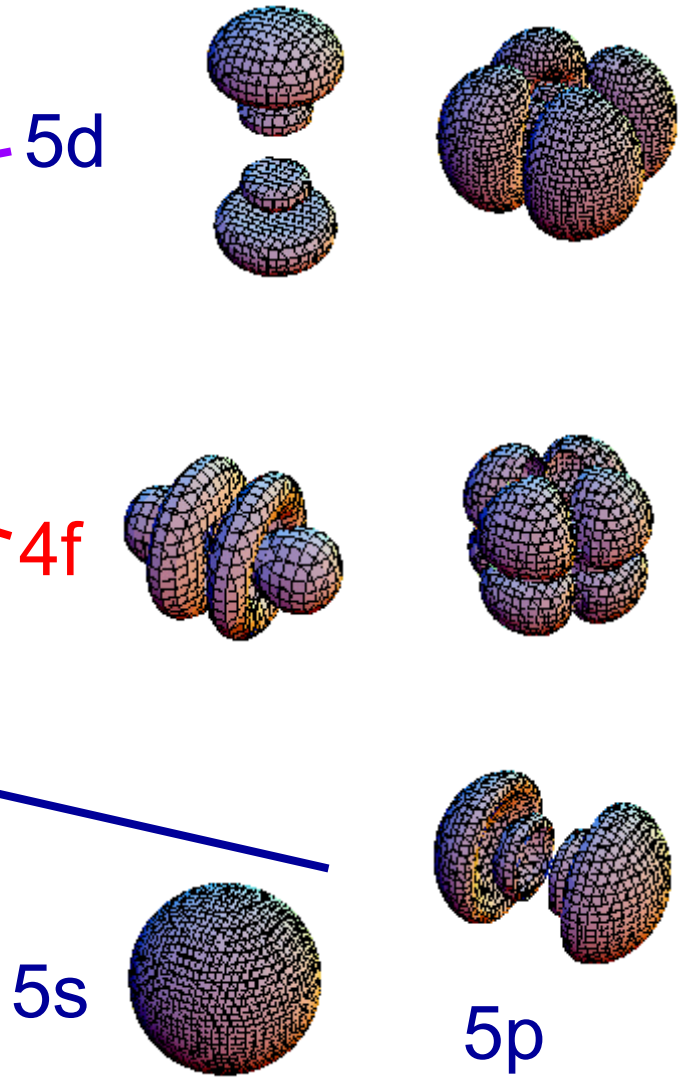

4f orbitals are shielded from environment.
Sharp lines, long lifetimes.
S=1/2, L=3 → 14 states, $4f^N$, N=1-14
Many transitions available for applications.

“Dieke Diagram” 1960s

Carnall, Goodman,
Rajnak, Rana, 1988

4f: S=1/2, L=3, → 14 states
$4f^N$: N=1-14

Eu^{3+}, $4f^6$
3003 electronic states

20,000 cm^{-1}
500 nm
2.5 eV

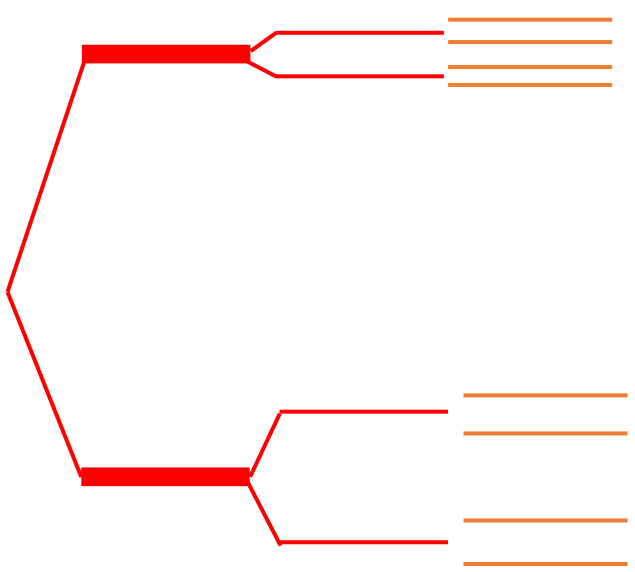

Free ion Crystal Field Hyperfine/Magnetic

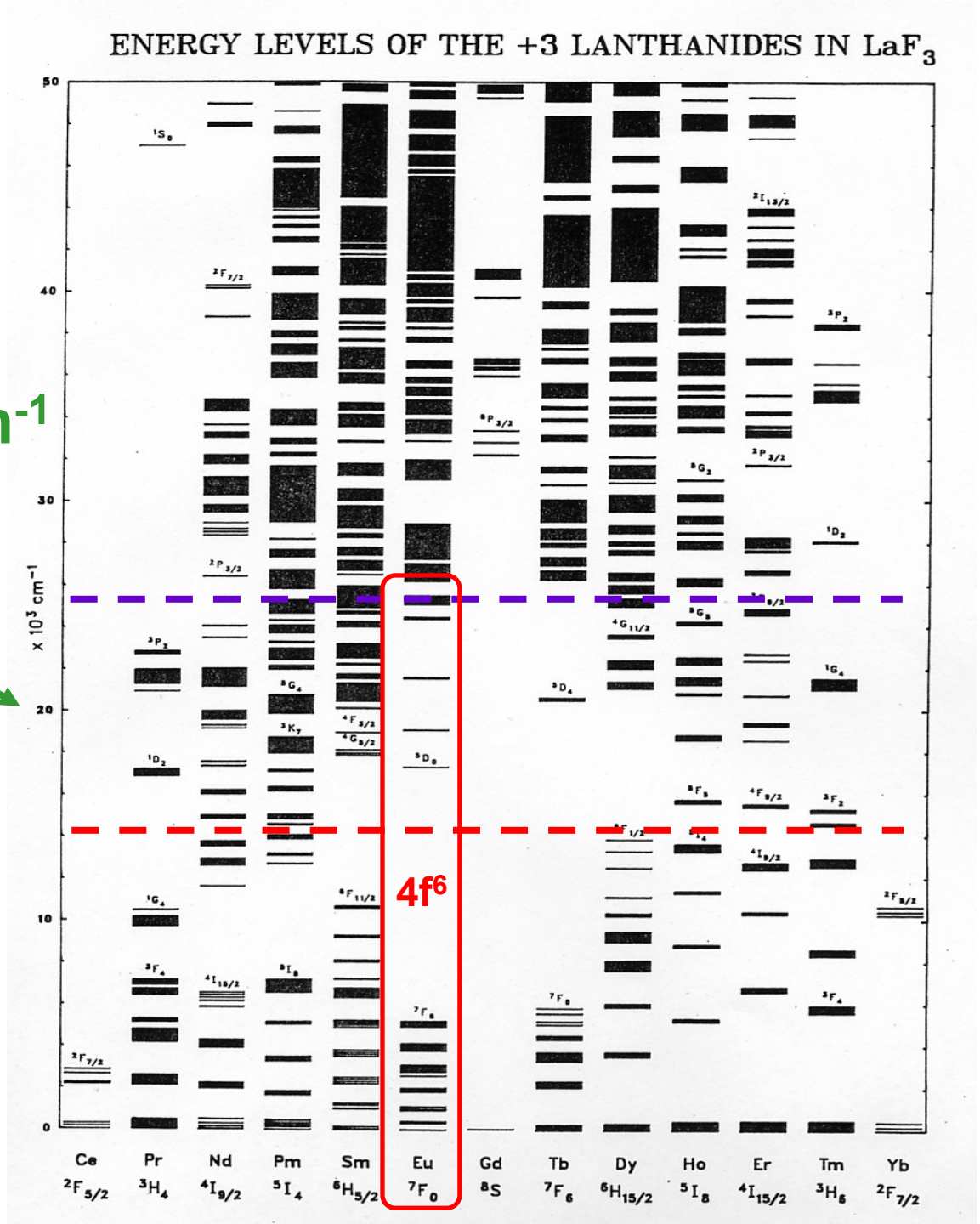

Modelling the $4f^N$ structure of rare-earth doped crystals

$$H = H_{FI} + H_{CF} + H_Z + H_{HF}$$

Free Ion Crystal Field Zeeman Hyperfine

$$H_{CF} = \sum_{k,q} B_q^k C_q^{(k)}$$

C_1 symmetry → 27 crystal-field parameters

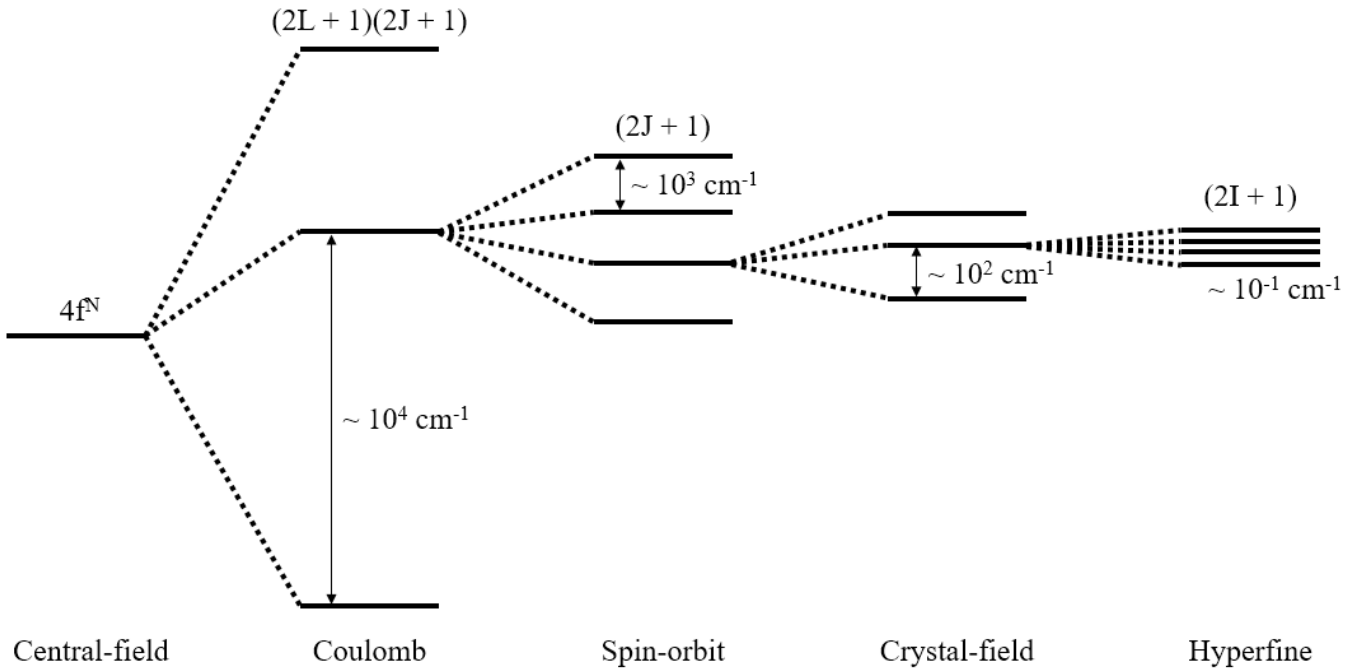

Zeeman

$H_Z = \mu_B \boldsymbol{B} \bullet (\boldsymbol{L} + 2\boldsymbol{S})$

Magnetic field can be experimentally varied.

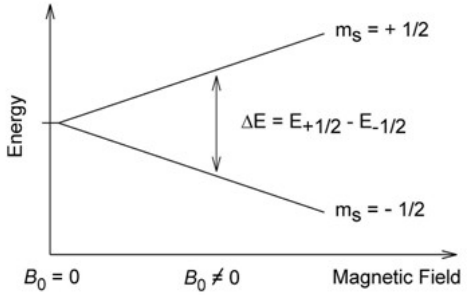

Hyperfine

$H_{HF} = A\,\boldsymbol{N} \bullet \mathbf{I} + Q\,H_Q$

A and Q are parameters

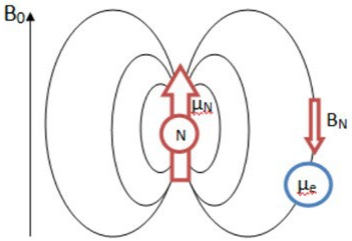

Eu^{3+} $^7F_0$ and $^5D_0$: electronic effects are small so Direct interaction of nucleus with magnetic field and lattice are important.

Parameter trends across the lanthanide series.

C-K Duan and P A Tanner, J. Phys. Chem. A, 2010, 114, pp 6055–6062

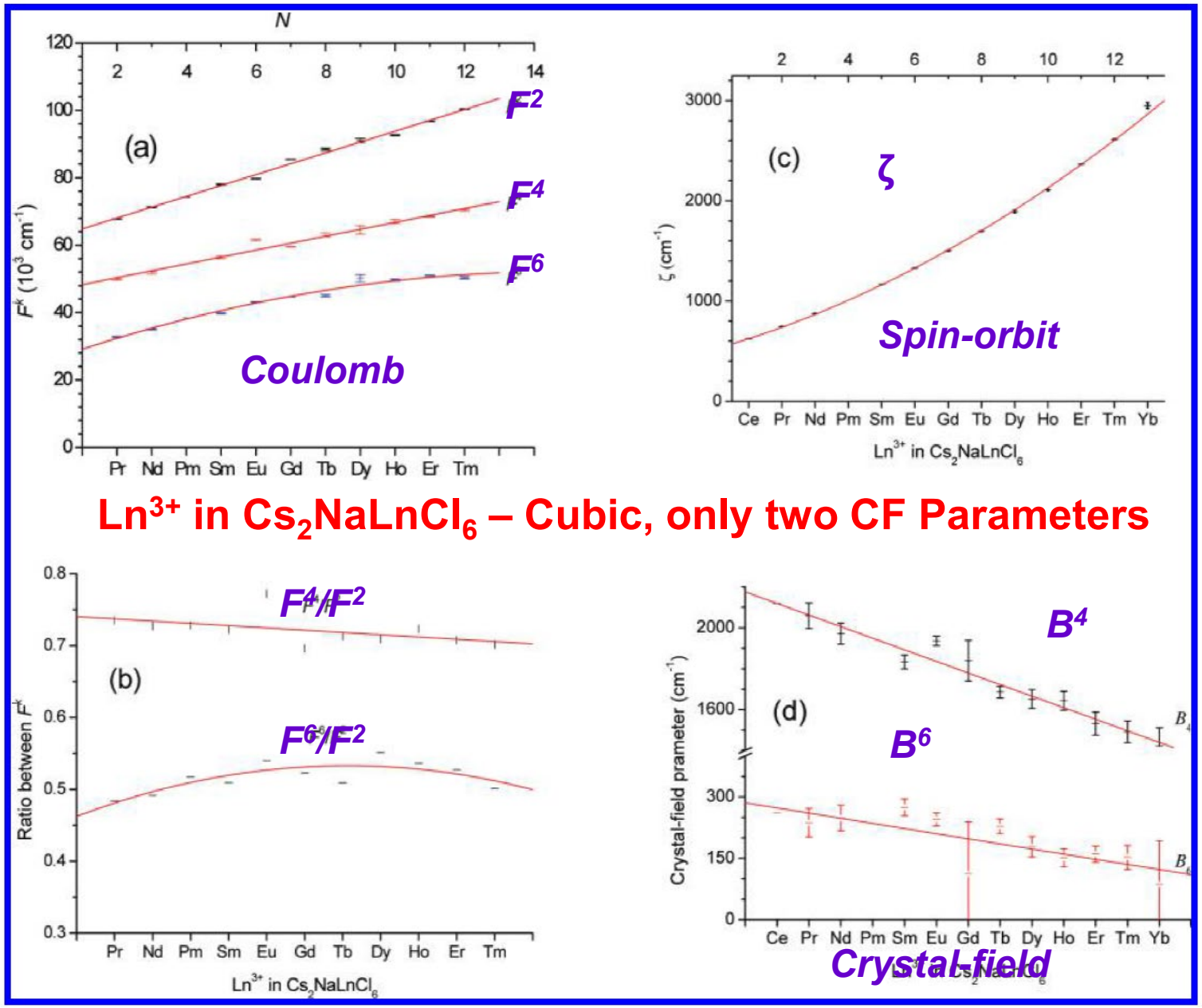

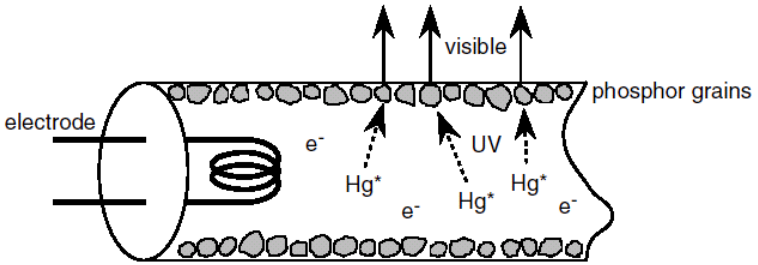

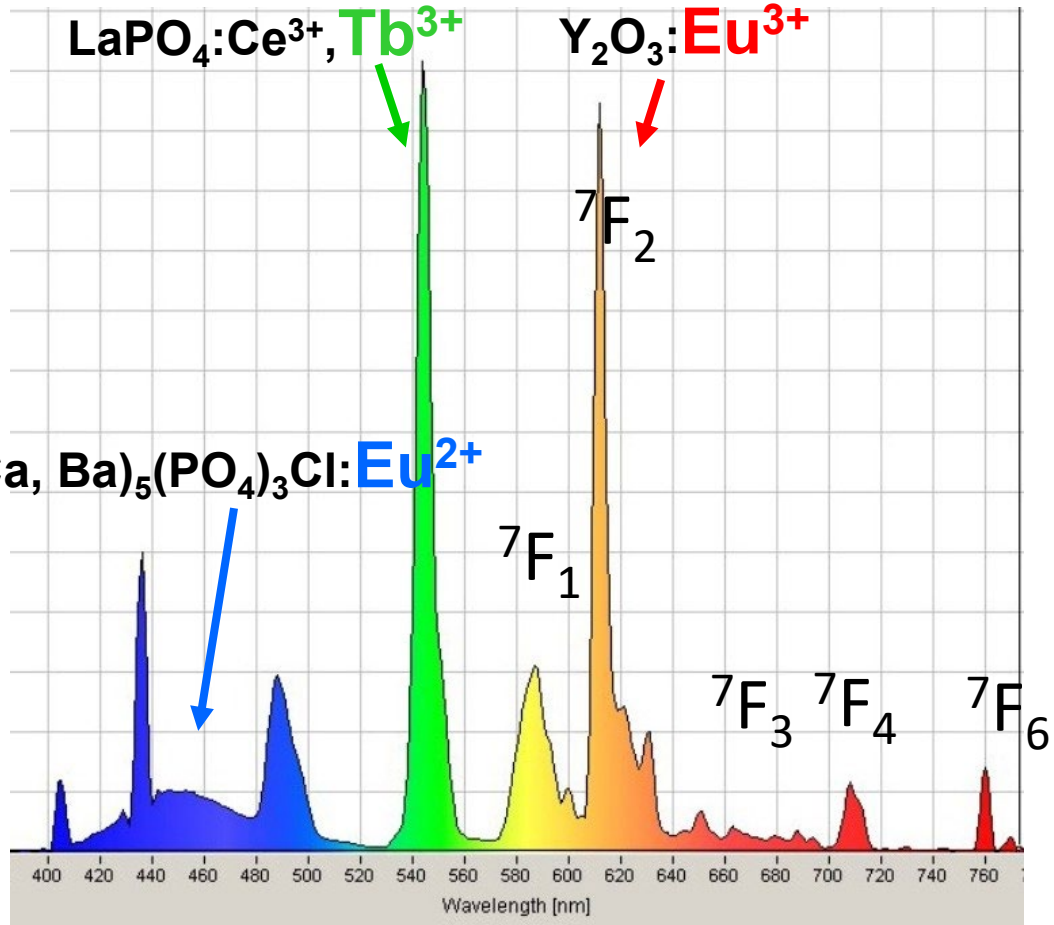

Reminiscencies of a quenched luminescence investigatory ☆

George Blasse

University Utrecht, Debye Institute, P.O. Box 80 000, 3508 TA Utrecht, The Netherlands

Journal of Luminescence 100 (2002) 65–67

Hypersensitivity: The emission of Eu^{3+} consists of an orange allowed magnetic-dipole transition ($^5D_0$–$^7F_1$), a red parity—forbidden electric-dipole (ED) transition ($^5D_0$–$^7F_2$), and further infrared ED transitions. For application, the emission should consist of as much $^5D_0$–$^7F_2$ emissions as possible. This requires Eu^{3+} to occupy a site without inversion symmetry. This, however, induces also the infrared emission. Fortunately, the rare-earth transitions with $\Delta J = 2$ are hypersensitive to the surroundings, i.e. a small deviation from inversion symmetry induces strong red emission whereas the infrared emission is still weak. By comparing many systems I found that a certain amount of covalency is a condition for this hypersensitivity. Later calculations by others confirmed this, but to me they are not transparent. It remains striking that the high quality of colour displays like in TV is due to this hypersensitivity effect.

George Blasse
1934-2020

Angular momentum states and tensor operators

$$[J_x, J_y] = iJ_z, \qquad \mathbf{J}^2 \equiv J_x^2 + J_y^2 + J_z^2$$

$$\begin{aligned} J_z|jm\rangle &= m|jm\rangle, \\ \mathbf{J}^2|jm\rangle &= j(j+1)|jm\rangle, \\ D(R)|jm\rangle &= \sum_{m'} D^{(j)}_{m'm}(R)|jm'\rangle \end{aligned}$$

Rather than classifying states by eigenvalues and operators by commutators, it is helpful to classify both in terms of behaviour under rotations.

$$[J_z, T^{(k)}_q] = qT^{(k)}_q$$

$$D(R)T^{(k)}_q D(R)^\dagger = \sum_{q'} D^{(k)}_{q'q}(R)T^{(k)}_{q'}$$

Wigner-Eckart theorem

$$\langle \alpha J M | T_q^{(k)} | \alpha' J' M' \rangle = (-1)^{J-M} \begin{pmatrix} J & k & J' \\ -M & q & M' \end{pmatrix} \langle \alpha J || T^{(k)} || \alpha' J' \rangle .$$

3j symbols or Clebsch-Gordan coefficients: "geometry"

Reduced matrix elements: "physics"

Selection rules: $M' + q = M$ and $|J - J'| \leq k \leq J + J'$.

Clearest proof is to express $T^{(k)}_q$ as a linear combination of $|jm\rangle\langle j'm'|$ kets and bras that transform as kq, recalling transformation properties:

$$D(R)|jm\rangle = \sum_{m'} D^{(j)}_{m'm}(R)|jm'\rangle$$

$$D(R) T_q^{(k)} D(R)^\dagger = \sum_{q'} D^{(k)}_{q'q}(R) T^{(k)}_{q'}$$

The linear combination of $|jm\rangle\langle j'm'|$ required gives the 3j symbol (or Clebsch-Gordan coeffient).

Spherical Harmonics and Spherical Tensors

$$Y_{lm}(\theta,\phi) = \sqrt{\frac{2l+1}{4\pi}}\sqrt{\frac{(l-m)!}{(l+m!)}}\,P_{lm}(\cos\theta)\,e^{im\phi}$$

$$C_q^{(k)}(\hat{\mathbf{r}}) = C_q^{(k)}(\theta,\phi) = \sqrt{\frac{4\pi}{2k+1}}\,Y_{kq}(\theta,\phi)$$

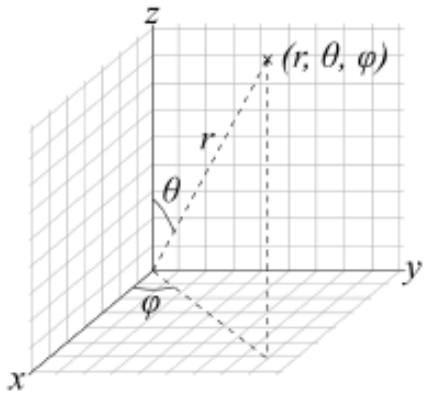

k	q	$C_q^{(k)}(x,y,z)$	$C_q^{(k)}(\theta,\phi)$
0	0	1	1
1	0	z/r	$\cos\theta$
1	±1	$\mp\sqrt{\frac{1}{2}}(x\pm iy)/r$	$\mp\sqrt{\frac{1}{2}}\sin\theta\,e^{\pm i\phi}$
2	0	$\sqrt{\frac{1}{4}}(3z^2-r^2)/r^2$	$\sqrt{\frac{1}{4}}(3\cos^2\theta-1)$
2	±1	$\mp\sqrt{\frac{3}{2}}z(x\pm iy)/r^2$	$\mp\sqrt{\frac{3}{2}}\cos\theta\sin\theta\,e^{\pm i\phi}$
2	±2	$\sqrt{\frac{3}{8}}(x\pm iy)^2/r^2$	$\sqrt{\frac{3}{8}}\sin^2\theta\,e^{\pm 2i\phi}$

Electric and Magnetic Dipoles

$$-e\mathbf{r} = -er\mathbf{C}^{(1)}$$

$$x = r\,\frac{1}{\sqrt{2}}\left(-C_1^{(1)} + C_{-1}^{(1)}\right), \qquad y = r\,\frac{i}{\sqrt{2}}\left(C_1^{(1)} + C_{-1}^{(1)}\right), \qquad z = r\,C_0^{(1)}.$$

k	q	$C_q^{(k)}(x,y,z)$
0	0	1
1	0	z/r
1	±1	$\mp\sqrt{\frac{1}{2}}(x \pm iy)/r$
2	0	$\sqrt{\frac{1}{4}}(3z^2 - r^2)/r^2$
2	±1	$\mp\sqrt{\frac{3}{2}}z(x \pm iy)/r^2$
2	±2	$\sqrt{\frac{3}{8}}(x \pm iy)^2/r^2$

x

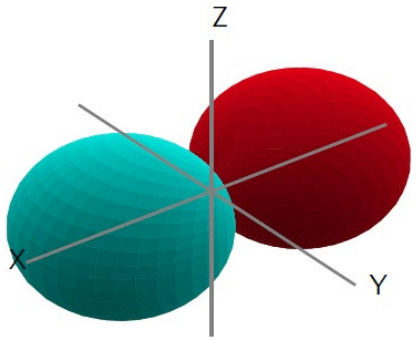

y

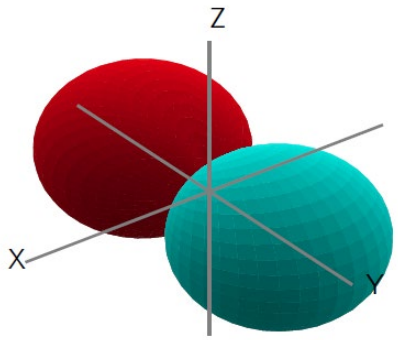

z

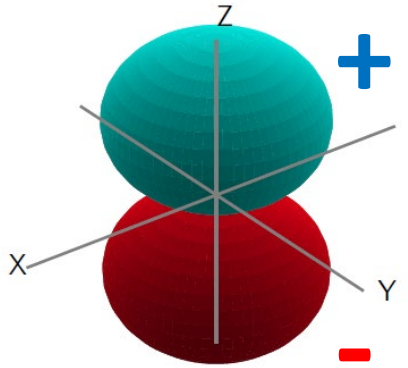

$$\mathbf{B}\cdot\mathbf{J} = \sum_{i=x,y,z} B_i J_i.$$

$$J_x = r\,\frac{1}{\sqrt{2}}\left(-J_1^{(1)} + J_{-1}^{(1)}\right), \qquad J_y = r\,\frac{i}{\sqrt{2}}\left(J_1^{(1)} + J_{-1}^{(1)}\right), \qquad J_z = r\,J_0^{(1)}.$$

Crystal Field Potential

$$Y_{lm}(\theta,\phi) = \sqrt{\frac{2l+1}{4\pi}}\sqrt{\frac{(l-m)!}{(l+m!)}}\,P_{lm}(\cos\theta)\,e^{im\phi}$$

$$C_q^{(k)}(\hat{\mathbf{r}}) = C_q^{(k)}(\theta,\phi) = \sqrt{\frac{4\pi}{2k+1}}\,Y_{kq}(\theta,\phi)$$

k	q	$C_q^{(k)}(x,y,z)$	$C_q^{(k)}(\theta,\phi)$
0	0	1	1
1	0	z/r	$\cos\theta$
1	±1	$\mp\sqrt{\frac{1}{2}}(x \pm iy)/r$	$\mp\sqrt{\frac{1}{2}}\sin\theta\, e^{\pm i\phi}$
2	0	$\sqrt{\frac{1}{4}}(3z^2-r^2)/r^2$	$\sqrt{\frac{1}{4}}(3\cos^2\theta-1)$
2	±1	$\mp\sqrt{\frac{3}{2}}z(x \pm iy)/r^2$	$\mp\sqrt{\frac{3}{2}}\cos\theta\sin\theta\, e^{\pm i\phi}$
2	±2	$\sqrt{\frac{3}{8}}(x \pm iy)^2/r^2$	$\sqrt{\frac{3}{8}}\sin^2\theta\, e^{\pm 2i\phi}$

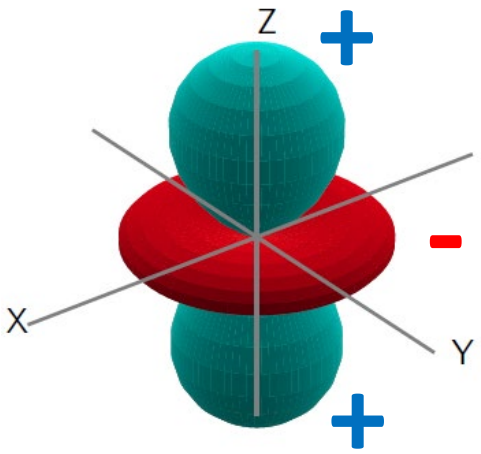

$C^2_0(r)$

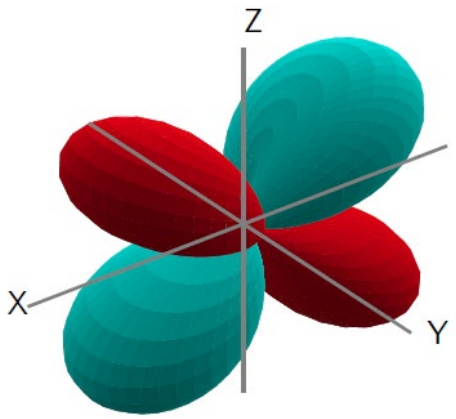

$C^2_1(r)$ - $C^2_{-1}(r)$

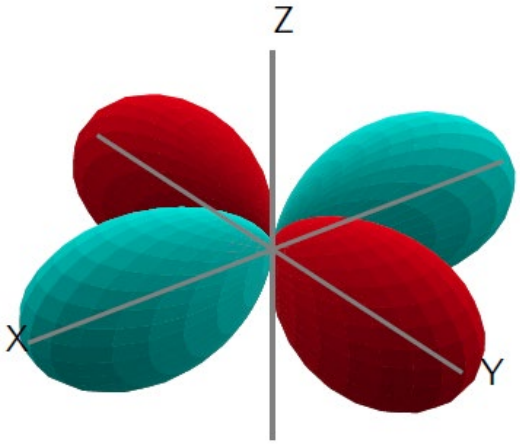

$C^2_2(r)$ - $C^2_{-2}(r)$

Note: Potential is **real**. **Phases** of parameters determine **orientation**, e.g. $e^{iq\phi}$

Coulomb interaction and crystal field: Addition theorem

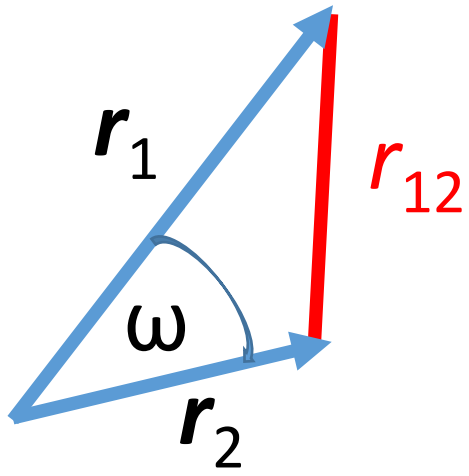

$$\frac{1}{r_{12}} = \sum_{k=0}^{\infty} \frac{r_<^k}{r_>^{k+1}} P_k(\cos\omega)$$

cos ω: -1..1

$$= \sum_{k=0}^{\infty} \frac{r_<^k}{r_>^{k+1}} \mathbf{C}^{(k)}(\hat{\mathbf{r}}_1) \cdot \mathbf{C}^{(k)}(\hat{\mathbf{r}}_2)$$

$$= \sum_{k=0}^{\infty} \frac{r_<^k}{r_>^{k+1}} \sum_{q=-k}^{+k} C_q^{(k)}(\hat{\mathbf{r}}_1) C_{-q}^{(k)}(\hat{\mathbf{r}}_2)(-1)^q.$$

Legendre Polynomials
orthogonal: -1..1

k	P_k
0	1
1	x
2	$(3x^2-1)/2$

k	q	$C_q^{(k)}(x,y,z)$
0	0	1
1	0	z/r
1	±1	$\mp\sqrt{\frac{1}{2}}(x \pm iy)/r$
2	0	$\sqrt{\frac{1}{4}}(3z^2-r^2)/r^2$
2	±1	$\mp\sqrt{\frac{3}{2}}z(x \pm iy)/r^2$
2	±2	$\sqrt{\frac{3}{8}}(x \pm iy)^2/r^2$

Addition Theorem - Example

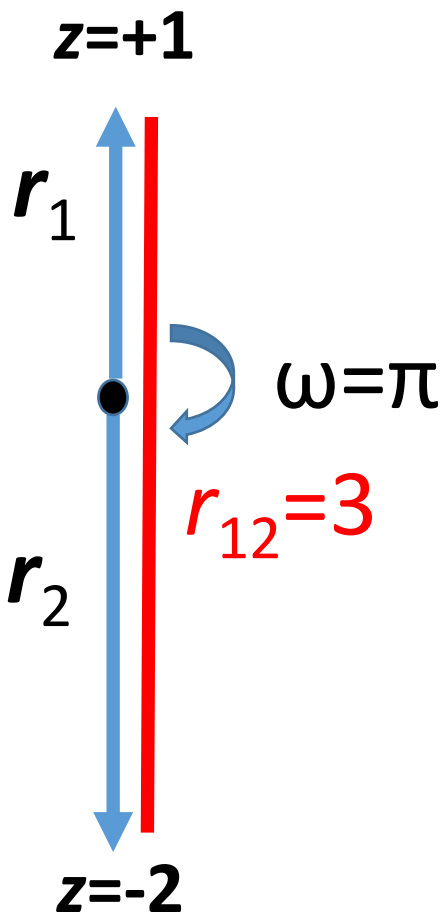

$$1/r_{12} = 1/3$$ cosω = cosπ = -1

$$\begin{aligned}
\frac{1}{r_{12}} &= \sum_{k=0}^{\infty} \frac{r_<^k}{r_>^{k+1}} P_k(\cos\omega) \\
&= \frac{1^0}{2^1} \times (1) + \frac{1^1}{2^2} \times (-1) + \frac{1^2}{2^3} \times \left(\frac{1}{2} \left(3 \times (-1)^2 - 1 \right) \right) + \dots \\
&= \frac{1}{2} - \frac{1}{4} + \frac{1}{8} + \dots
\end{aligned}$$

$$\begin{aligned}
\frac{1}{r_{12}} &= \sum_{k=0}^{\infty} \frac{r_<^k}{r_>^{k+1}} \sum_{q=-k}^{+k} C_q^{(k)}(\hat{\mathbf{r}}_1) C_{-q}^{(k)}(\hat{\mathbf{r}}_2)(-1)^q \\
&= \frac{1^0}{2^1} \times 1 \times 1 + \frac{1^1}{2^2} \times (+1) \times (-1) + \frac{1^2}{2^3} \times \left(\left(\sqrt{\frac{1}{4}}(3-1) \right) \times \left(\sqrt{\frac{1}{4}}(3-1) \right) \right) + . \\
&= \frac{1}{2} - \frac{1}{4} + \frac{1}{8} + \dots
\end{aligned}$$

Legendre Polynomials
orthogonal: -1..1

k	P_k
0	1
1	x
2	$(3x^2-1)/2$

k	q	$C_q^{(k)}(x,y,z)$
0	0	1
1	0	z/r
1	± 1	$\mp\sqrt{\frac{1}{2}}(x \pm iy)/r$
2	0	$\sqrt{\frac{1}{4}}(3z^2 - r^2)/r^2$
2	± 1	$\mp\sqrt{\frac{3}{2}}z(x \pm iy)/r^2$
2	± 2	$\sqrt{\frac{3}{8}}(x \pm iy)^2/r^2$

Coulomb Interaction

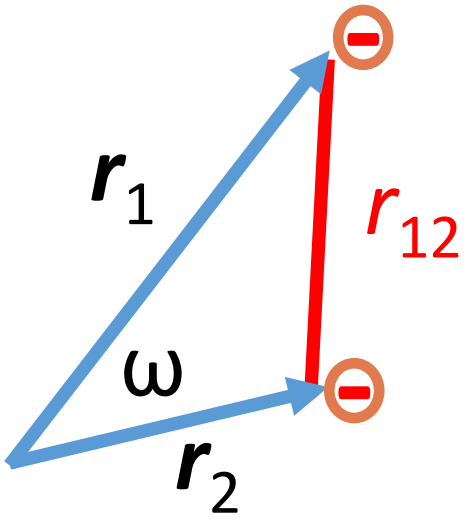

$$\frac{1}{r_{12}} = \sum_{k=0}^{\infty} \frac{r_<^k}{r_>^{k+1}} P_k(\cos\omega)$$

$$= \sum_{k=0}^{\infty} \frac{r_<^k}{r_>^{k+1}} \mathbf{C}^{(k)}(\hat{\mathbf{r}}_1) \cdot \mathbf{C}^{(k)}(\hat{\mathbf{r}}_2)$$

$$= \sum_{k=0}^{\infty} \frac{r_<^k}{r_>^{k+1}} \sum_{q=-k}^{+k} C_q^{(k)}(\hat{\mathbf{r}}_1) C_{-q}^{(k)}(\hat{\mathbf{r}}_2)(-1)^q.$$

$$H_{\text{Coulomb}} = \frac{e^2}{4\pi\epsilon_0} \sum_{k}^{\text{even}} \sum_{i<j} \frac{r_<^k}{r_>^{k+1}} \left[\mathbf{C}^{(k)}(\hat{\mathbf{r}}_i) \cdot \mathbf{C}^{(k)}(\hat{\mathbf{r}}_j)\right]$$

$$= \sum_{k}^{\text{even}} F^k \left[\sum_{i<j} \mathbf{C}^{(k)}(\hat{\mathbf{r}}_i) \cdot \mathbf{C}^{(k)}(\hat{\mathbf{r}}_j)\right]$$

$$= \sum_{k}^{\text{even}} F^k f_k.$$

Two-centre addition theorem: Ligand polarization(dynamic coupling) and energy transfer

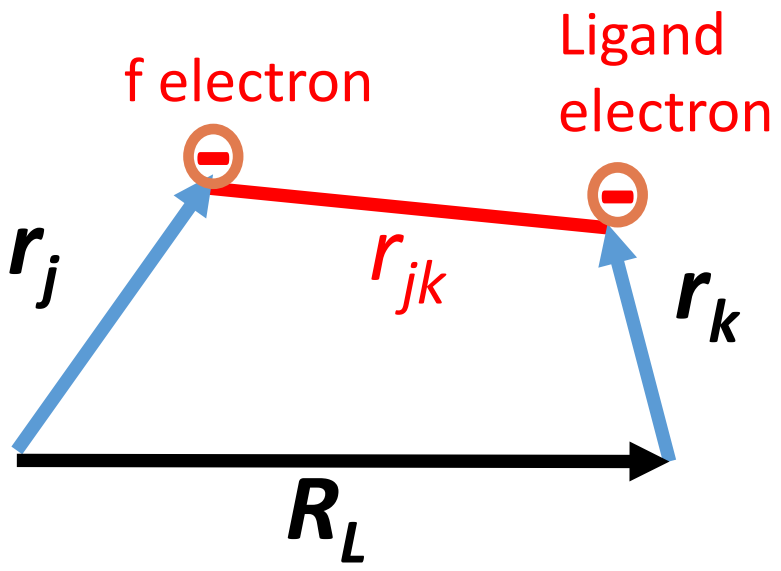

Ionic transitions hypersensitive to environment

B. R. Judd

Physics Department, The Johns Hopkins University, Baltimore, Maryland 21218
(Received 5 February 1979)

$$r_{jk}^{-1} = \sum_{l,t} r_j^l r_k^t {}_L R_L^{-l-t-1} [(2l+2t)!/(2l)!(2t)!]^{1/2}$$

$$\times (-1)^t (C_j^{(l)} C_{kL}^{(t)})^{(l+t)} \cdot C_L^{(l+t)} \ .$$

Interaction between f electron and Ligand electron

Energy transfer

In this case there is an interaction between f electrons on two ions.
Dipole-dipole is l=t=1, so we have $1/R^3$. Square gives $1/R^6$.
Exchange interaction gives a different distance dependence.

Electrostatic Crystal Field

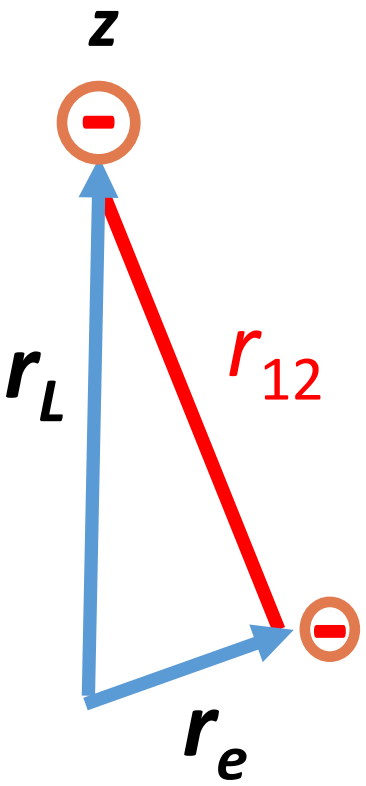

$$\frac{1}{r_{12}} = \sum_{k=0}^{\infty} \frac{r_<^k}{r_>^{k+1}} P_k(\cos\omega)$$
$$= \sum_{k=0}^{\infty} \frac{r_<^k}{r_>^{k+1}} \mathrm{C}^{(k)}(\hat{\mathrm{r}}_1)\cdot\mathrm{C}^{(k)}(\hat{\mathrm{r}}_2)$$
$$= \sum_{k=0}^{\infty} \frac{r_<^k}{r_>^{k+1}} \sum_{q=-k}^{+k} C_q^{(k)}(\hat{\mathrm{r}}_1) C_{-q}^{(k)}(\hat{\mathrm{r}}_2)(-1)^q.$$

$$\begin{aligned} V &= \frac{e^2}{4\pi\epsilon_0} \sum_{kq} \langle r^k \rangle C_q^{(k)}(\theta_e,\phi_e) \frac{1}{r_L^{k+1}} C_{-q}^{(k)}(\theta_L,\phi_L)(-1)^q \\ &= \sum_{kq} \left[\frac{e^2}{4\pi\epsilon_0} \langle r^k \rangle \frac{1}{r_L^{k+1}} C_{-q}^{(k)}(\theta_L,\phi_L)(-1)^q \right] \left[C_q^{(k)}(\theta_e,\phi_e) \right] \\ &= \sum_{kq} B_q^k \, C_q^{(k)}. \end{aligned}$$

$$\begin{aligned} C_0^{(2)} &= \sqrt{\frac{1}{4}}(3z^2 - r^2)/r^2 = 1, \\ r_L &= 3\,\text{Å} = 3 \times 10^{-10}\,\text{m}, \\ \langle r^2 \rangle &= 0.2\,\text{Å} = 0.2 \times 10^{-20}\,\text{m}^2. \end{aligned}$$

$$B_0^2 = \frac{e^2}{4\pi\epsilon_0} \times \frac{1}{r_L^3} C_0^{(2)}(0,0)(-1)^0 = \frac{(1.6\times10^{-19})^2}{4\pi \times 8.85 \times 10^{-12}} \times \frac{0.2\times10^{-20}}{(3\times10^{-10})^3} = 1.7 \times 10^{-20}\,\text{J}.$$

We can convert to eV by dividing by $1.6 \times 10^{-19}\,\text{C}$, and multiply by 8066 to convert to cm^{-1}.
So B_0^2 is 0.11 eV, or $860\,\text{cm}^{-1}$.

“Crystal Field” $\sum_{k,q} B_q^k C_q^{(k)}$

[Diagrams use p orbitals for simplicity.]

Do the ``Ligand Field'' Parameters in Lanthanides Represent Weak Covalent Bonding?
C.K. Jorgensen, R. Pappalardo, H.H. Schmidtke
J. Chem. Phys. 1963

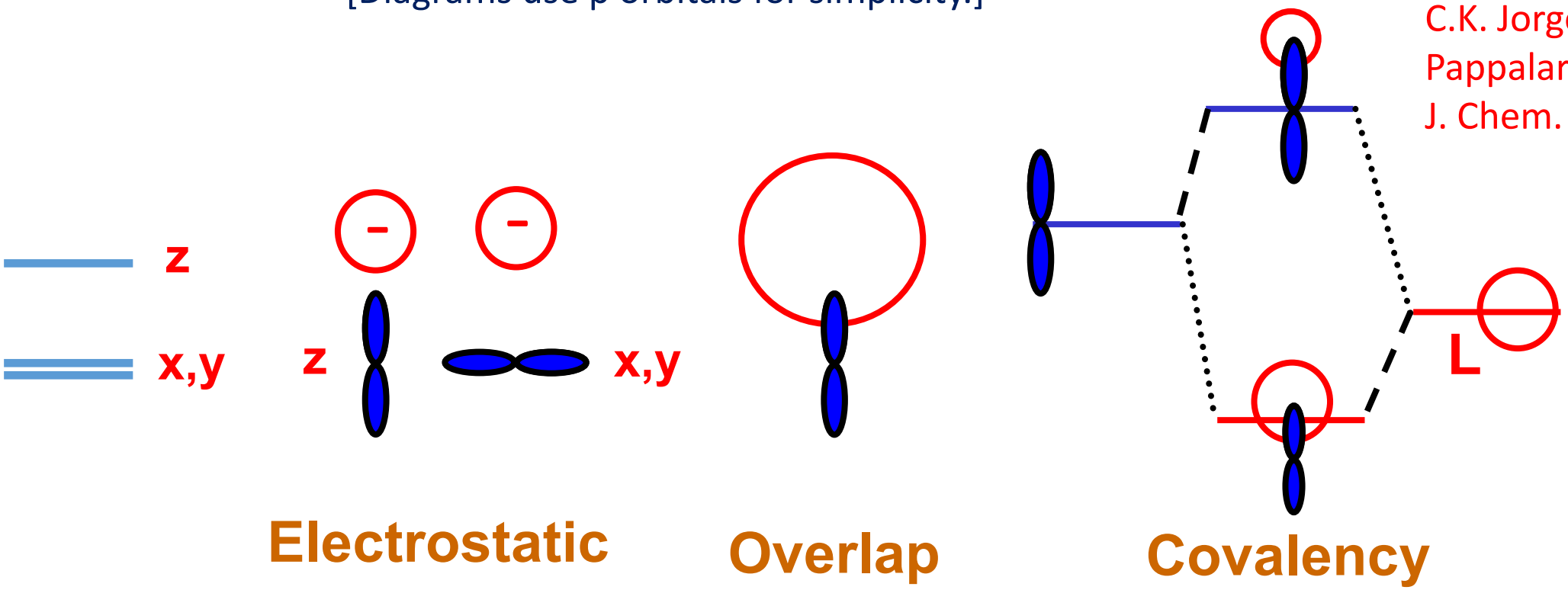

All increase energy of z orbital more than x,y

Orbital energies or Hamiltonian matrix ↔ crystal-field parameters

Do the ``Ligand Field'' Parameters in Lanthanides Represent Weak Covalent Bonding?

C.K. Jorgensen, R. Pappalardo, H.H. Schmidtke, J. Chem. Phys. 1963

Abstract: Instead of explaining the seven different f-orbital energies or five different d-orbital energies by parameters $A_{nm}\ \langle r_n \rangle$ of the electrostatic ligand field model, we propose to classify the energy levels according to the actual one-electron energies and to interpret these quantities by the weak effects of σ antibonding on the partly filled shell. Calculations of the relative angular dependence of such effects are made in a simple model and compared with experimental data for nine- and eight-coordinated lanthanide compounds The agreement is judged to be much more satisfactory than when the electrostatic model is applied, and the number of freely chosen parameters is much smaller.

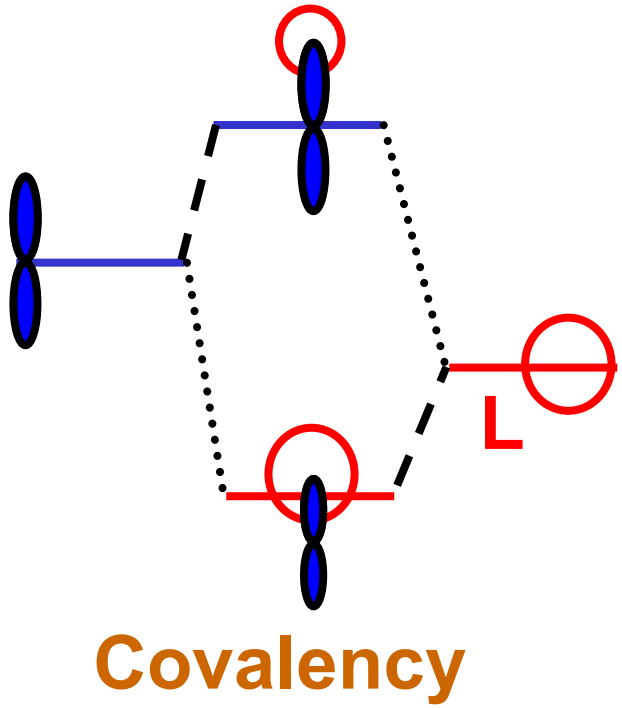

Rotations and the Superposition Model

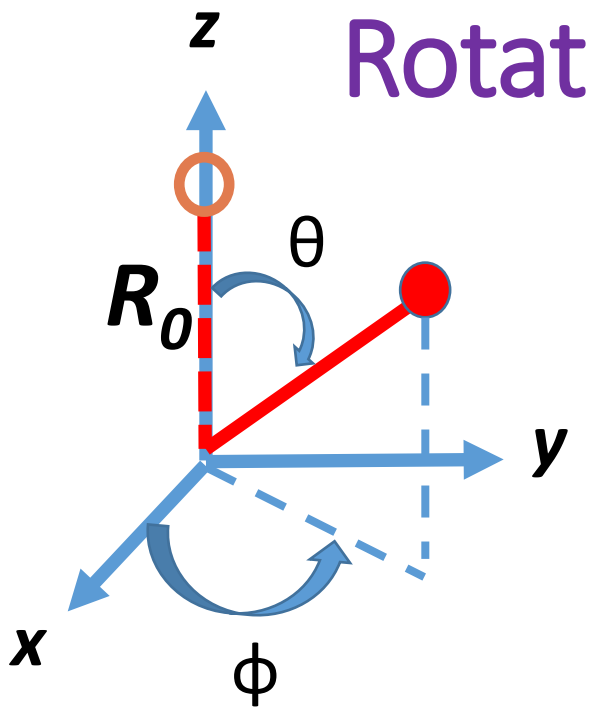

Electrostatic model:

$$B_q^k = \frac{e^2}{4\pi\epsilon_0}\langle r^k\rangle \sum_L \frac{1}{r_L^{k+1}} C_{-q}^{(k)}(\theta_L,\phi_L)(-1)^q$$

Rotation matrix is related to the spherical tensors:

$$D_{q'0}^{(j)}(\alpha=\phi,\beta=\theta,\gamma=0) = (-1)^{q'} C_{-q'}^{(K)}(\theta,\phi).$$

Rotate from Z and change the distance to build up CF in terms of single ligand CF:

$$B_q^k = \bar{B}_k(R_0)\sum_L C_{-q}^{(k)}(\theta_L,\phi_L)(-1)^q \left(\frac{R_0}{R_L}\right)^{t_k}$$

$$B_0^k(R_L) \equiv \bar{B}_k(R_L)$$

Table A.1. The Wigner rotation matrices $D^1_{m',m}(\alpha,\beta,\gamma)$.

	m		
m'	1	0	-1
1	$\frac{1+\cos\beta}{2}\, e^{-i(\alpha+\gamma)}$	$-\frac{1}{\sqrt{2}}\sin\beta e^{-i\alpha}$	$\frac{1-\cos\beta}{2} e^{-i(\alpha-\gamma)}$
0	$\frac{1}{\sqrt{2}}\sin\beta e^{-i\gamma}$	$\cos\beta$	$-\frac{1}{\sqrt{2}}\sin\beta e^{i\gamma}$
-1	$\frac{1-\cos\beta}{2}\, e^{i(\alpha-\gamma)}$	$\frac{1}{\sqrt{2}}\sin\beta e^{i\alpha}$	$\frac{1+\cos\beta}{2}\, e^{i(\alpha+\gamma)}$

k	q	$C_q^{(k)}(x,y,z)$	$C_q^{(k)}(\theta,\phi)$
0	0	1	1
1	0	z/r	$\cos\theta$
1	±1	$\mp\sqrt{\frac{1}{2}}(x\pm iy)/r$	$\mp\sqrt{\frac{1}{2}}\sin\theta\, e^{\pm i\phi}$

Relating ab-initio and crystal-field calculations

- Modern quantum-chemistry calculations for rare-earth materials:
  - DFT calculation using VASP.
  - 4f energies (without spin-orbit) using AIMP embedded cluster approach
  - [Seijo et al J. Chem. Phys. 114, 118 (2001).]
  - SA-CASSCF calculation using MOLCAS.

- Use calculations for Ce^{3+} to estimate parameters for the series.
  - For high symmetry we can just fit the energy levels of the ab-initio calculation.
  - Not possible in low symmetries such as D_2 (YAG), C_1 (YSO)
  - Need to relate the matrices.
  - Project the Hamiltonian into the model space.
    (Hurtubise and Freed, Adv. Chem. Phys. 83, 465, 1993).

Relate H_{eff} to full H

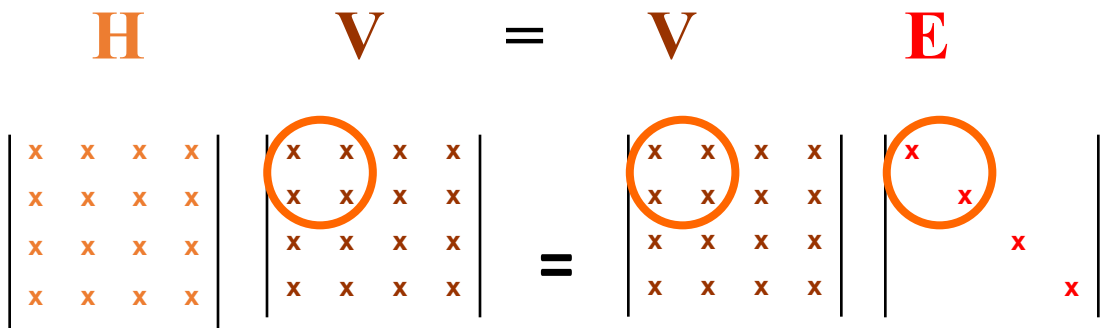

$$H = V\ E\ V^{-1}$$

Use a subset of energies and eigenvectors from ab-initio calculation:

$$H_{eff}^{NH} = V_p\ E_p\ V_p^{-1}$$ (non-Hermitian) ['p' is the small, 'projected' matrix]

$$V_k = (Vp\ Vp^{+})^{-1/2}\ Vp$$ (orthonormal)

$$H_{eff} = V_k\ Ep\ V_k^{-1}$$ (Hermitian)

Can Solve: $H_{eff} = \Sigma_\alpha P_\alpha T_\alpha$ for parameters P_α

Reid MF., Duan CK. and Zhou HW. (2009) Crystal-field parameters from ab initio calculations. Journal of Alloys and Compounds 488: 591-594.

Example: $LiYF_4:Ce^{3+}$

J. Phys. Chem. C 2012, 116, 20513−20521

A Theoretical Study on the Structural and Energy Spectral Properties of Ce^{3+} Ions Doped in Various Fluoride Compounds

Jun Wen,[†] Lixin Ning,[‡] Chang-Kui Duan,*[,†] Yonghu Chen,[†] Yongfan Zhang,[§] and Min Yin[†]

DFT calculation using VASP.
4f energies (without spin-orbit) using AIMP embedded cluster approach
[Seijo et al J. Chem. Phys. 114, 118 (2001).]
SA-CASSCF calculation using MOLCAS.

	$LiYF_4$		
	CF	CF + SO	exptl[b]
	0	0	0
	196	247	
4f [1]	196	481	
	297	2214	
	504	2255	
	504	2409	
	1321	3016	
	32389	33378	33433
	40274	41142	41101
	48640	49404	48564
5d[1]	48640	50144	50499
	52213	53520	52790
	44431	45518	45277

(4f from Pr^{3+})

Parameter	Experiment	Theory
$B_0^2(4f)$	481	310
$B_0^4(4f)$	−1150	−1104
$B_4^4(4f)$	−1228	−1418
$B_0^6(4f)$	−89	−70
$B_4^6(4f)$	−1213	$-1140 + 237i$
$B_0^2(5d)$	4673	4312
$B_0^4(5d)$	−18649	−18862
$B_4^4(5d)$	−23871	−23871

Temperature dependent infrared absorption, crystal-field and intensity analysis of Ce^{3+} doped $LiYF_4$

Jon-Paul R. Wells[a,b,*], S. P. Horvath[a], Michael F. Reid[a,c]

Optical Materials, **47**, 33 (2015)

Table 1: Experimental, fitted, and ab-initio [21] energy levels ($cm^{-1}\pm0.1$), ground state g-values for Ce^{3+} in $LiYF_4$.

State	Experiment	Fitted	Ab-initio
$Z_1\gamma_{7,8}$	0.0	1.5	0
$Z_2\gamma_{5,6}$	216	213.8	247
$Z_3\gamma_{7,8}$	-	414.4	481
$Y_1\gamma_{5,6}$	2216.1	2215.5	2214
$Y_2\gamma_{7,8}$	2312.8	2312.1	2255
$Y_3\gamma_{5,6}$	2428.8	2430.1	2409
$Y_4\gamma_{7,8}$	3157.8	3158.6	3016
$g_\parallel$	2.765	2.751	
$g_\perp$	1.473	1.514	

Table 2: Fitted and ab-initio [21] spin-orbit and S_4 symmetry crystal-field parameters (cm^{-1}) for Ce^{3+} in $LiYF_4$.

Parameter	Fitted	Ab-initio
ζ	626	-
B_0^2	298	310
B_0^4	-1328	-1104
B_4^4	-1282	-1418
B_0^6	-192	-70
B_4^6	-1743	-1140
$B_4^{6'}$	693	237

Note use of magnetic splittings in crystal-field fit. We now expand on this idea.

CF calculations with magnetic splittings

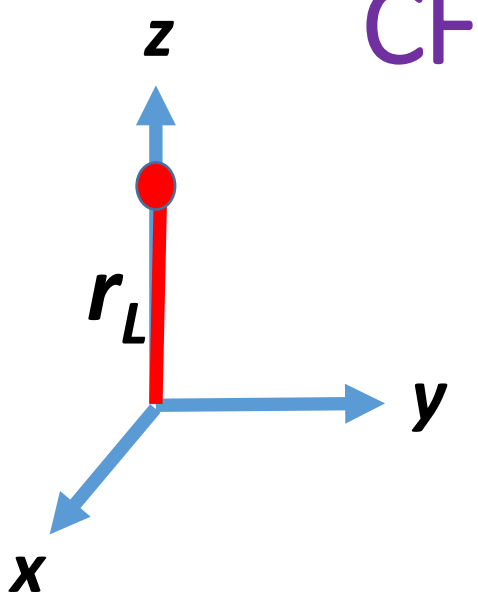

$$B_q^k = \bar{B}_k(R_0) \sum_L C_{-q}^{(k)}(\theta_L, \phi_L)(-1)^q \left(\frac{R_0}{R_L}\right)^{t_k}$$

Consider the $^4F_{3/2}$ multiplet of Nd^{3+}.
We only need B^2_q in this case.

E.g. Single ligand on Z, $B^2_0 = 500\ cm^{-1}$

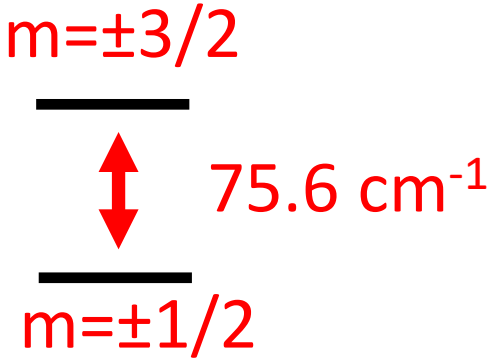

But there are many sets of parameters that would give the same splitting.

We can use magnetic splittings to determine the orientation of the potential…

Potential

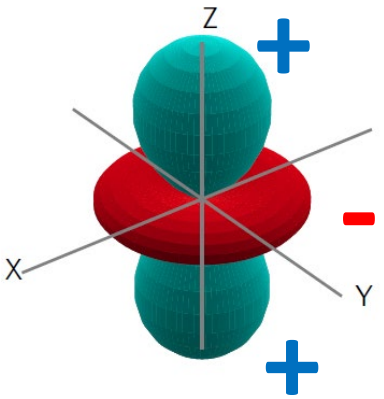

$C^2_0(r)$

f orbitals:

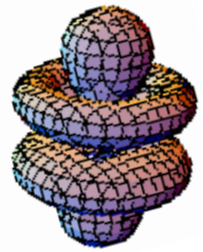

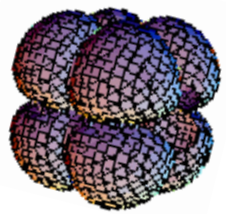

k	q	$C_q^{(k)}(x,y,z)$
0	0	1
1	0	z/r
1	±1	$\mp\sqrt{\frac{1}{2}}(x \pm iy)/r$
2	0	$\sqrt{\frac{1}{4}}(3z^2 - r^2)/r^2$
2	±1	$\mp\sqrt{\frac{3}{2}}z(x \pm iy)/r^2$
2	±2	$\sqrt{\frac{3}{8}}(x \pm iy)^2/r^2$

CF calculations with magnetic splittings

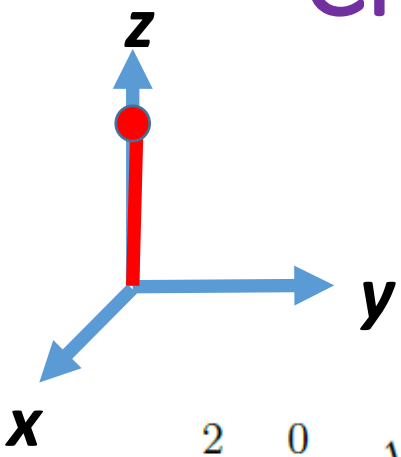

Single ligand on Z, B^2_0 = 500 cm^{-1}

Calculate magnetic splitting of upper state: B=4T

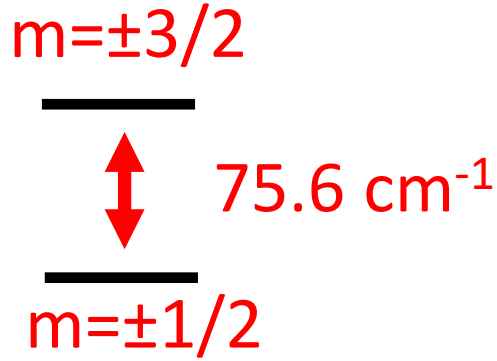

2	0	$\sqrt{\frac{1}{4}}(3z^2 - r^2)/r^2$
2	±1	$\mp\sqrt{\frac{3}{2}}z(x \pm iy)/r^2$
2	±2	$\sqrt{\frac{3}{8}}(x \pm iy)^2/r^2$

Potential

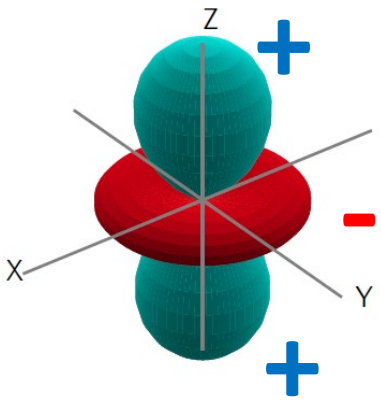

$C^2_0(r)$

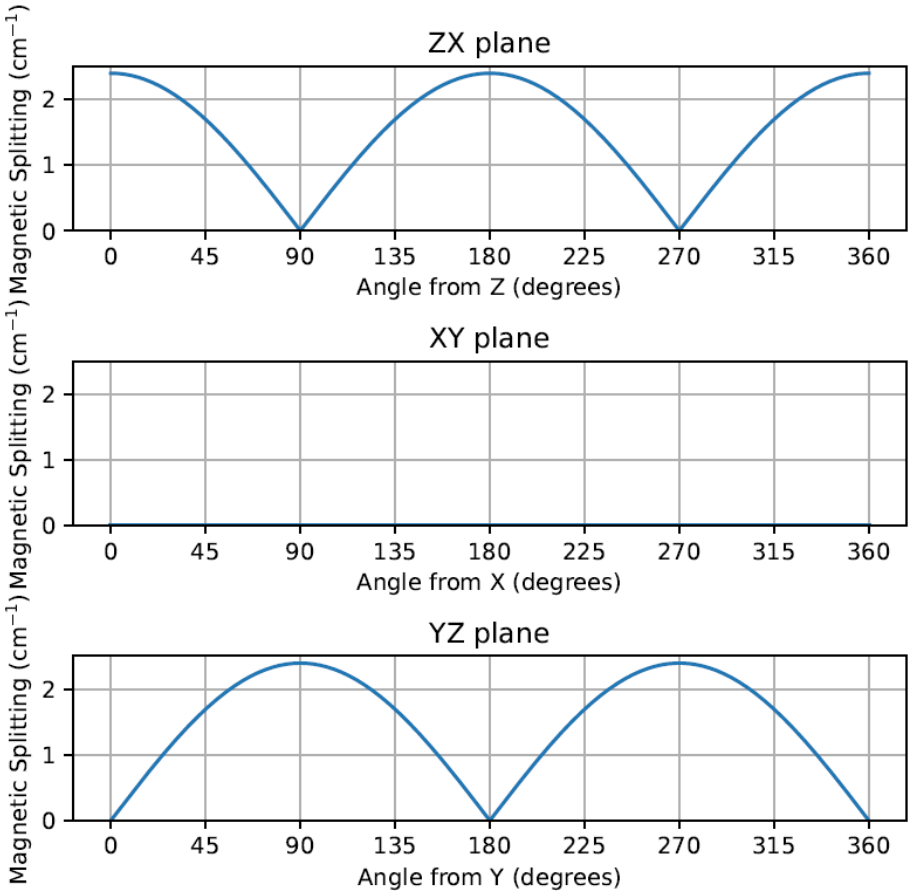

Magnetic Splitting

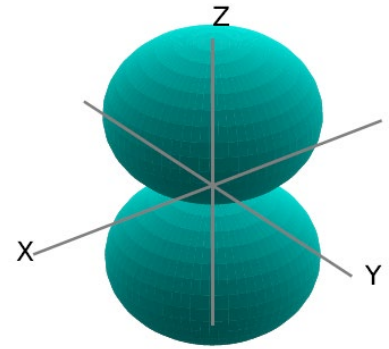

Change orientation!

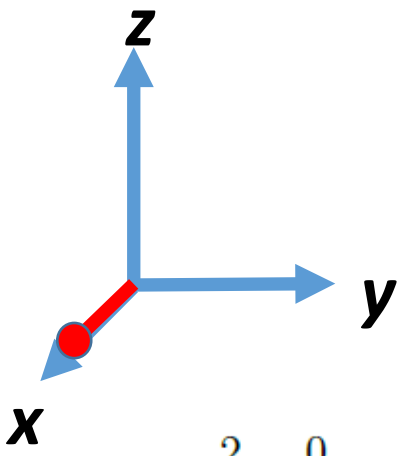

Single ligand on X, B^2_0 = -250 cm^{-1} B^2_2 = +306 cm^{-1}
Calculate magnetic splitting of upper state: B=4T

m=mixture

75.6 cm^{-1}

m=mixture

2	0	$\sqrt{\frac{1}{4}}(3z^2 - r^2)/r^2$
2	±1	$\mp\sqrt{\frac{3}{2}}z(x \pm iy)/r^2$
2	±2	$\sqrt{\frac{3}{8}}(x \pm iy)^2/r^2$

Potential

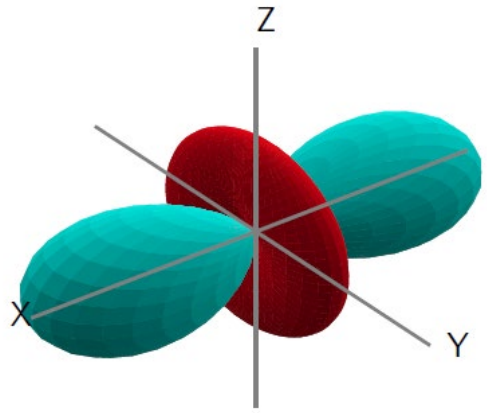

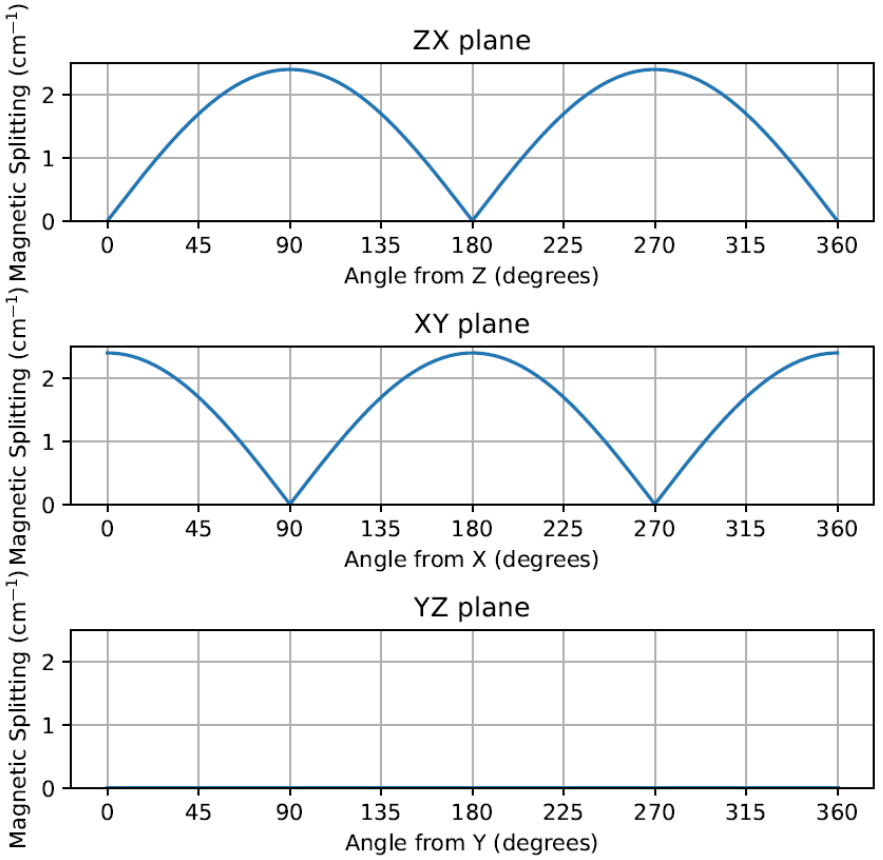

Magnetic Splitting

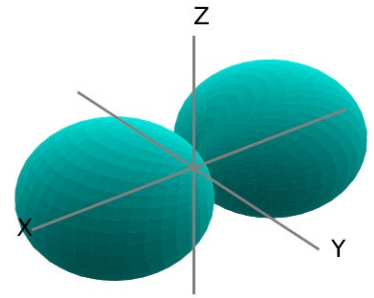

Quantum Information Applications?

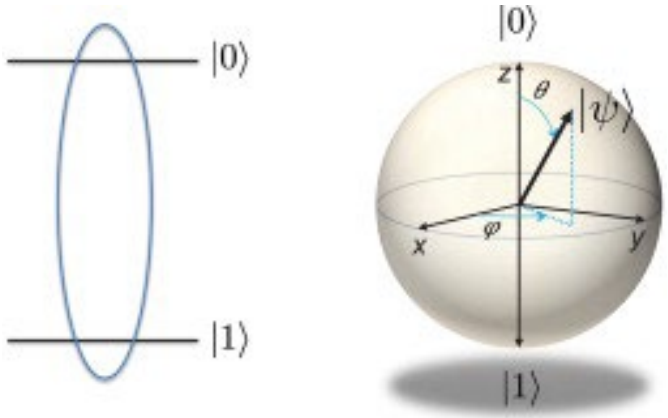

$$|\psi\rangle = \cos(\theta/2)\,|0\rangle + e^{i\phi}\sin(\theta/2)\,|1\rangle$$

$$X = \begin{pmatrix} 0 & 1 \\ 1 & 0 \end{pmatrix}$$

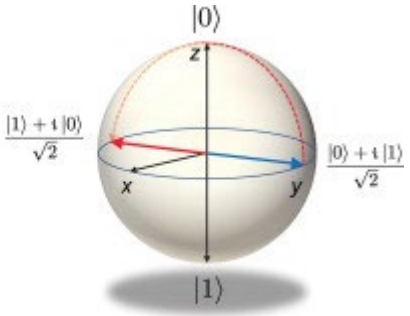

$$|\psi'\rangle = X\,|\psi\rangle$$

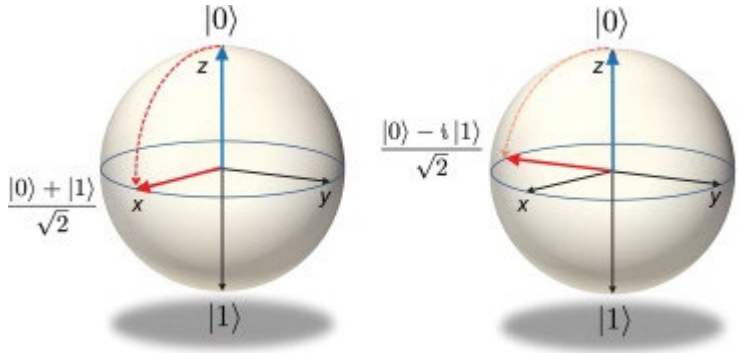

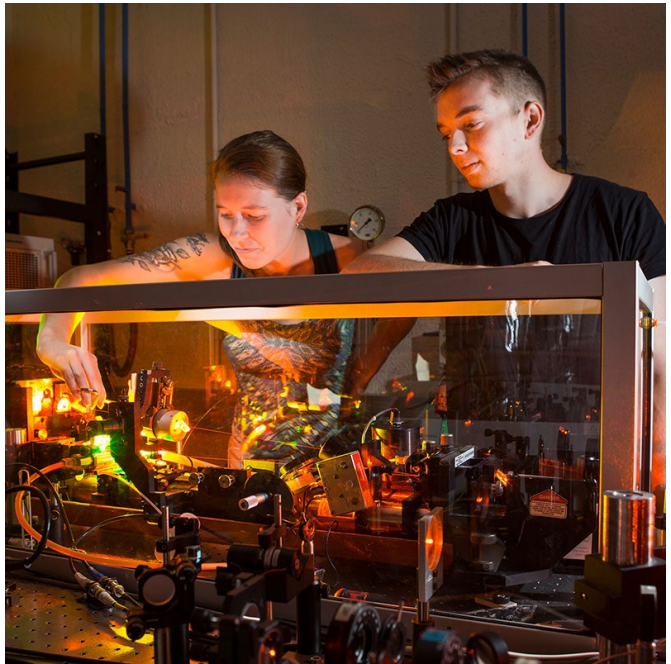

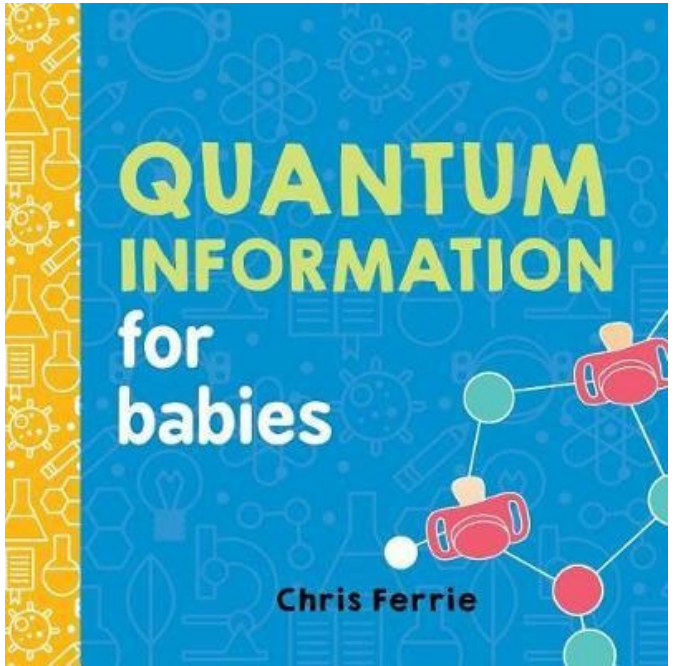

Spin Echoes*†

E. L. HAHN‡
Physics Department, University of Illinois, Urbana, Illinois
(Received May 22, 1950)

30MHz/0.7T
$\tau \approx 100\mu s$

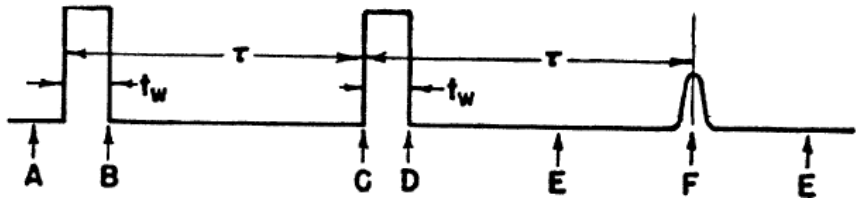

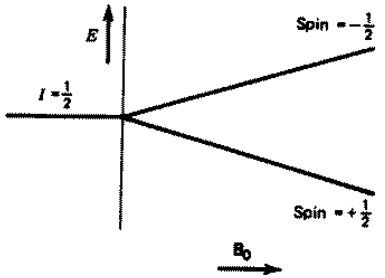

Modern NMR
600MHz/14T

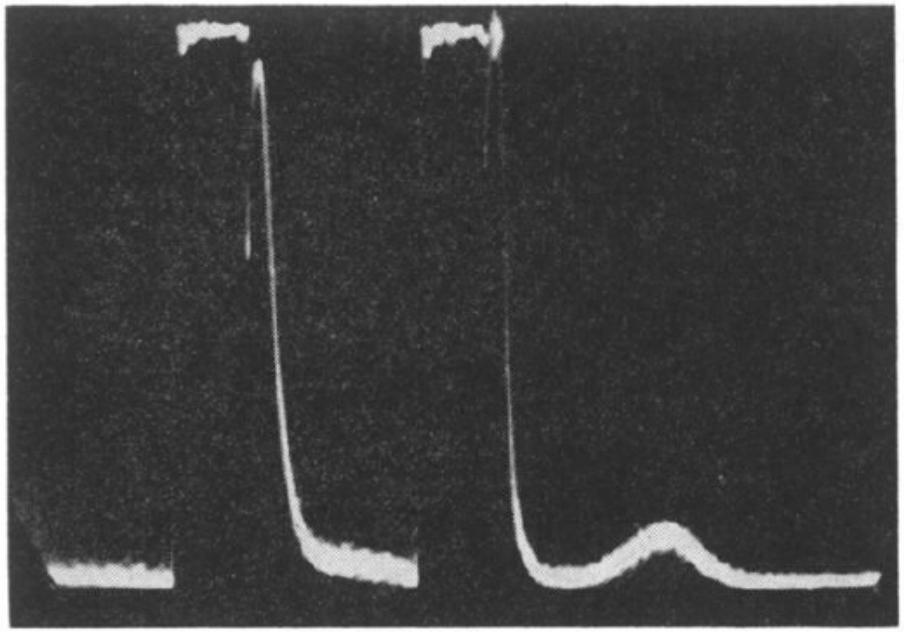

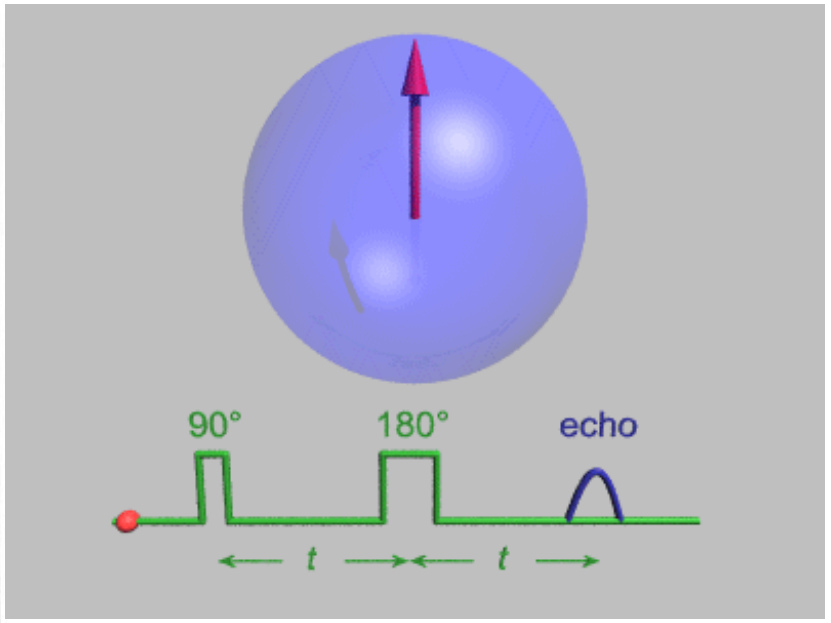

(N)MRI

FIG. 11. Free induction signals for protons in paraffin. The echo lasts for $\sim 1.4 \times 10^{-5}$ sec. The r-f pulses, about 25 μsec. wide, cause some blocking of the i.f. amplifier. The echo envelope decay time is also of the order of the single echo lifetime.

Spin Echo: Wikipedia

Six-Hour Coherence: $^{151}Eu^{3+}$

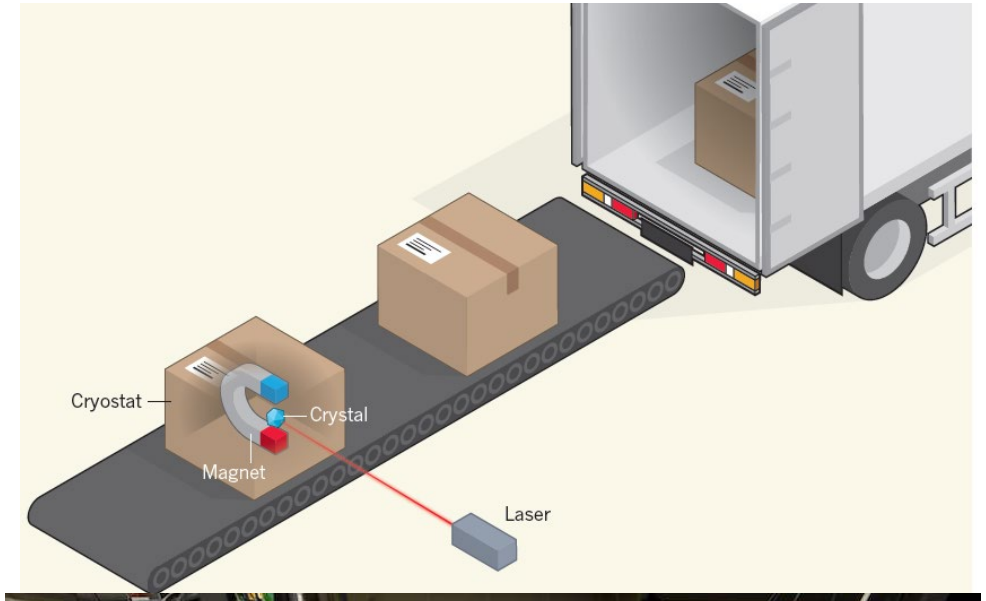

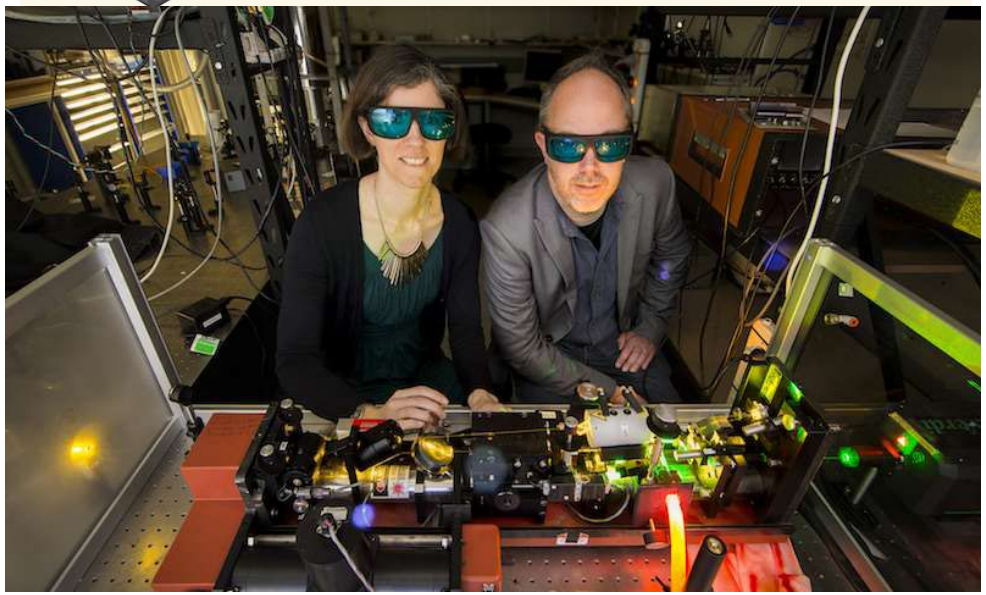

Rose Ahlefeldt, Matt Sellars, ANU, Australia.

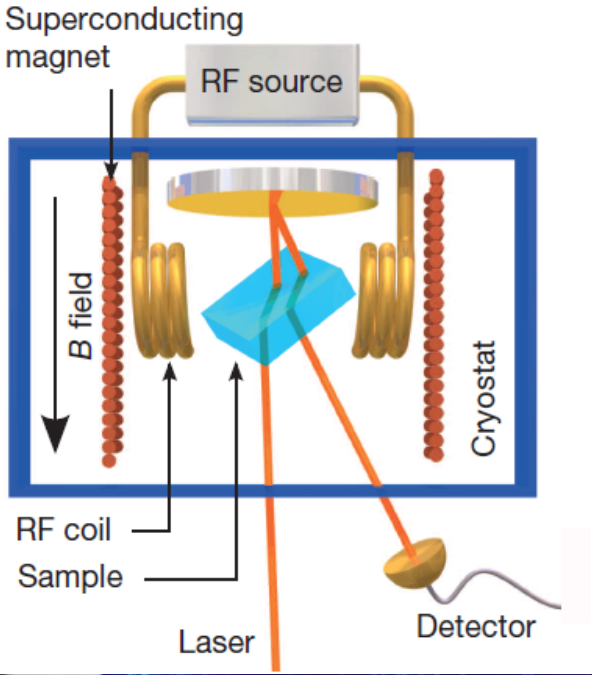

Manjin Zhong, SUSTech, Shenzhen

Optically addressable nuclear spins in a solid with a six-hour coherence time

Manjin Zhong[1], Morgan P. Hedges[1,2], Rose L. Ahlefeldt[1,3], John G. Bartholomew[1], Sarah E. Beavan[1,4], Sven M. Wittig[1,5], Jevon J. Longdell[6] & Matthew J. Sellars[1]

8 JANUARY 2015 | VOL 517 | NATURE | 177

$^{151}Eu^{3+}:Y_2SiO_5$

ZEro First Order Zeeman

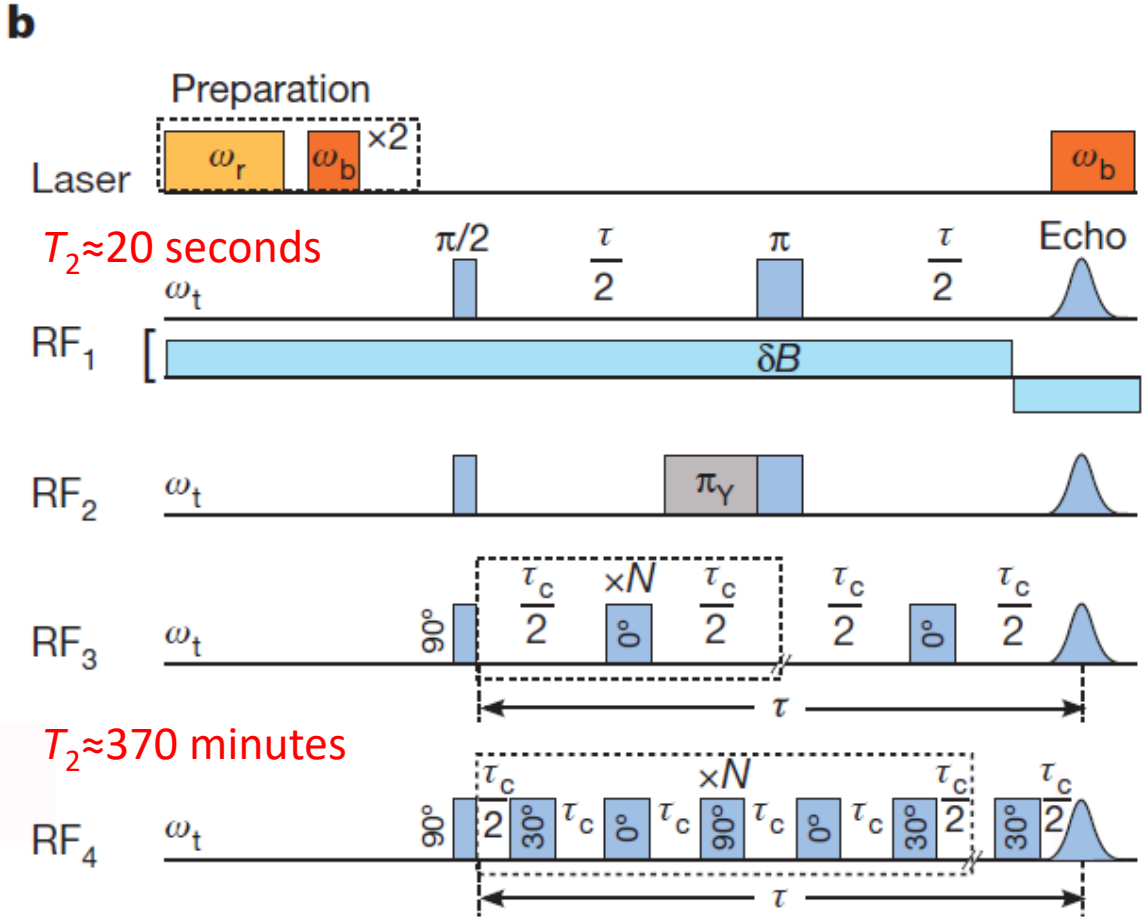

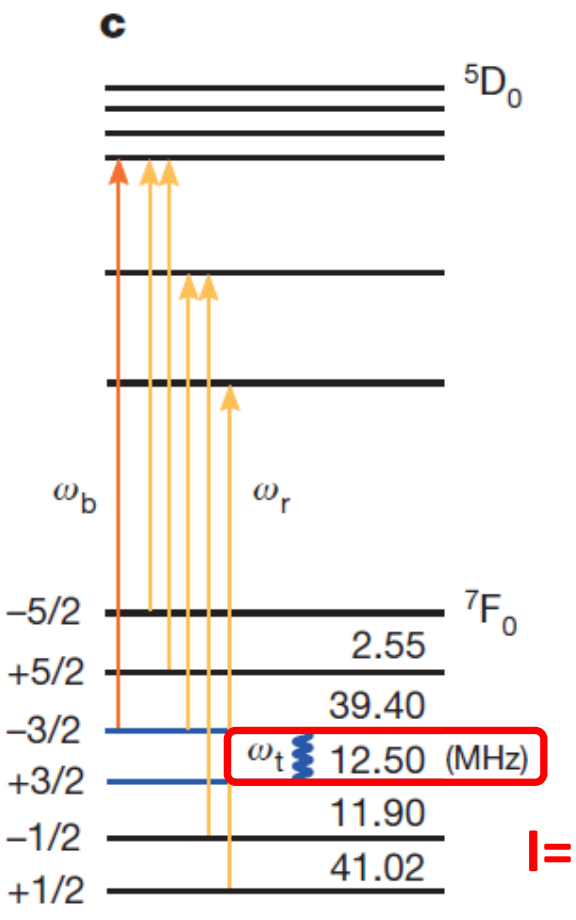

I=5/2

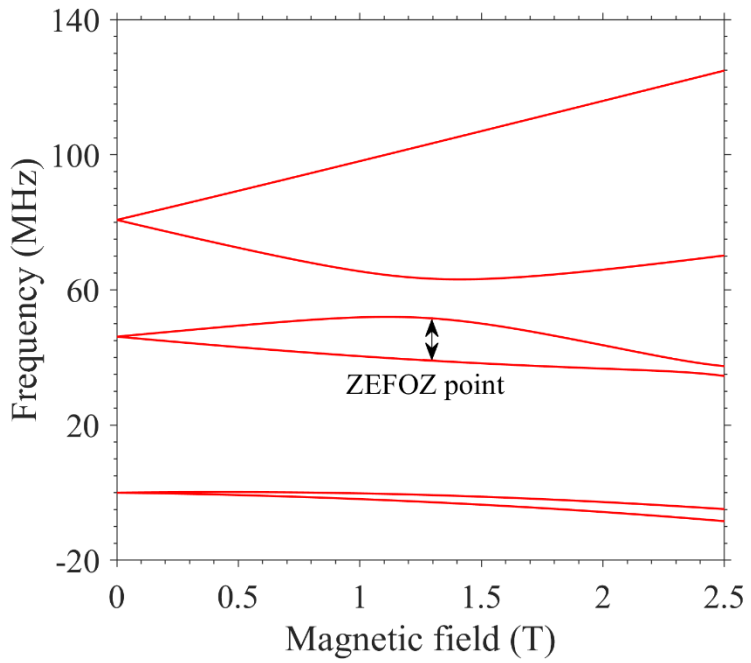

(Note that recent work has re-ordered the states relative to those shown on the left.)

Crystal-Field Calculation for $^{167}Er^{3+}$:YSO Site 2

$$H = H_{\mathrm{FI}} + H_{\mathrm{CF}} + H_{\mathrm{Z}} + H_{\mathrm{HF}} + H_{\mathrm{Q}}.$$

- Use literature and new data for electronic energy levels, magnetic, and hyperfine splitting.
- Directional magnetic data is crucial to fixing orientation of CF Hamiltonian for low-symmetry sites.
- Separately calculate:
  - Electronic energy levels
  - Magnetic splitting for various field orientations
  - Hyperfine splitting.
- Data (Effectively 95 data points)
  - 35 Electronic energies
  - 12 Ground-state hyperfine levels
  - 12 Zeeman rotation points
  - Raman heterodyne hyperfine data (15 MHz accuracy)
- 34 Parameters (similar to spin-Hamiltonian parameter number…)

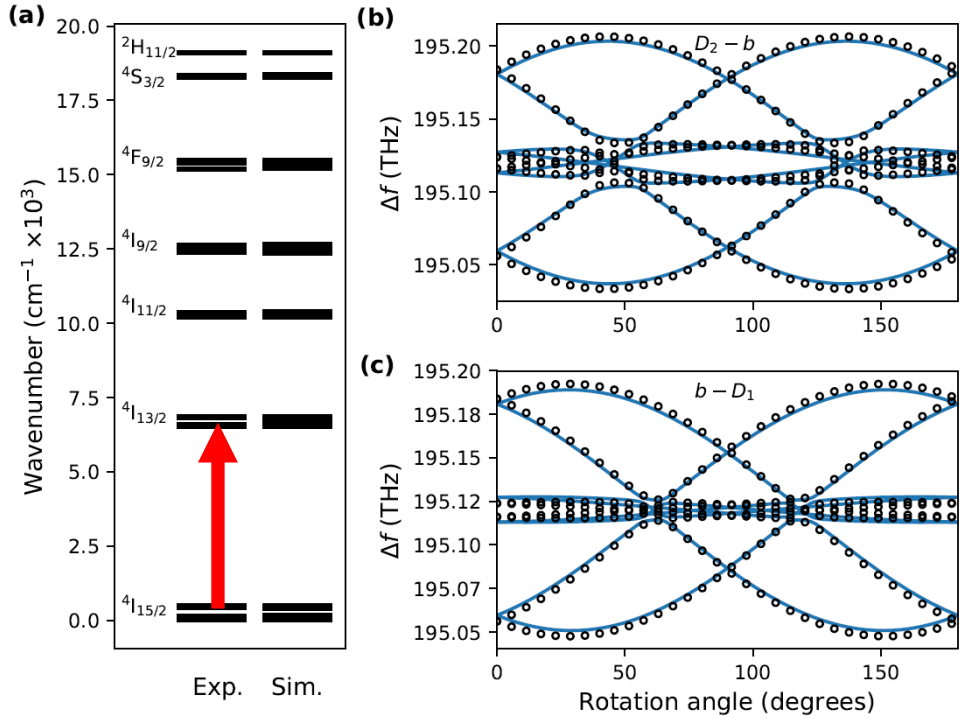

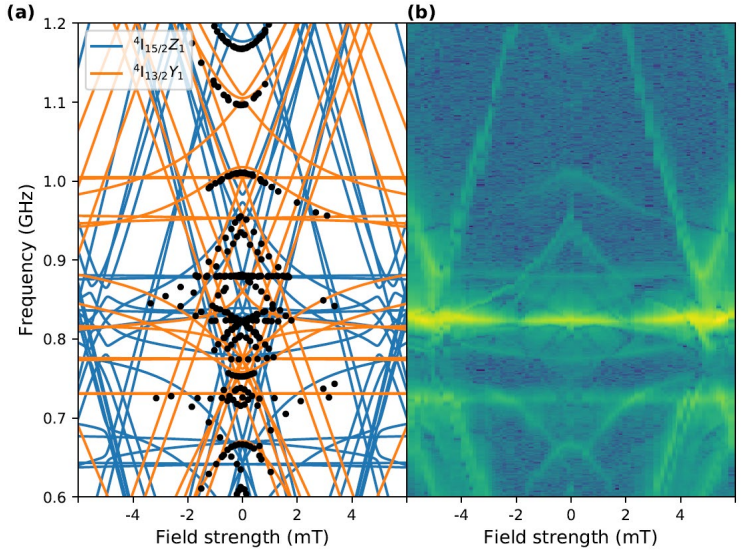

Sebastian Horvath et al. Phys. Rev. Lett. **123**, 057401 (2019)

Extension to other ions: Zeeman spectroscopy of $Sm^{3+}:Y_2SiO_5$

N.L. Jobbitt et al. J. Phys. Condensed Matter 34:325502 (2022)

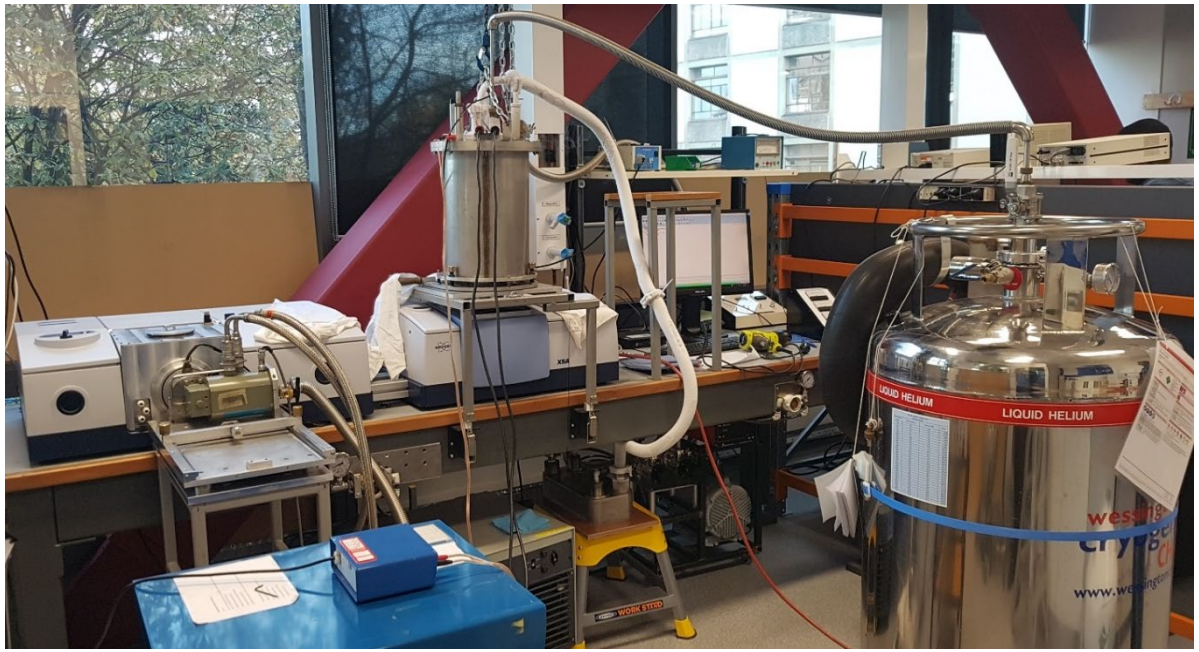

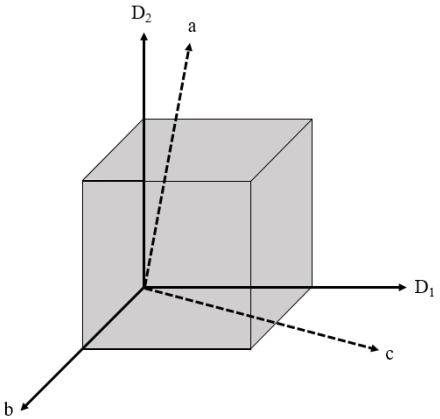

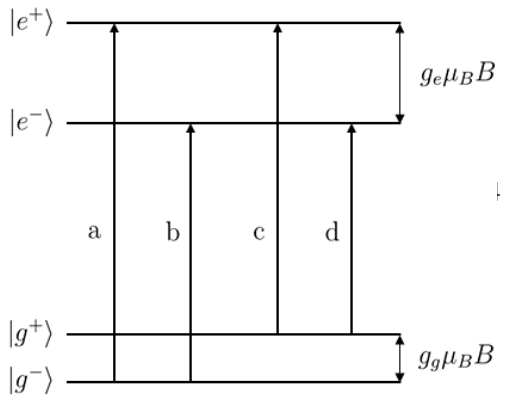

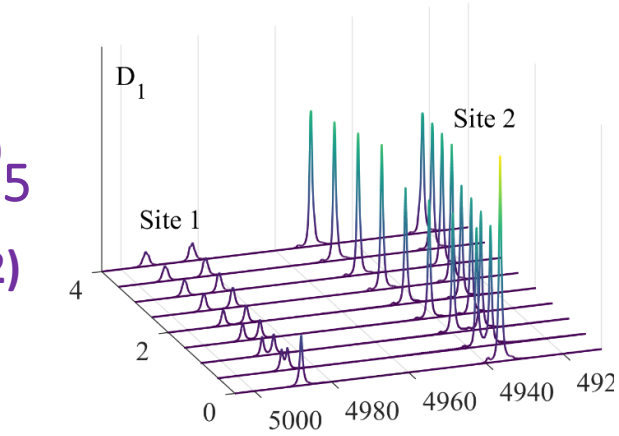

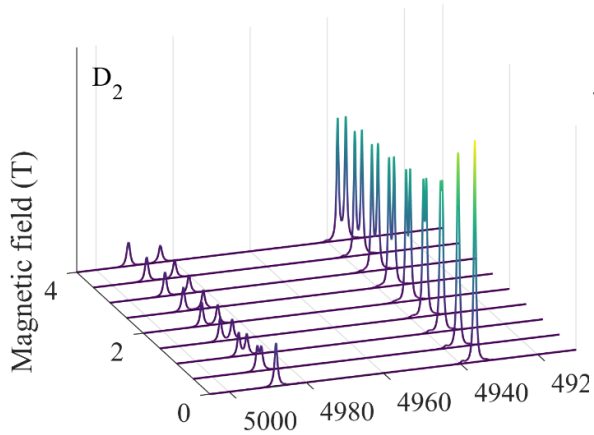

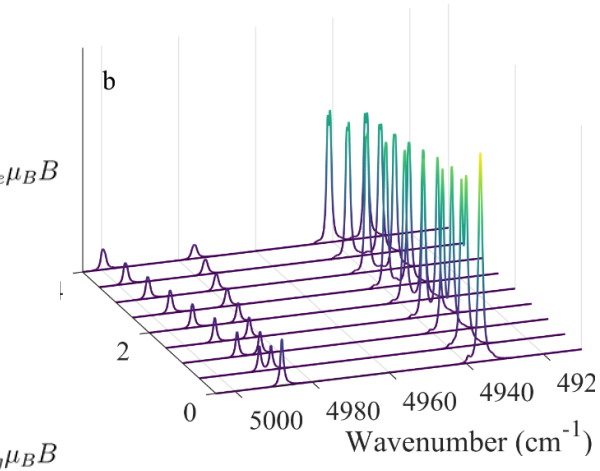

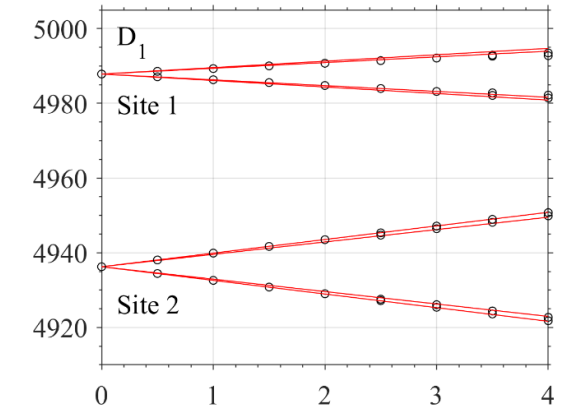

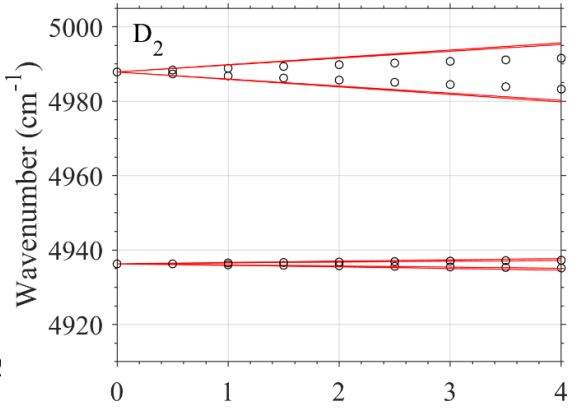

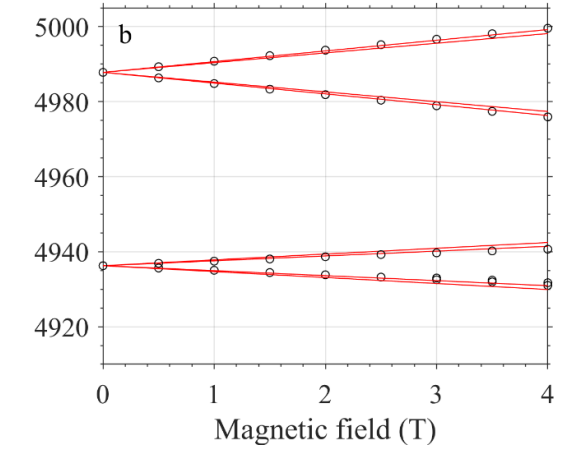

Er^{3+}:YSO N.L. Jobbitt et al. Phys. Rev. B 104, 155121 (2021)

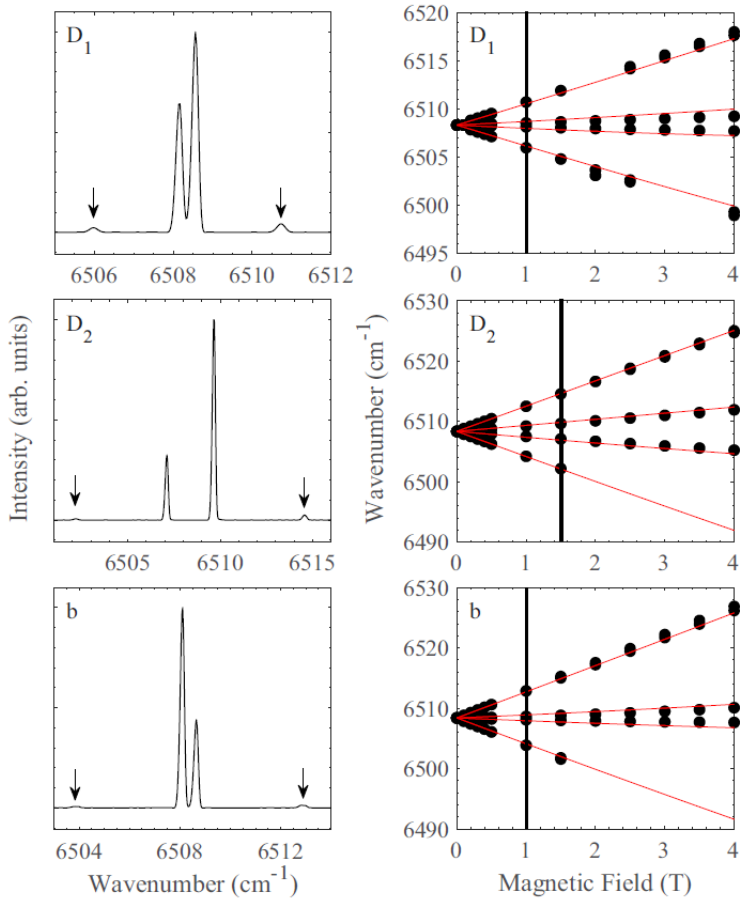

FIG. 2. Magnetic splittings of the site 1 $Z_1 \rightarrow Y_1$ transition for magnetic fields applied along the three crystallographic axes of Y_2SiO_5. The top, middle, and bottom panels shows $B \parallel D_1$, $B \parallel D_2$, and $B \parallel b$, respectively. The left panels show 4.2-K Zeeman absorption spectra at magnetic field strengths represented by the vertical lines in the right panels. The weak outer transitions are labeled with arrows to assist the reader. The right panels show the experimental splittings, represented by the circles, and the calculated splittings are represented by the red lines.

Site 1

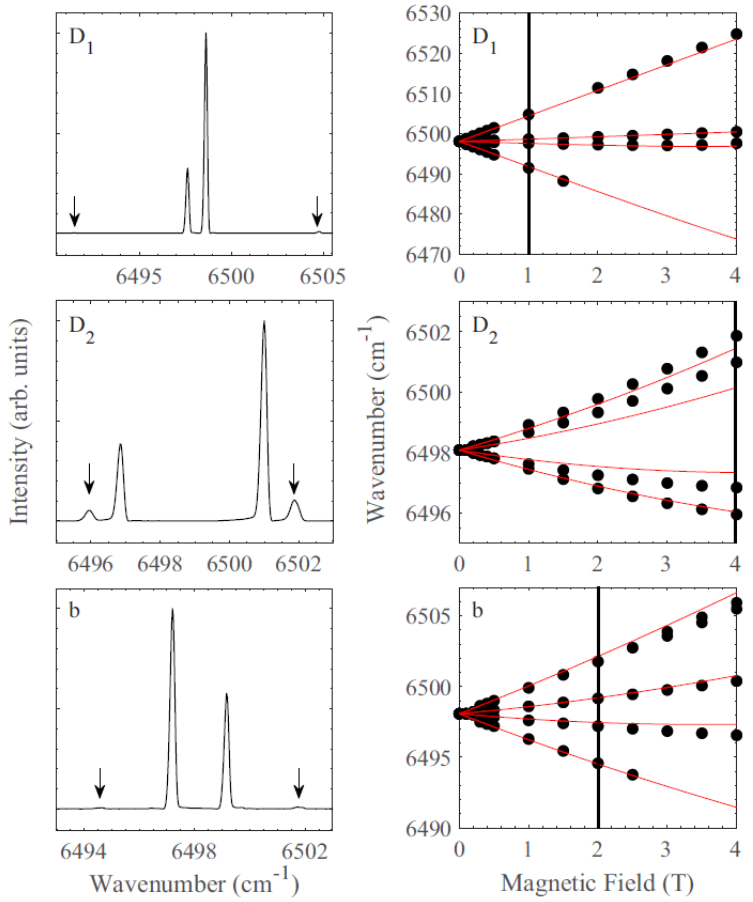

FIG. 3. Magnetic splittings of the site 2 $Z_1 \rightarrow Y_1$ transition for magnetic fields applied along the three crystallographic axes of Y_2SiO_5. The top, middle and bottom panels shows $B \parallel D_1$, $B \parallel D_2$, and $B \parallel b$, respectively. The left panels show 4.2-K Zeeman absorption spectra at magnetic field strengths represented by the vertical lines in the right panels. The weak outer transitions are labeled with arrows to assist the reader. The right panels show the experimental splittings, represented by the circles, and the calculated splittings are represented by the red lines.

Site 2

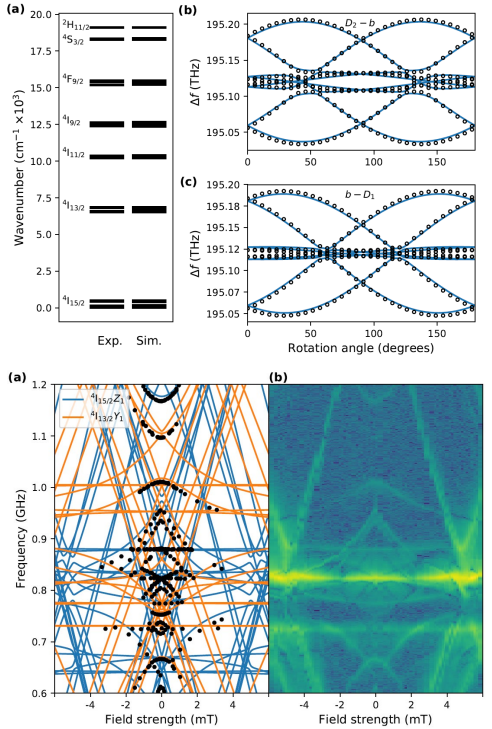

Site 1 ground state magnetic splitting

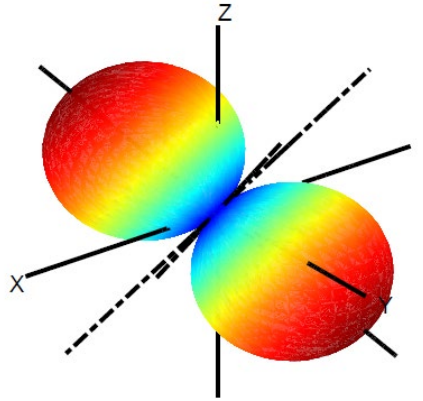

g value max: 14

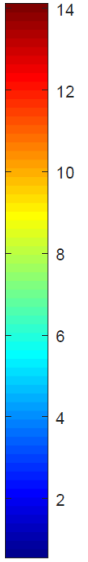

Er^{3+}:YSO Nick Jobbitt et al. Phys. Rev. B 104, 155121 (2021)

TABLE III. Fitted values for the free-ion, crystal-field and hyperfine parameters and their related uncertainties of site 1 and site 2 in Er^{3+}:Y_2SiO_5. All values are in cm^{-1}. Parameters determined by Horvath *et al.* are also included for comparison [16,18].

	Site 1				Site 2		
Parameter	This study	Uncertainty	Ref. [16]	Ref. [18]	This study	Uncertainty	Ref. [18]
E_{avg}	35491.3	0.1	35503.5	–	35507.5	0.1	–
F^2	95805.7	1.0	96029.6	95346	96121.9	1.3	95721
F^4	67869.7	3.4	67670.6	68525	67722.4	4.5	68564
F^6	53148.2	2.5	53167.1	52804	53241.2	3.1	52999
ζ	2360.5	0.1	2362.9	2358	2362.3	0.1	2356
B_0^2	−479.6	6.1	−149.8	−563	389.0	3.7	354
B_1^2	471.4+143.8i	2.9 + 3.0i	420.6+396.0i	558+280i	−325.7 − 95.8i	2.7 + 3.0i	498.6807+274i
B_2^2	125.5−2.0i	2.8 + 2.3i	−228.5+27.6i	143−121i	−368.5+53.7i	1.8 + 2.0i	−75.8028+60i
B_0^4	−640.6	31.3	1131.2	−125	17.2	15.5	226
B_1^4	288.8+924.1i	7.2 + 25.3i	985.7+34.2i	225−831i	−378.7 − 519.5i	5.1 + 9.3i	−657.8381+593i
B_2^4	−273.9+320.9i	11.1 + 16.7i	296.8+145.0i	−48 − 945i	−72.0 − 146.0i	5.7 + 6.7i	335.7827+253i
B_3^4	−873.7 − 367.8i	20.7 + 9.7i	−402.3 − 381.7i	−615 − 688i	−890.8+570.4i	9.5 + 7.3i	−71.3262 − 46i
B_4^4	−600.8+1210.5i	23.7 + 9.2i	−282.3+1114.3i	744−102i	−198.7 − 567.9i	7.8 + 5.2i	−813.9654+64i
B_0^6	145.7	13.2	−263.2	−28	73.4	4.3	219
B_1^6	−105.9 − 329.0i	2.9 + 4.0i	111.9+222.9i	49+199i	−37.5+49.9i	3.4 + 5.7i	−127+197i
B_2^6	−119.9+164.1i	7.7 + 8.8i	124.7+195.9i	120−107i	135.5+60.6i	4.5 + 1.5i	−36 − 47i
B_3^6	1.1+133.3i	6.7 + 4.5i	−97.9+139.7i	195−55i	−166.7+131.8i	2.6 + 4.0i	17−108i
B_4^6	−84.6+36.9i	5.0 + 4.5i	−93.7 − 145.0i	−287 − 161i	227.2+47.6i	1.2 + 3.0i	−100+77i
B_5^6	75.5+6.9i	4.3 + 6.6i	13.9+109.5i	−117+162i	119.5+64.3i	3.7 + 3.2i	−263+103i
B_6^6	−48.5+118.0i	6.2 + 4.2i	3.0−108.6i	136+186i	37.6−41.3i	3.5 + 2.8i	12−26i
S^2	386.6	–	399.0	483.0	363.1	–	397.9
S^4	948.2	–	862.9	824.6	653.3	–	607.5
S^6	183.8	–	189.6	218.6	151.5	–	171.4
a_I	0.005306	0.000008	0.005466	0.0059	0.005389	0.000012	0.0069
a_Q	0.0554	0.0020	0.0716	0.0800	0.0240	0.0024	0.0808

Note that 34 parameters is the same as the number of spin Hamiltonian parameters for Z1 and Y1.

g, A, Q tensors: (6+6+5)*2

$Er^{3+}:Y_2SiO_5$ predictions: Polarization Measurements

Polarization measurements for 1550 µm transitions

Y. Petit et al. Opt. Mater. X, **8**, 100062 (2020)

Blue: E‖b → Magnetic dipole variation.

Red: M‖b → Electric dipole variation.

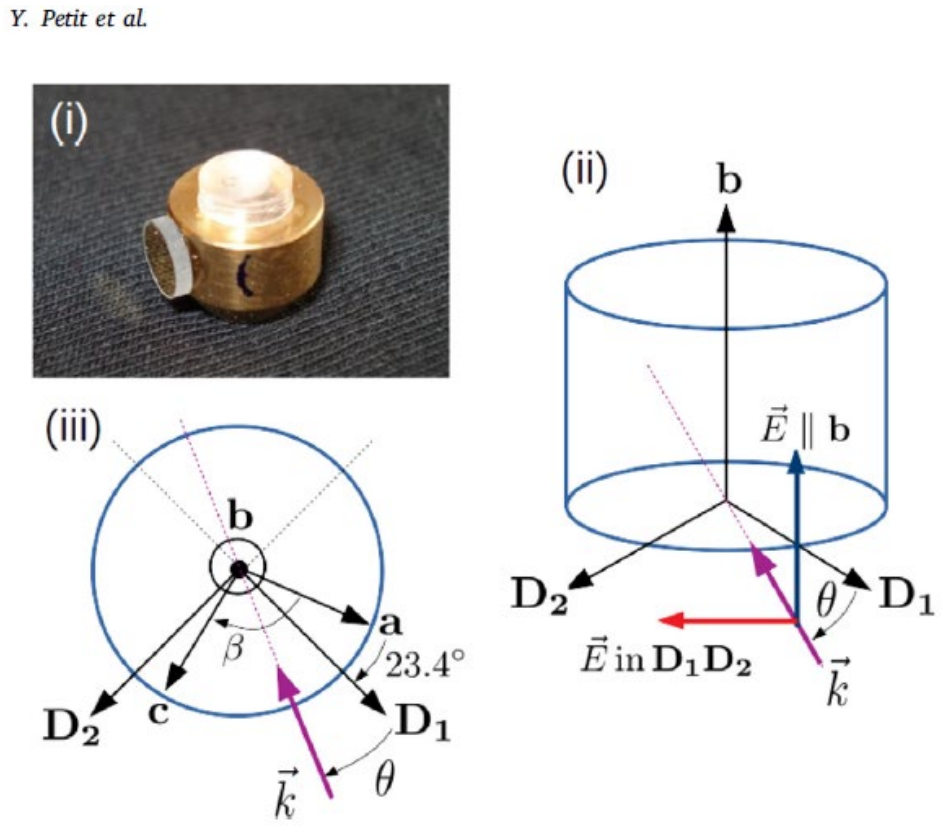

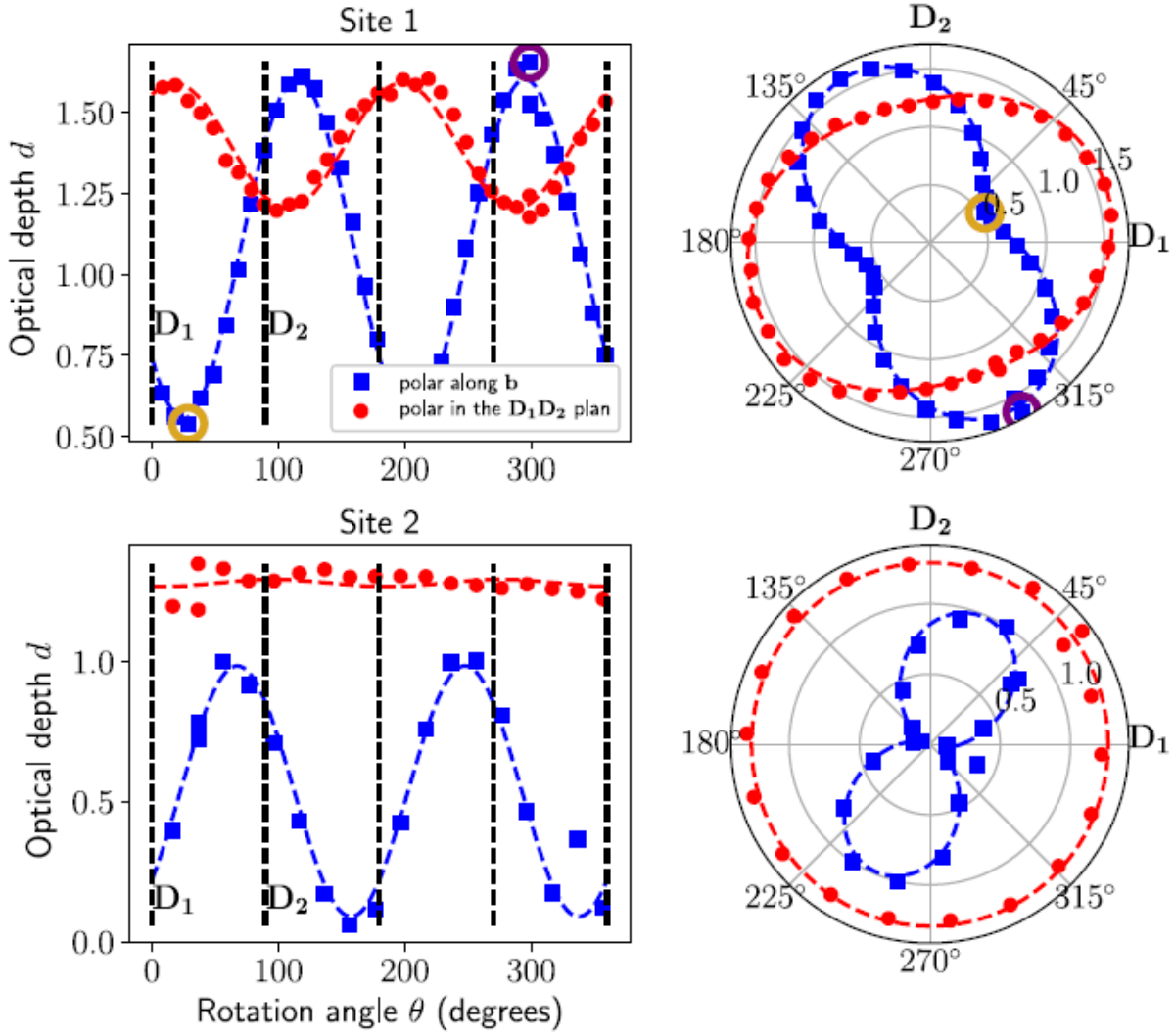

$Er^{3+}:Y_2SiO_5$ Predictions: Polarization

- We cannot (yet) calculate electric-dipole moments in low symmetry, but can calculate magnetic dipole moments (same matrix elements as Zeeman).
- Our predictions for Site 1 have improved with more data.
- Site 2 is still out of phase…
  Calculation or measurement?
- Interesting that all fits reproduce Zeeman splitting, but not dipole moments **between** states.

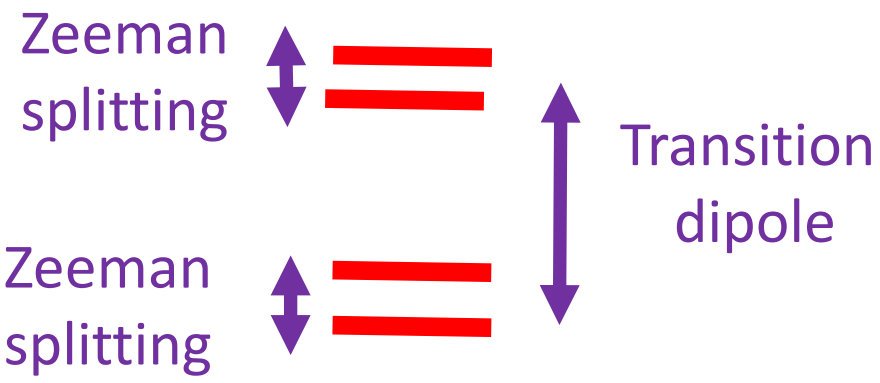

Site 1 – magnetic dipole

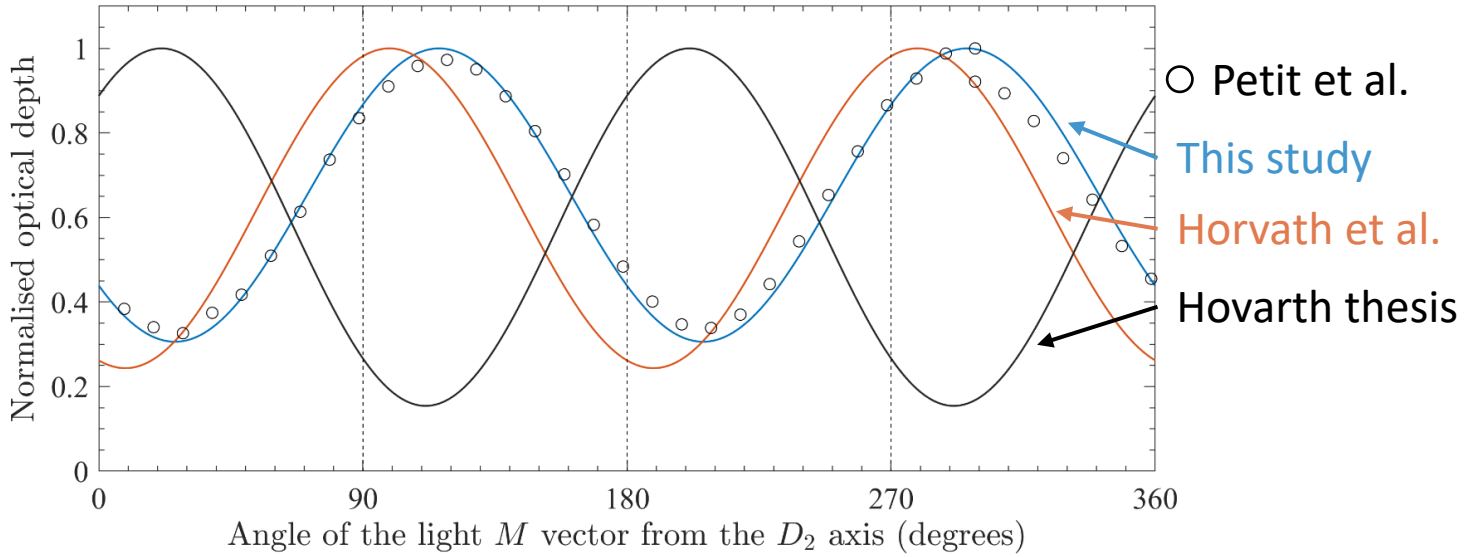

Site 2 – magnetic dipole

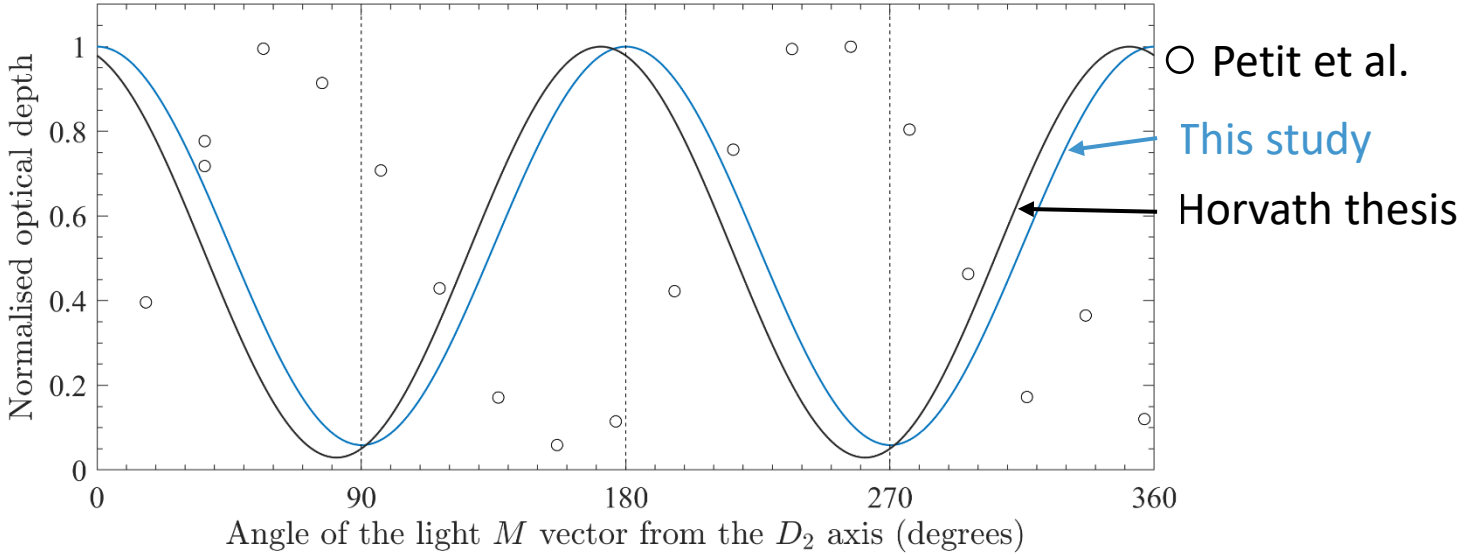

$Er^{3+}:Y_2SiO_5$ predictions: high-field hyperfine

Hyperfine structure of Site 2 1.5µm transition:

7T along D_1.

Miloš Rančić et al. Nat. Phys., **4**, 50-54 (2018)

Non-linear regime where spin-Hamiltonian approach breaks down.

Unlike Site 1, our Site 2 fit does not include Y_1 hyperfine data – this is a *prediction*.

Splittings	$^4I_{15/2}Z_1$		$^4I_{13/2}Y_1$	
ΔE	This study	Ref. [5]	This study	Ref. [5]
$\Delta(1,2)$	897	995	928	994
$\Delta(2,3)$	881	943	912	972
$\Delta(3,4)$	865	898	895	953
$\Delta(4,5)$	849	862	879	935
$\Delta(5,6)$	833	831	863	918
$\Delta(6,7)$	817	810	847	903
$\Delta(7,8)$	801	796	831	889

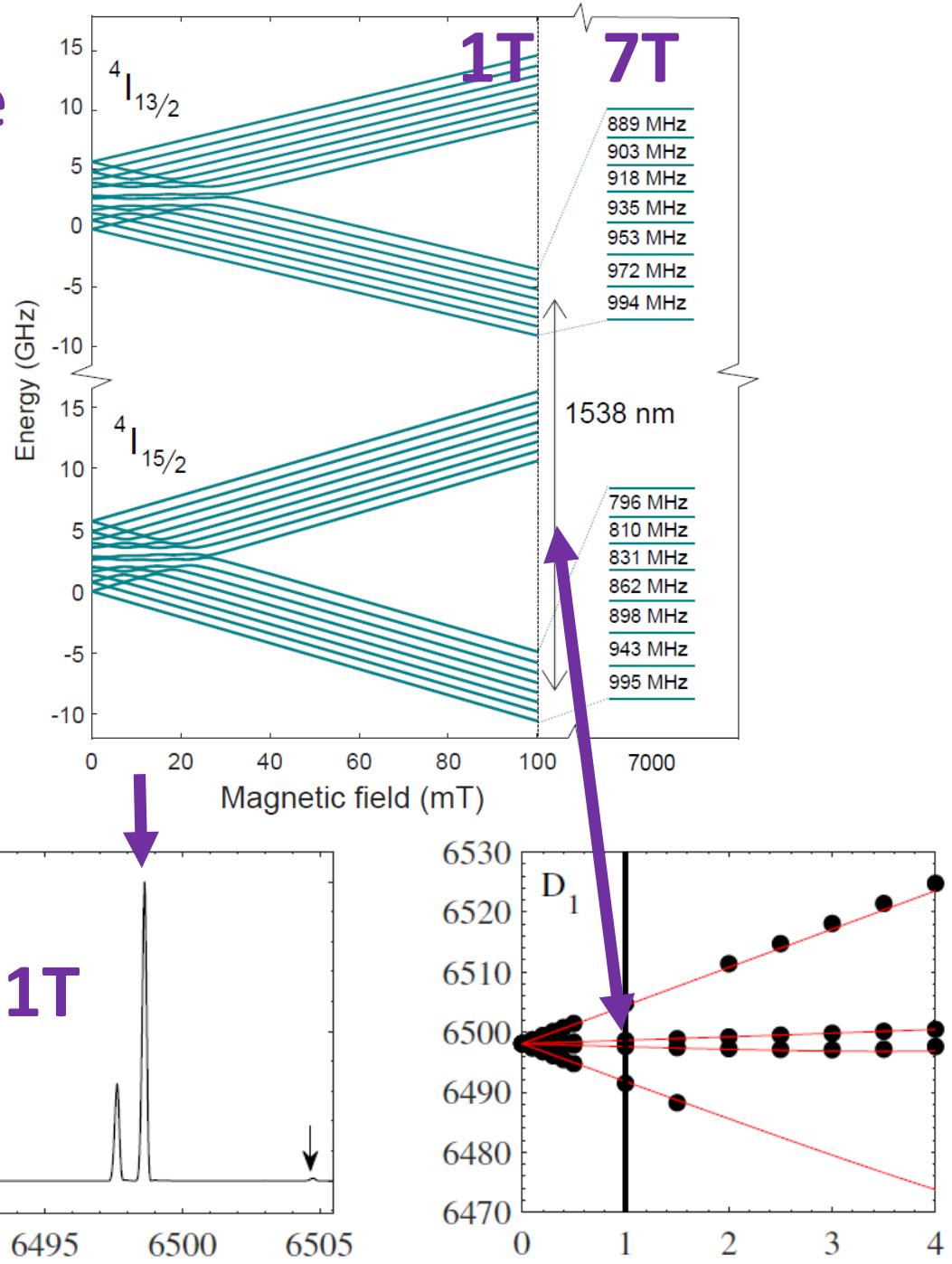

Other work by our group on Y_2SiO_5

$Ce^{3+}:Y_2SiO_5$

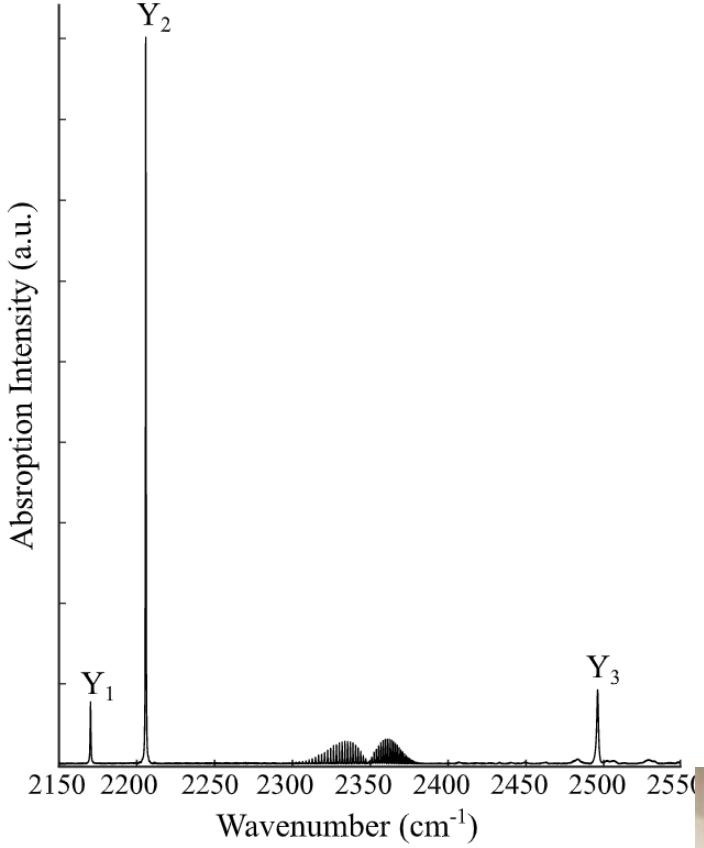

Yashar Alizadeh et al.
Opt. Mater., **117**, 111114 (2021)

$Nd^{3+}:Y_2SiO_5$

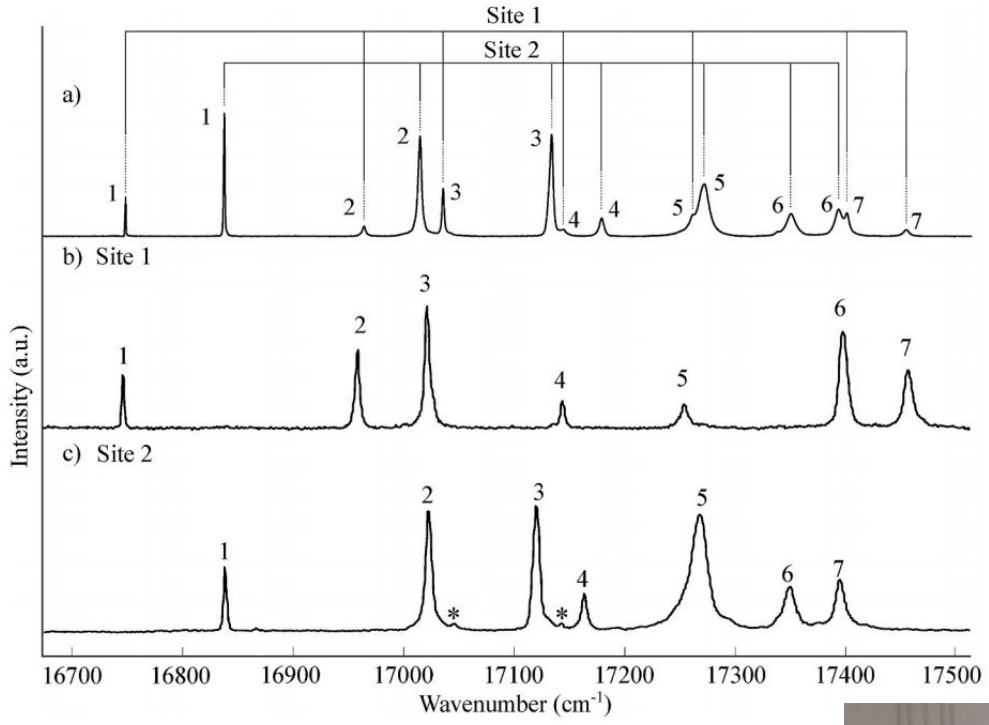

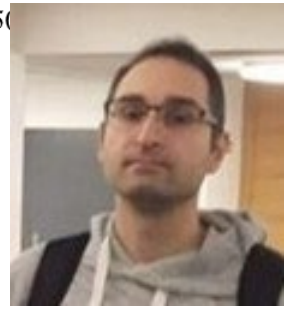

Yashar Alizadeh et al.
J. Lumin., **234**, 117959 (2021)

$Ho^{3+}:Y_2SiO_5$

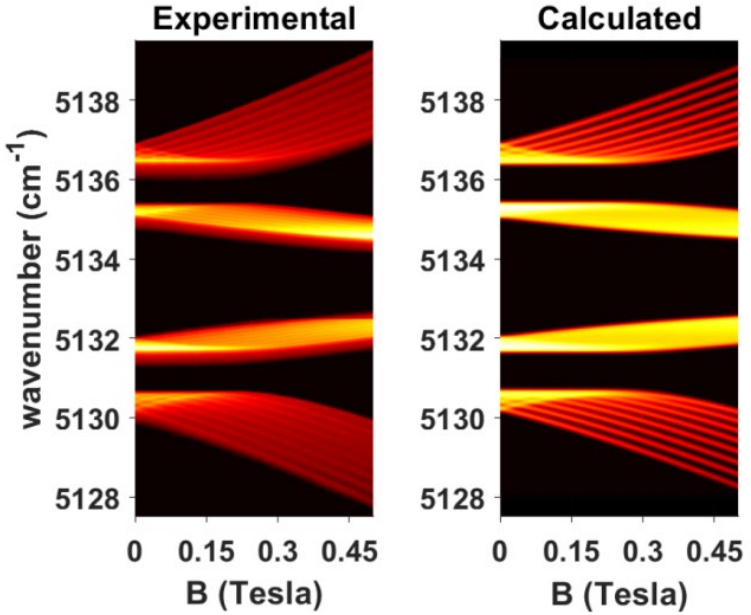

Sagar Mothkuri et al.
Phys. Rev. B, **103**, 104109 (2021)

THE JOURNAL OF PHYSICAL CHEMISTRY A

Article

pubs.acs.org/JPCA

The Journal of Physical Chemistry A, 2014, 118.

Spectroscopic Distinctions between Two Types of Ce^{3+} Ions in X2-Y_2SiO_5: A Theoretical Investigation

Jun Wen,*,† Chang-Kui Duan,‡ Lixin Ning,*,§ Yucheng Huang,§ Shengbao Zhan,† Jie Zhang,† and Min Yin‡

Table 5. Calculated Principal Values of the g-Tensors for Ce^{3+} Ions in X2-YSO in Comparison with the Experimental Values for Ce^{3+} Ions in LSO

	site 1 (CN = 6)		site 2 (CN = 7)	
principal values	calcd	exptl[a]	calcd	exptl[a]
g_x	0.015	0	0.394	0.55
g_y	1.317	1.3	1.743	1.69
g_z	2.297	2.3	2.216	2.25

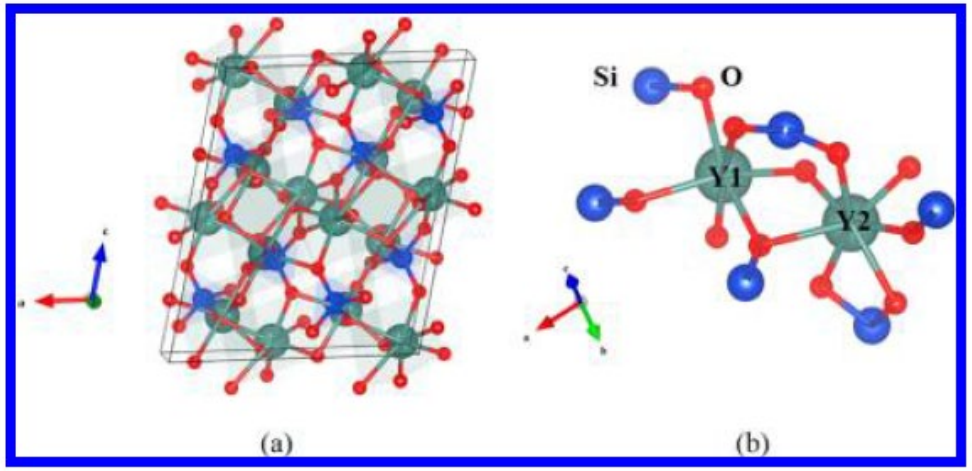

Figure 1. Schematic representations of local atomic structures around the two types of yttrium (Y1 and Y2) sites along with the unit cell of X2-YSO.

Ce^{3+} in X2-YSO

郝锐杰 (Ruijie HAO), 景伟国 (Weiguo JING)*

Chang-Kui Duan

USTC, Hefei, China

K=2 Spherical Harmonics - Potential

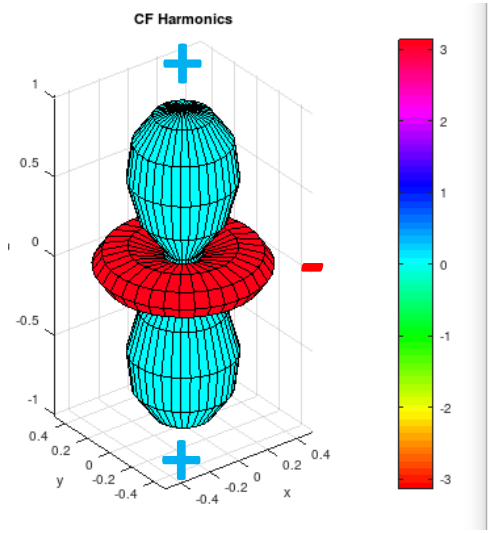

$C^2_0(\mathbf{r})$

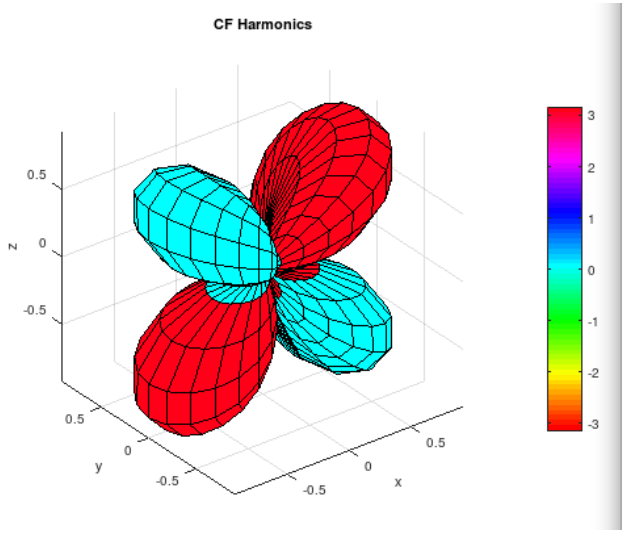

$C^2_1(\mathbf{r}) - C^2_{-1}(\mathbf{r})$

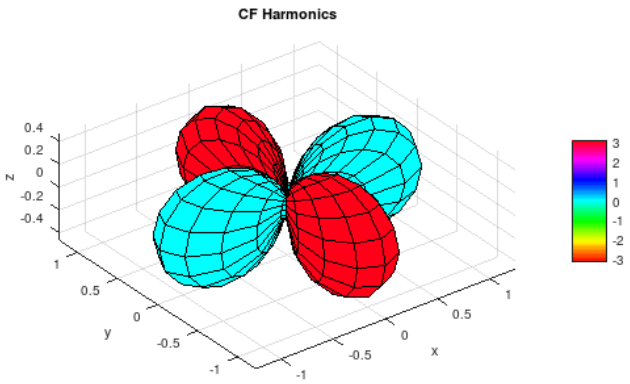

$C^2_2(\mathbf{r}) + C^2_{-2}(\mathbf{r})$

$C^2_0(\mathbf{r}) \sim 3z^2 - r^2 \sim 3\cos^2\theta - 1$, etc.

Potential acts on 4f orbitals:

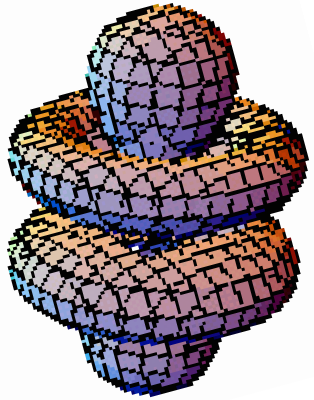

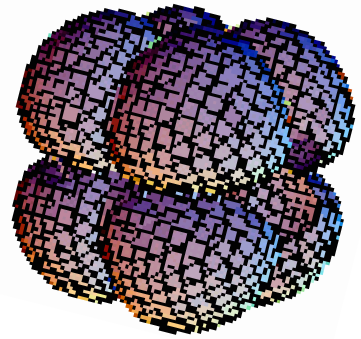

Fitted and ab-initio parameters for the k=2 part of the crystal-field potential (Er^{3+}:YSO, site 1).

$$H_{CF} = \sum_{k,q} B_q^k C_q^{(k)}$$

Parameter fit

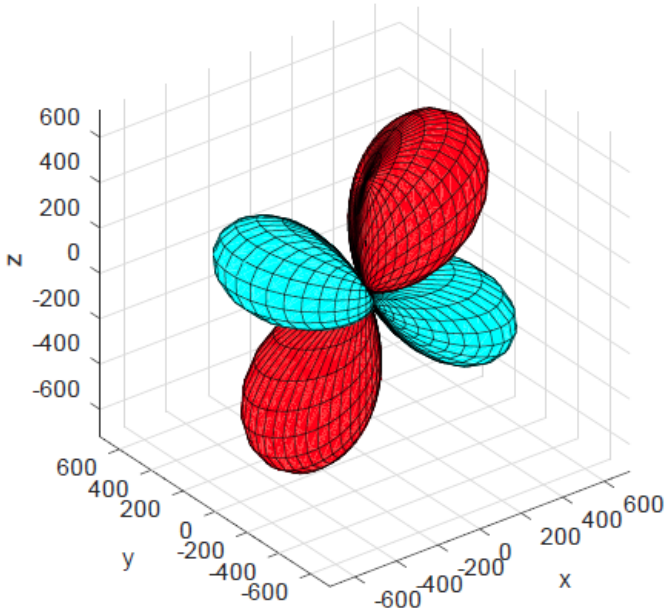

Ab-initio calculation

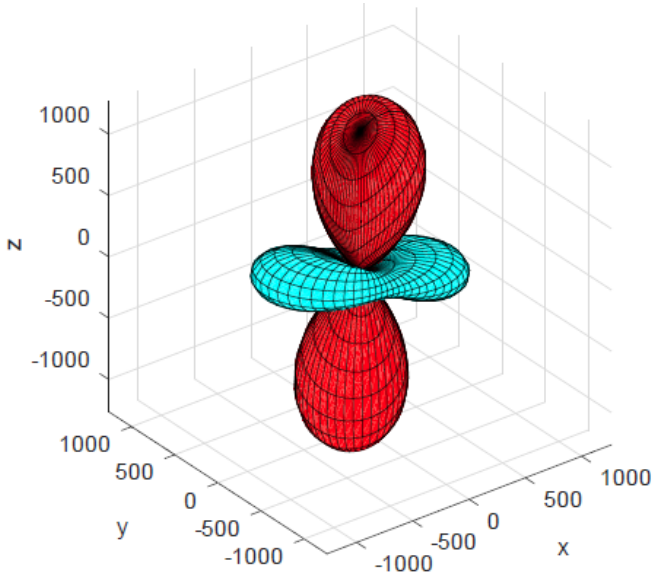

Parameter fit for Er^{3+}

B20 = -479.6
B21 = 471.4+143.8i
B22 = 125.5-2.0i

Ab-initio calculation for Ce^{3+}

B20 = -1162;
B21 = 362-198i;
B22 = 129+76i;

$C^2_0(\mathbf{r})$

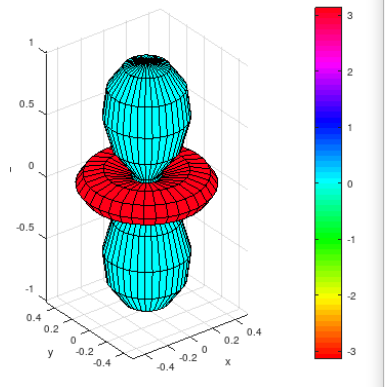

$C^2_1(\mathbf{r}) - C^2_{-1}(\mathbf{r})$

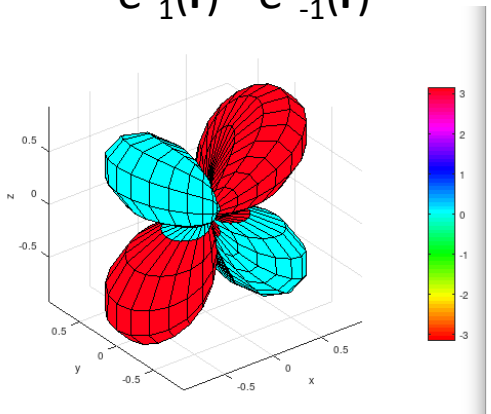

$C^2_2(\mathbf{r}) + C^2_{-2}(\mathbf{r})$

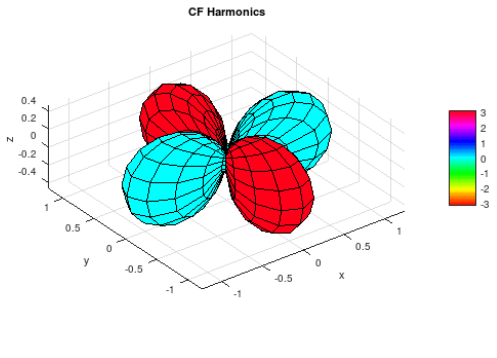

Fitted and ab-initio parameters for the k=2 part of the crystal-field potential (Er^{3+}:YSO, site 2).

$$H_{CF} = \sum_{k,q} B_q^k C_q^{(k)}$$

Parameter fit

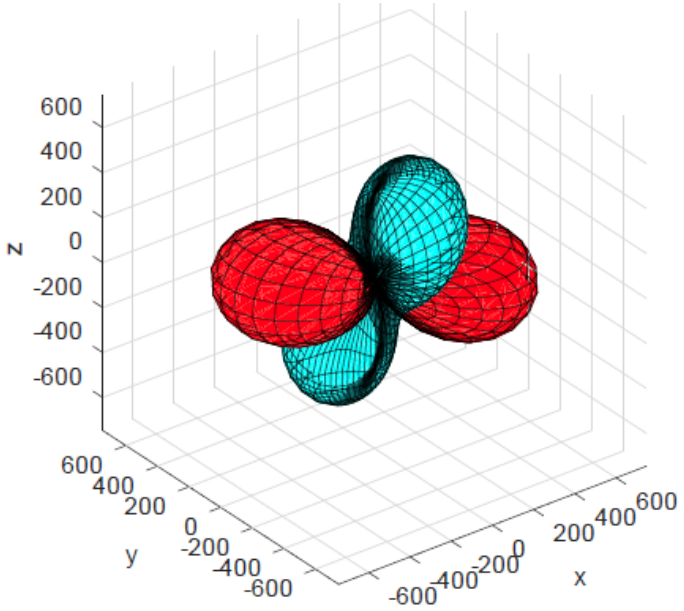

Ab-initio calculation

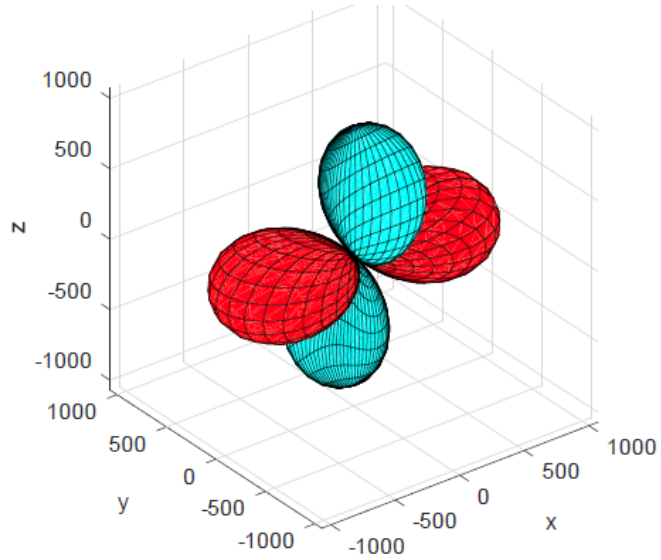

Parameter fit for Er^{3+}

B20 = 389
B21 = -325.7-95.8i
B22 = -368.5+53.7i

Ab-initio calculation for Ce^{3+}

B20 = 925;
B21 = -30-219i
B22 = -496+46i

$C^2_0(\mathbf{r})$

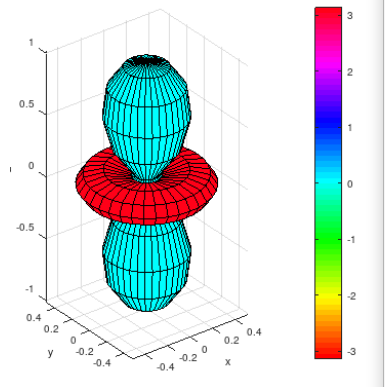

$C^2_1(\mathbf{r}) - C^2_{-1}(\mathbf{r})$

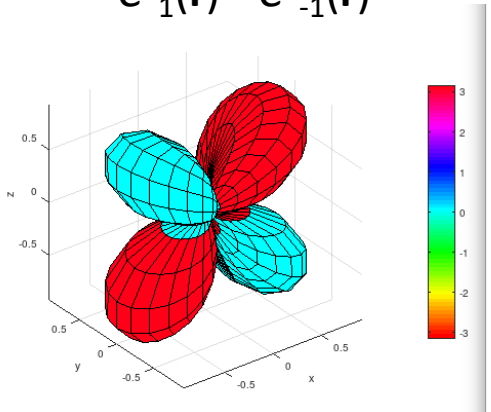

$C^2_2(\mathbf{r}) + C^2_{-2}(\mathbf{r})$

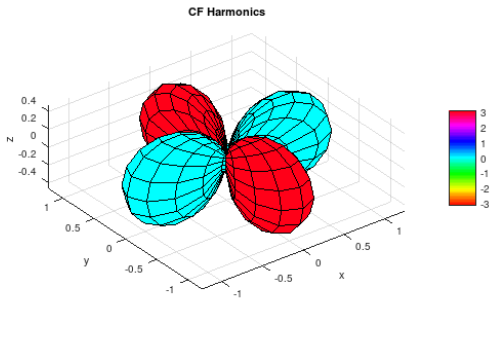

Fitted and ab-initio parameters for the k=2,4,6 parts of the crystal-field potential (Er^{3+}:YSO, site 1).

k=2 **k=4** **k=6**

Parameter fit

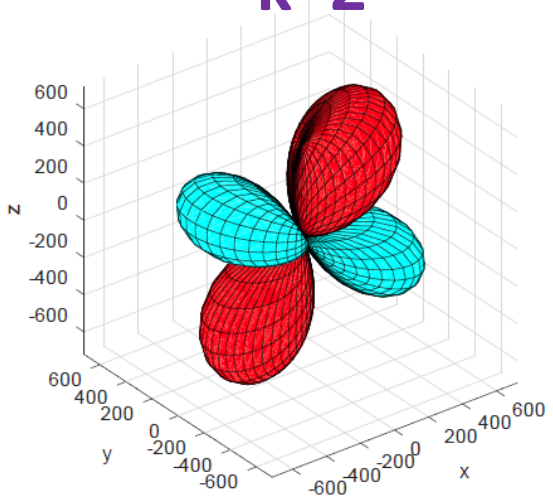

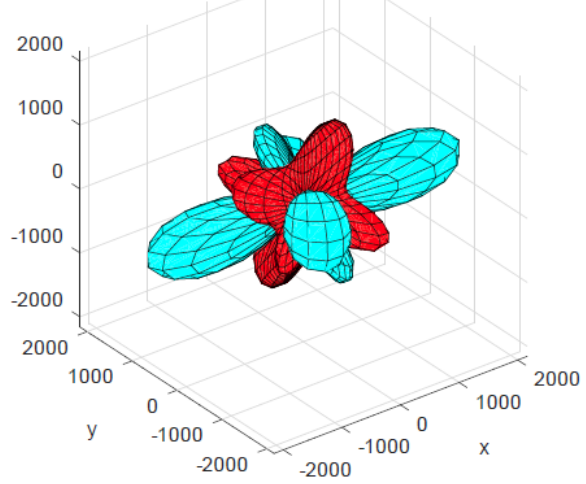

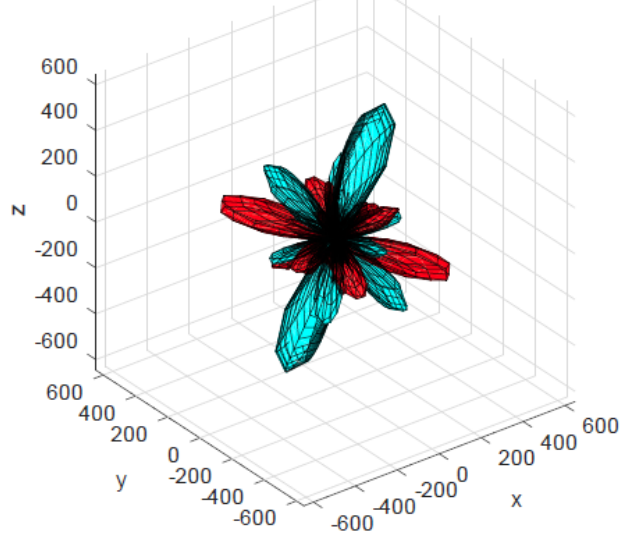

Ab-initio

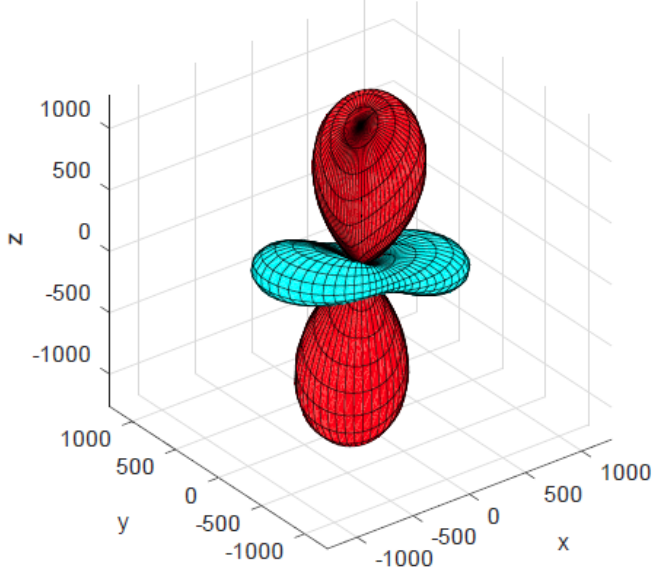

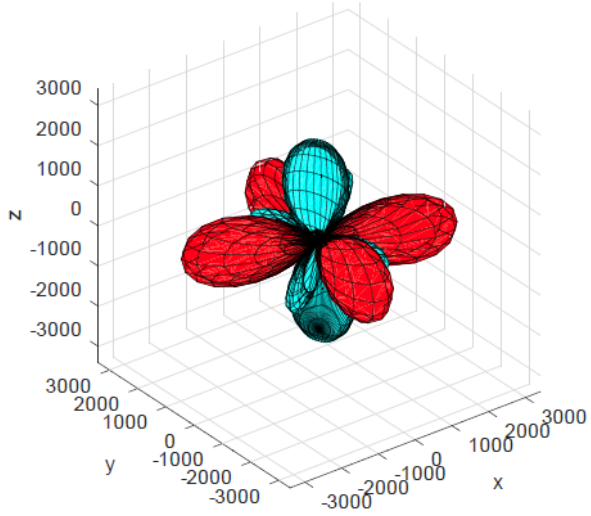

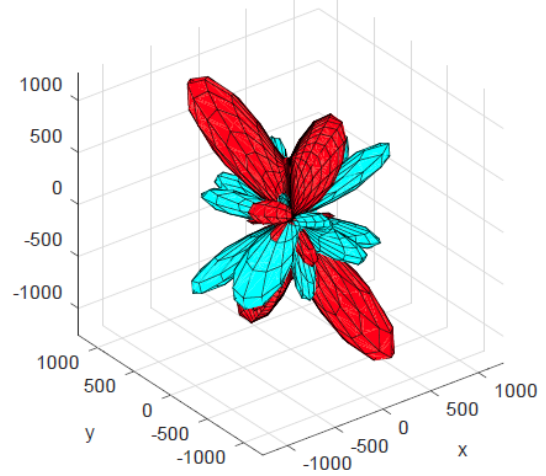

Fitted and ab-initio parameters for the k=2,4,6 part of the crystal-field potential (Er^{3+}:YSO, site 2).

k=2 **k=4** **k=6**

Parameter fit

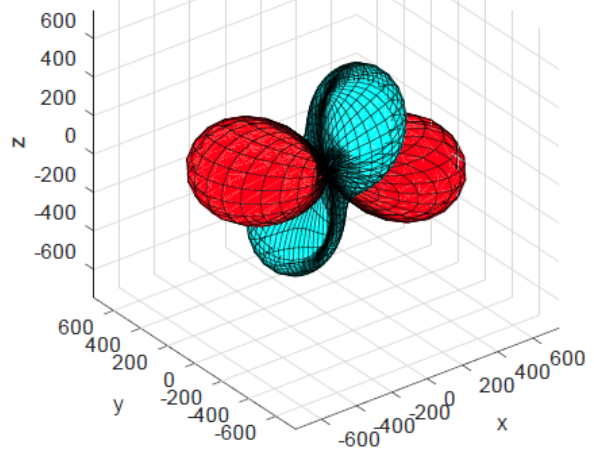

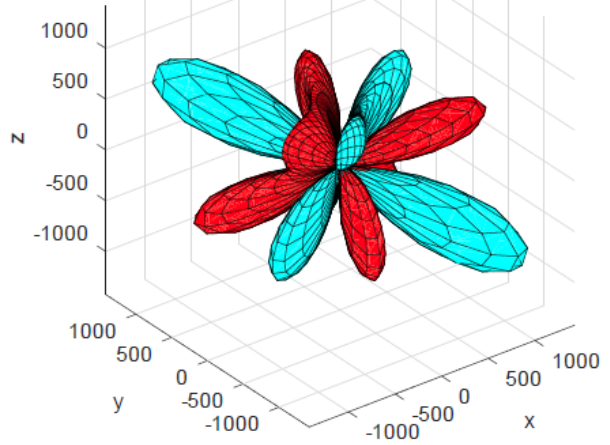

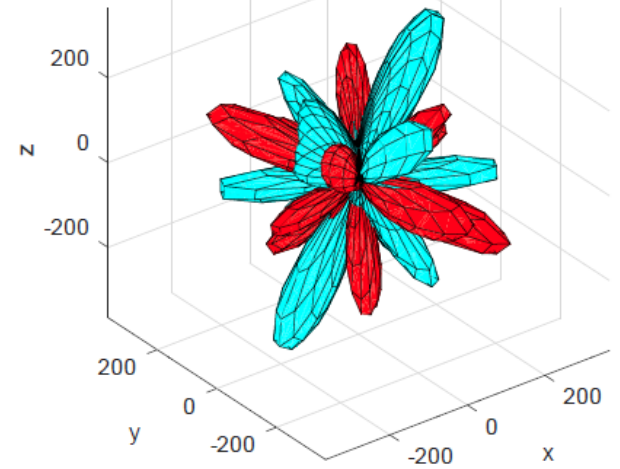

Ab-initio

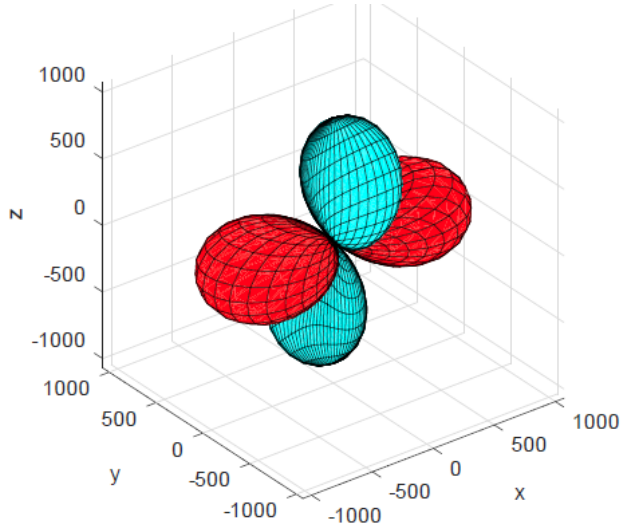

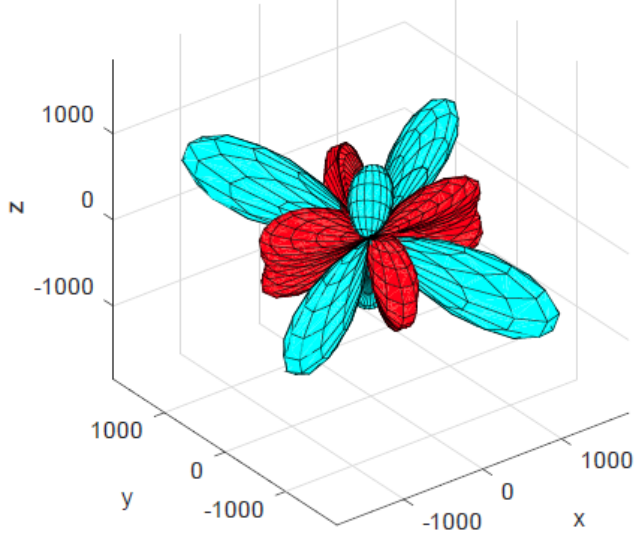

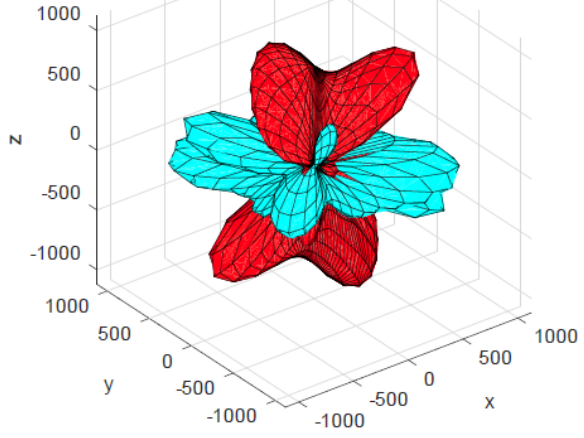

In Progress: Micro and nanocrystal Y_2SiO_5

- Basic laser spectroscopy of some ions, such as Ho^{3+} and Eu^{3+} are difficult at low concentrations.
- We can now make micro/nano crystals with higher concentration to do the preliminary work.
- Nano-crystals may also be useful for cavity enhancement.
- Lily Williams, Jamin Martin

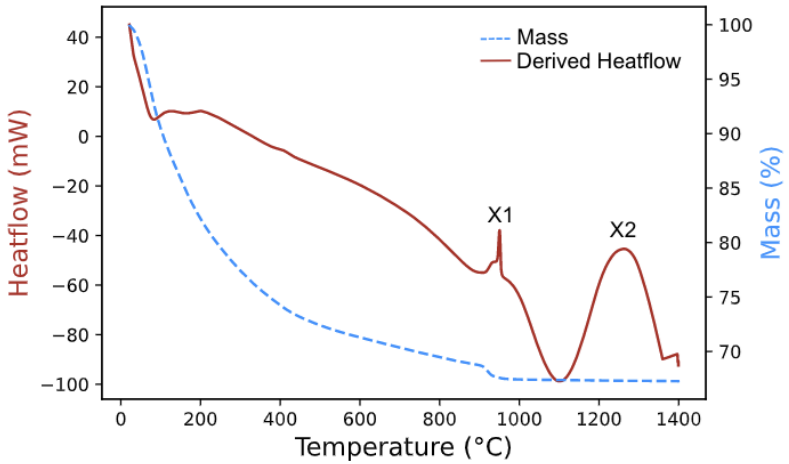

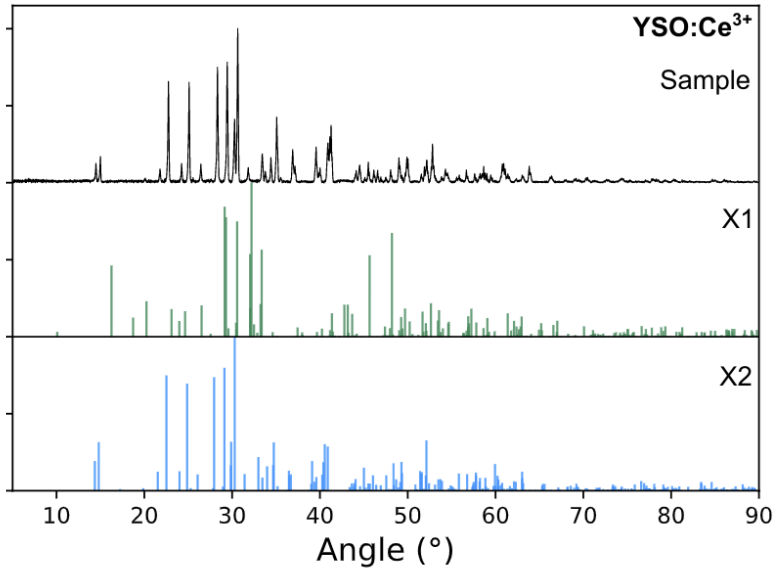

YSO:Eu site selective emission

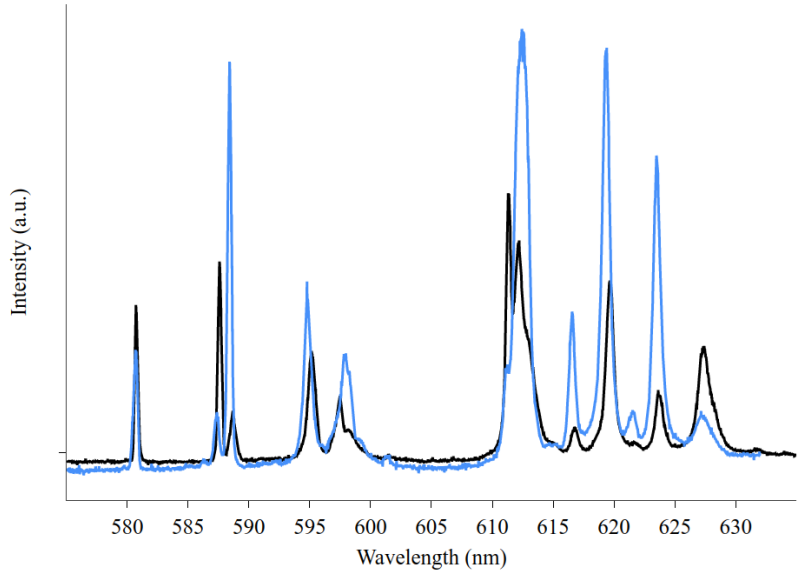

Magnetic field effects in nanoparticles
Jamin Martin

Review: Y. Luo, Z. Chen, S. Wen, Q. Han, L. Fu, L. Yan, D. Jin, J.-C. G. Bünzli, G. Bao, Magnetic regulation of the luminescence of hybrid lanthanide-doped nanoparticles, Coordination Chemistry Reviews 469 (2022) 214653

We use KY_3F_{10}, which has high symmetry (C_{4v}) and so calculations are possible of energy levels and intensities.

Magnetic Fields

Yb/Er $NaYF_4$

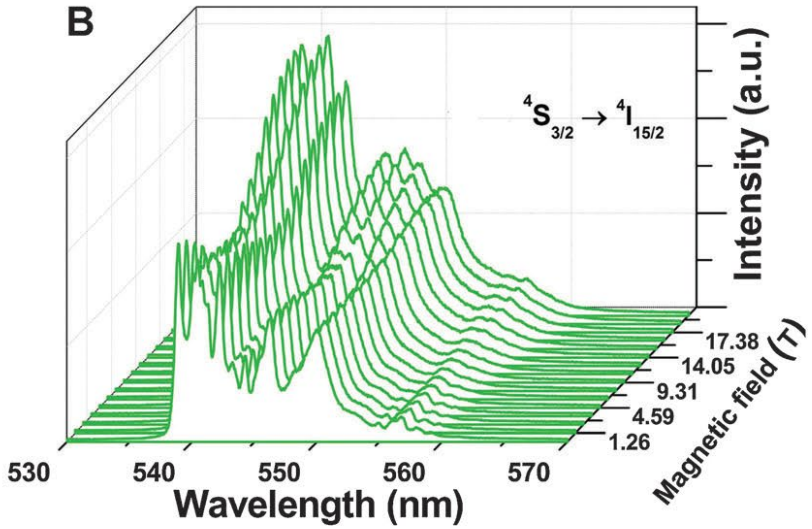

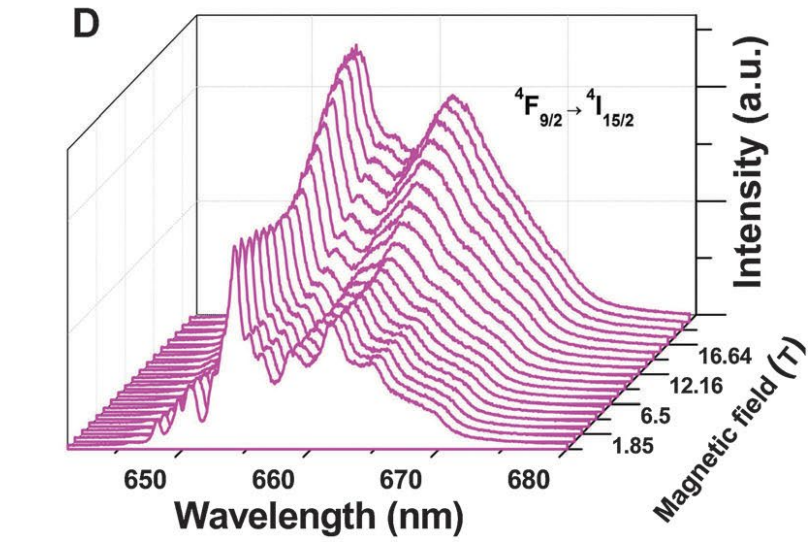

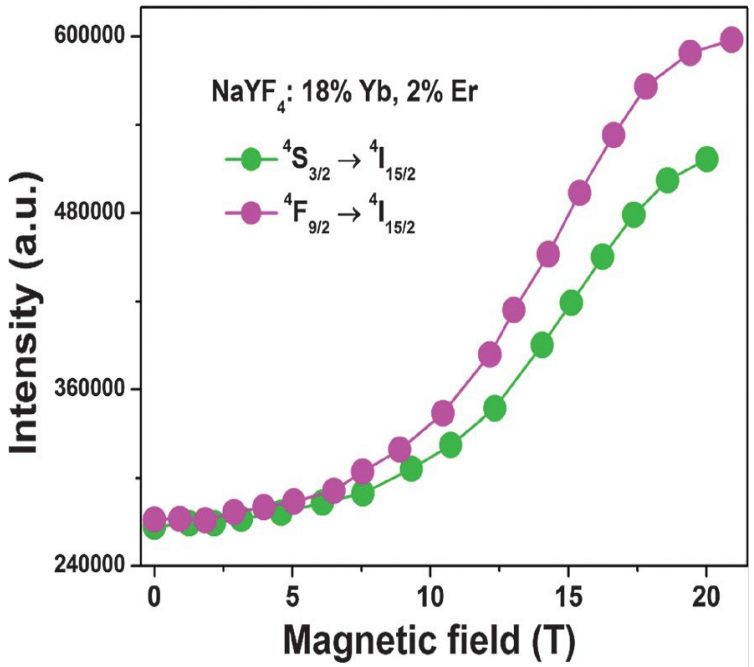

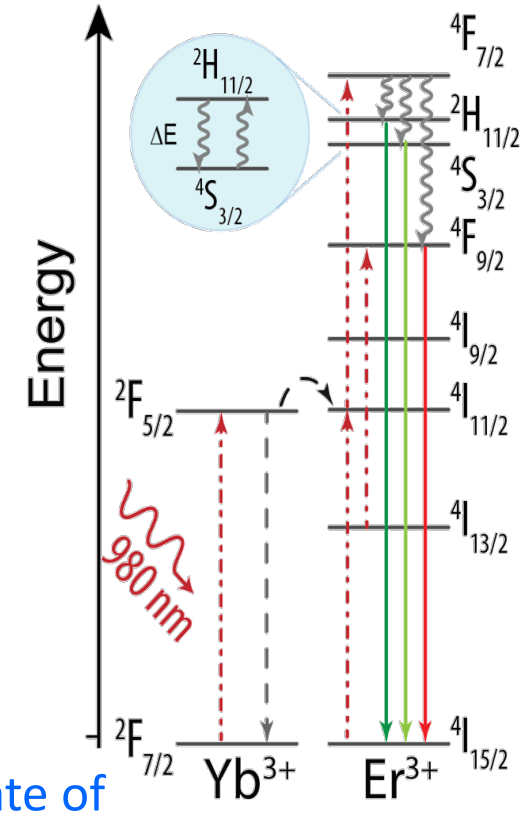

"… It is **highly possible** that the rate of excited state absorption of Er^{3+} is enhanced with magnetic field, because the energy level splitting **might** reduce the energy difference between the excitation light (975 nm) and the gap between the $^4I_{11/2}$ and $4F_{7/2}$ levels of Er^{3+}…"

Yb/Er $NaYF_4$: P. Chen et al, J. Mater. Chem. C, 2015, 3, 8794

$Er^{3+}/Nd^{3+}/ :KY_3F_{10}$

Jamin Martin

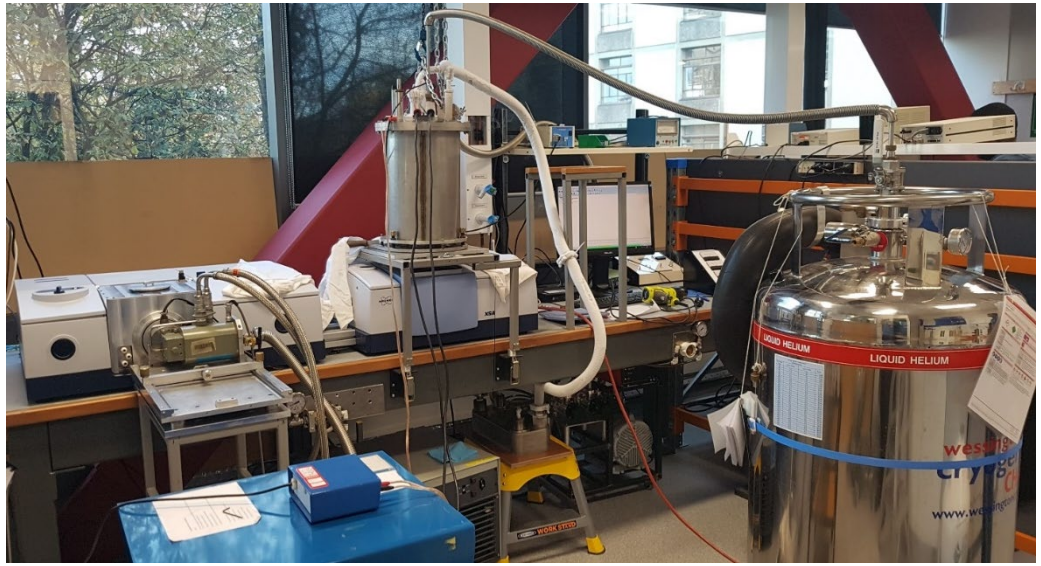

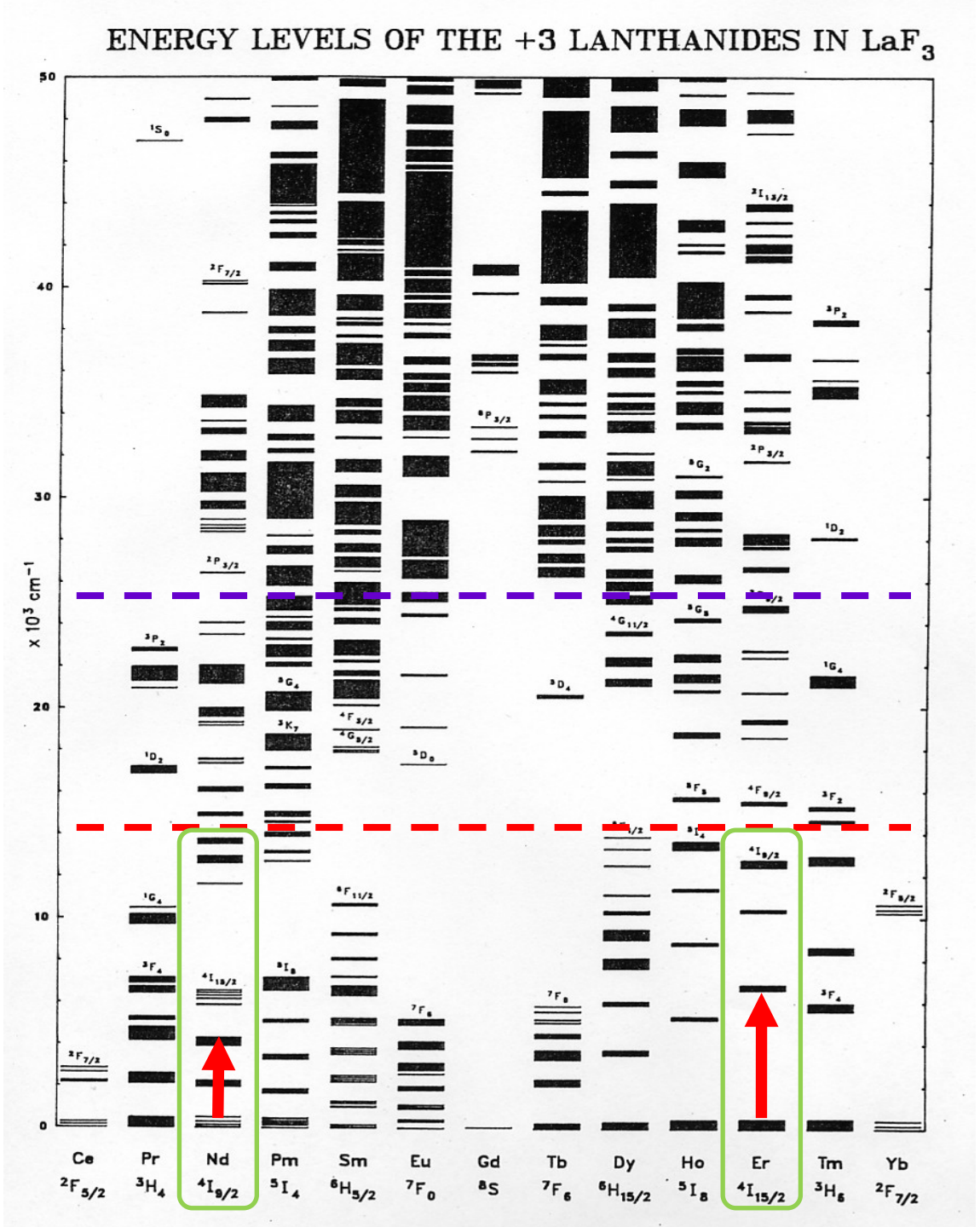

$Er^{3+}:KY_3F_{10}$ nanoparticles

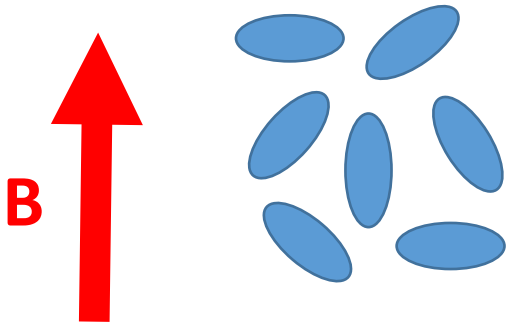

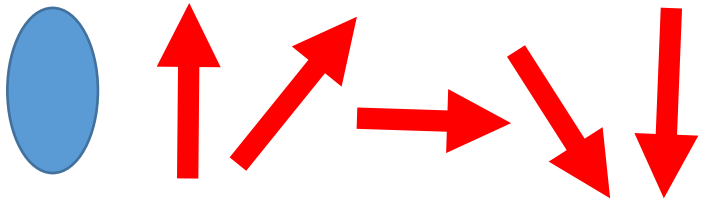

Not symmetrical: Transitions from lower ground state are more intense due to Boltzmann factors.

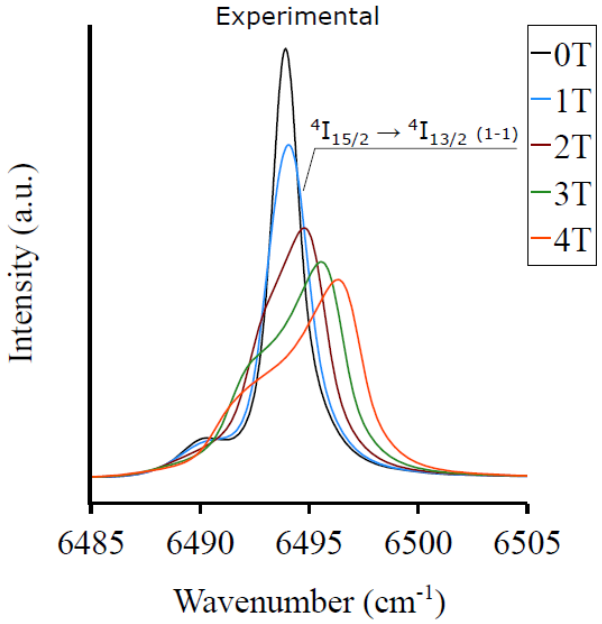

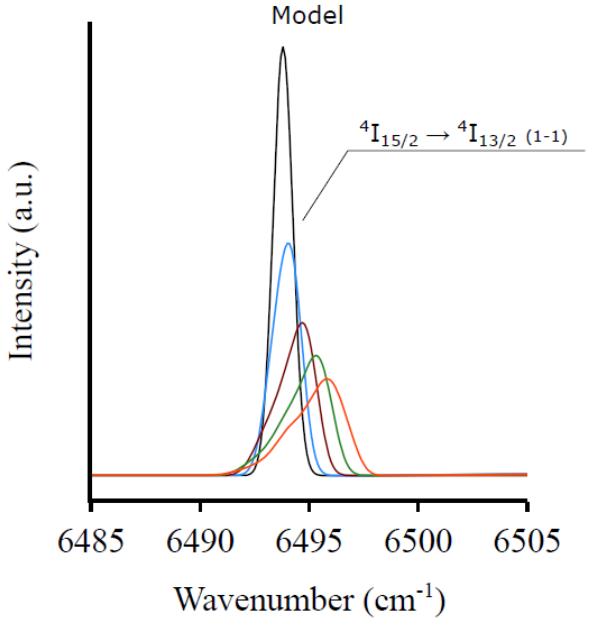

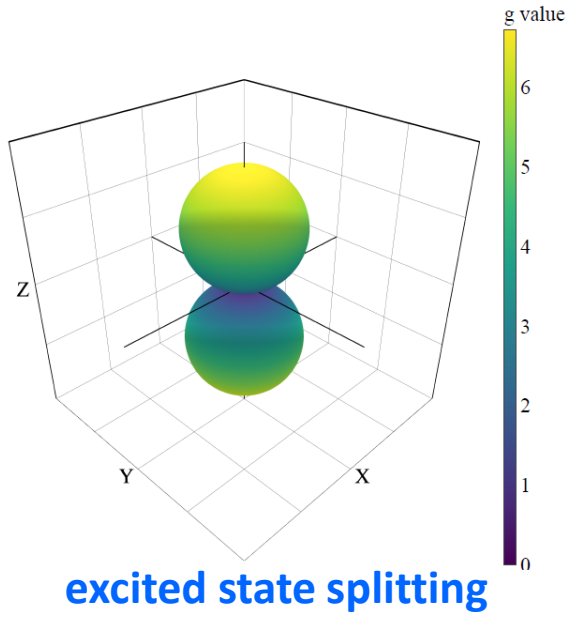

excited state splitting

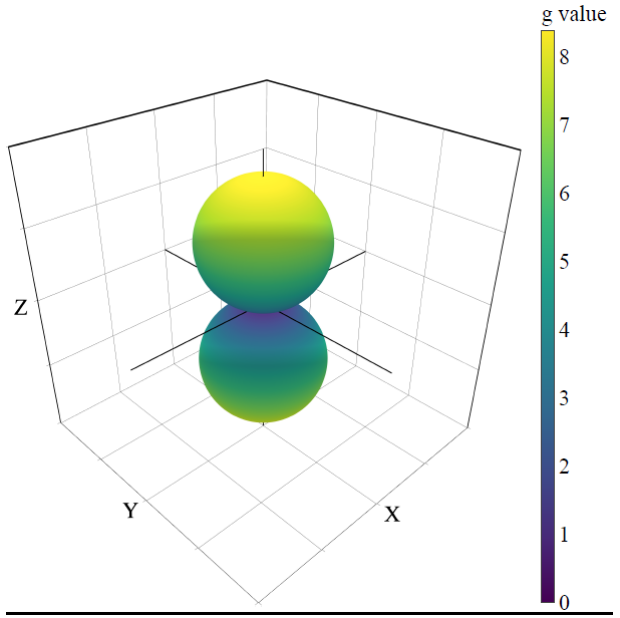

ground state splitting

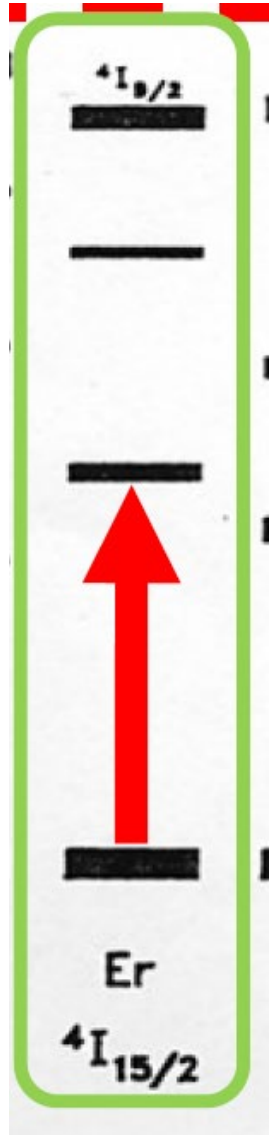

$Er^{3+}:KY_3F_{10}$

Model

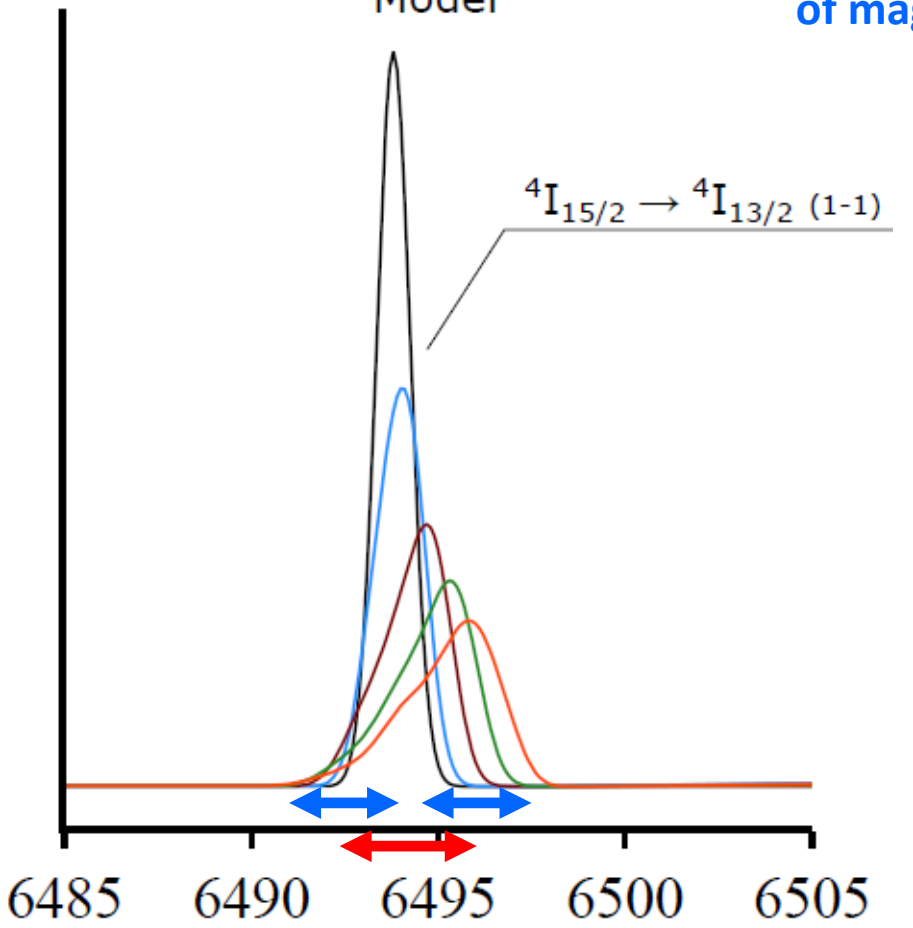

1 2 3 4

1 2 3 4 ← lower ground state – higher population

Random orientation probes populations at various angles of magnetic field.

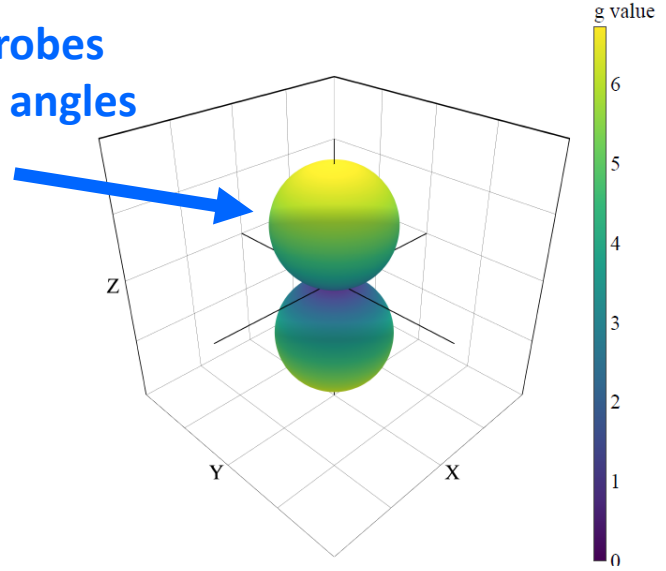

excited state splitting

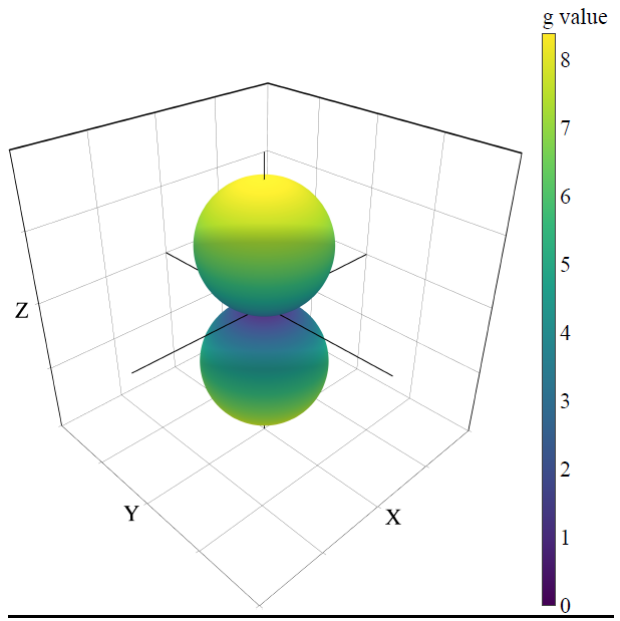

ground state splitting

Peak splitting not at maximum possible splitting.
This has to do with integral over solid angle of splitting function.

$Nd^{3+}:KY_3F_{10}$

Transition selected for isotropic splitting

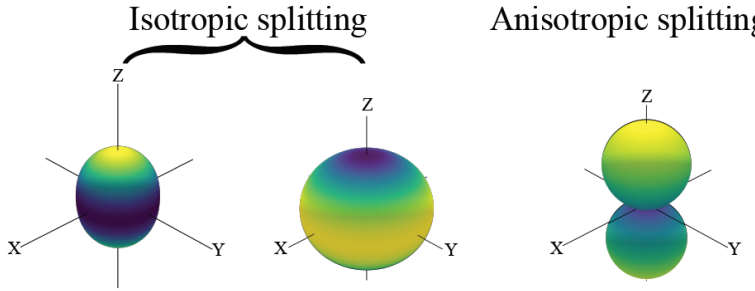

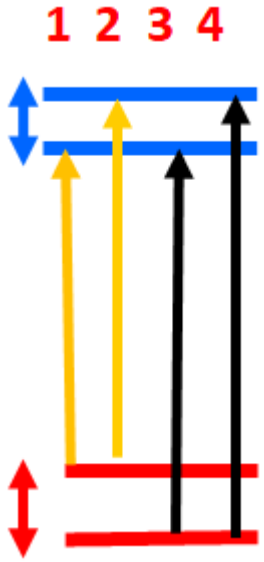

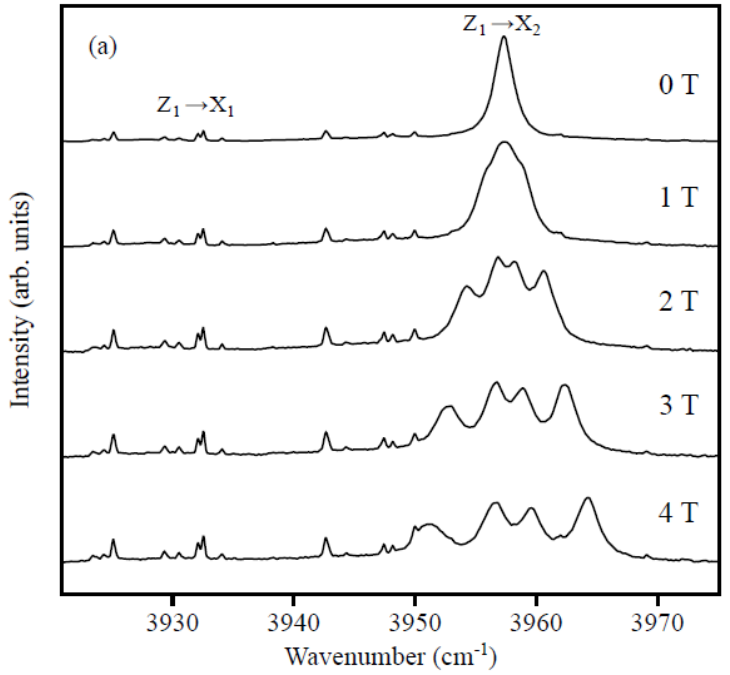

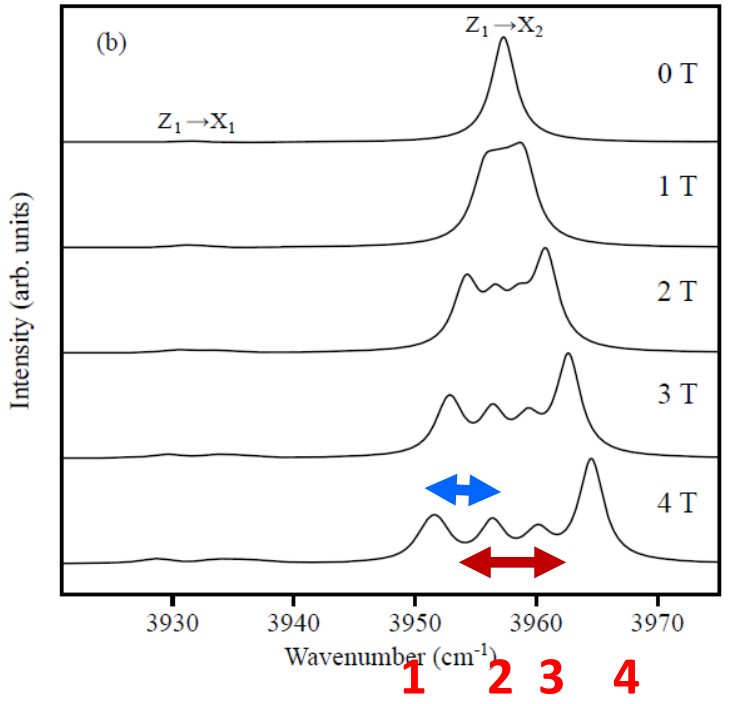

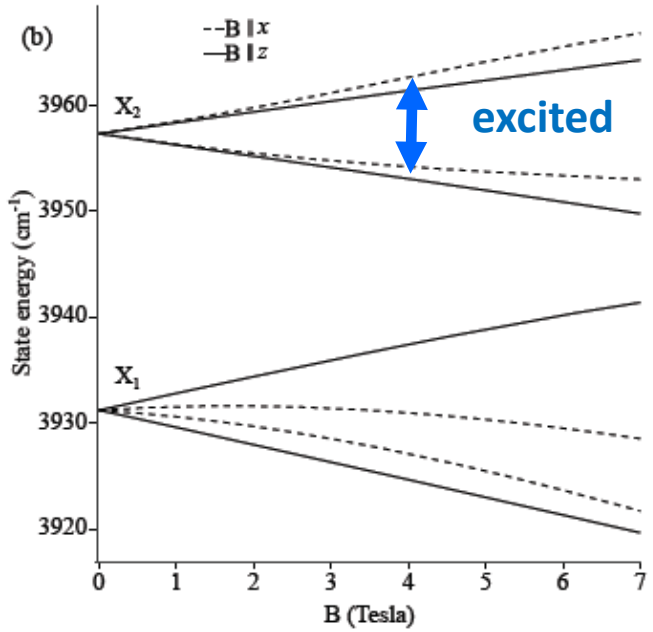

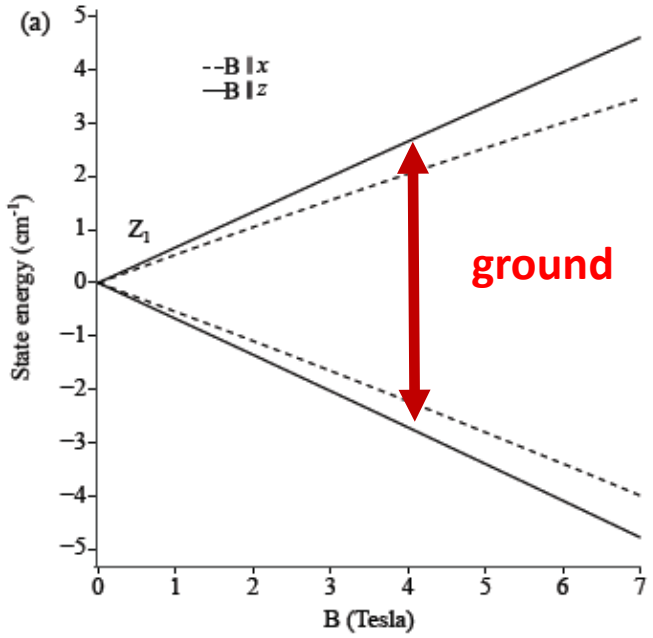

Crystal-field and Zeeman interactions in lanthanide doped nanocrystals: $KY_3F_{10}:Nd^{3+}$

Jamin L. B. Martin,Jon-Paul R. Wells,Michael F. Reid

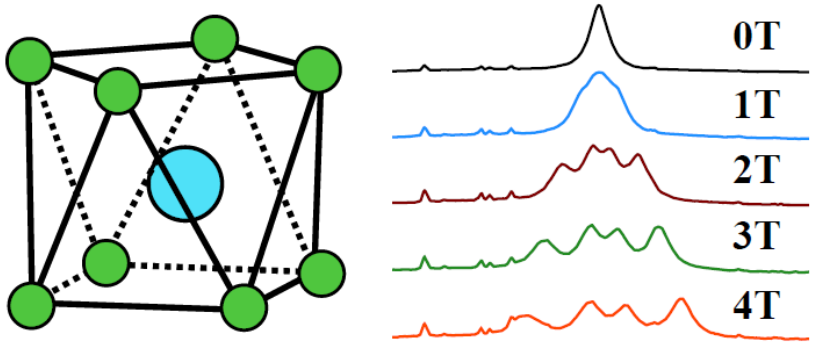

Fit including magnetic splittings gives a good reproduction in the splittings, including non-linear effects.

Jamin Martin et al.
Optical Materials X, 2022, 100181.

Energy-level fit only

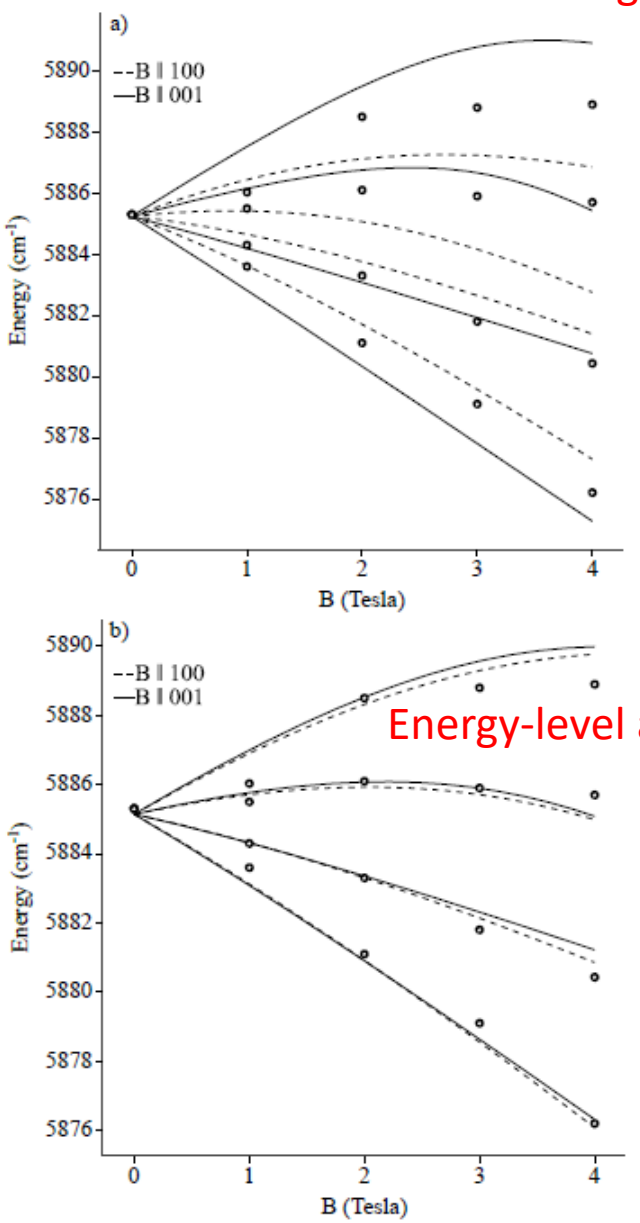

Figure 3: Calculated Zeeman splittings for the $Z_1\gamma_6 \longrightarrow W_1\gamma_7$ transition. Energies only fit (a) and energies + splittings fit (b)

Energy-level and magnetic-splitting fit

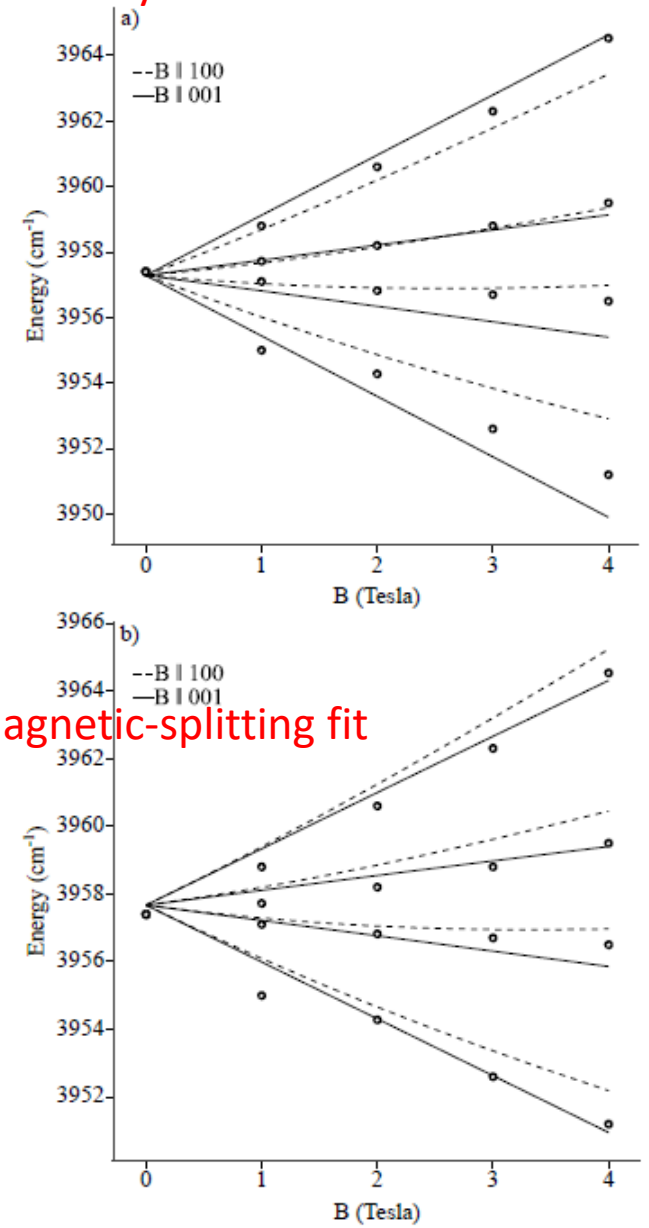

Figure 4: Calculated Zeeman splittings for the $Z_1\gamma_6 \longrightarrow X_2\gamma_6$ transition. Energies only fit (a) and energies + splittings fit (b)

Tutorials on Electronic Structure

www2.phys.canterbury.ac.nz/~mfr24/

Google: **Mike Reid, Personal Home Page Canterbury**

mike.reid@canterbury.ac.nz

The Dodd-Walls Centre
for Photonic and Quantum Technologies

UC
UNIVERSITY OF CANTERBURY
Te Whare Wānanga o Waitaha
CHRISTCHURCH NEW ZEALAND

In Progress: Prediction of the hyperfine structure of $^{151}Eu^{3+}:Y_2SiO_5$

The $Sm^{3+}:Y_2SiO_5$ parameters are scaled and fitted to predict the hyperfine structure of the $^7F_0$ ground state of $Eu^{3+}:Y_2SiO_5$ (Site 1)

Spin Hamiltonian: $\mathscr{H} = \mu_B \mathbf{B}\cdot\mathbf{g}\cdot\mathbf{S} + \mathbf{I}\cdot\mathbf{A}\cdot\mathbf{S} + \mathbf{I}\cdot\mathbf{Q}\cdot\mathbf{I} - \mu_n g_n \mathbf{B}\cdot\mathbf{I}$

Contributions from

1. Electronic effects due to mixing of $^7F_2$ with $^7F_0$ by crystal field.
2. Direct interaction of lattice and magnetic field with nucleus.

See: Smith et al, Complete crystal-field calculation of Zeeman hyperfine splittings in europium. Phys. Rev. B 105: 125141

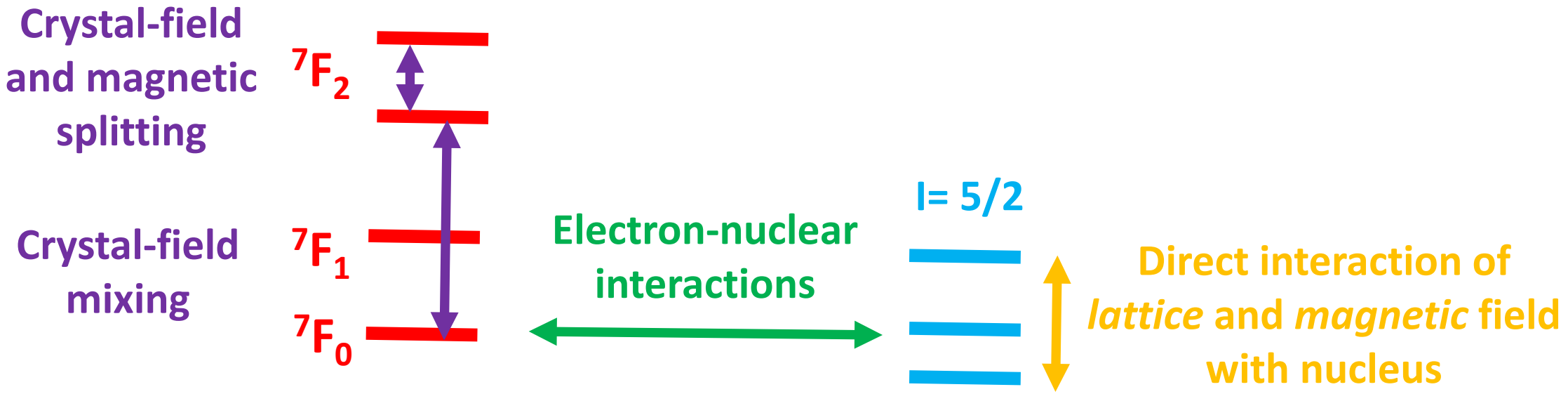

In Progress: Predictions of the hyperfine structure of $^{151}Eu^{3+}:Y_2SiO_5$

Nuclear spin: I=5/2

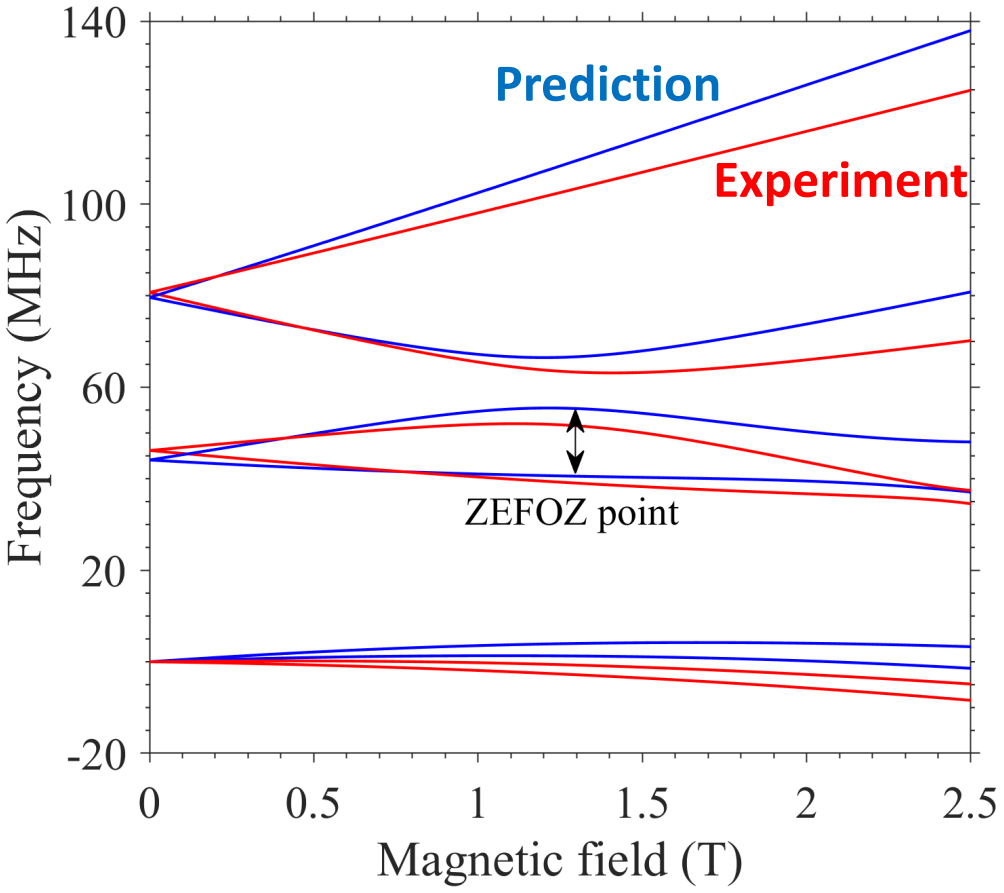

The $Sm^{3+}:Y_2SiO_5$ parameters were scaled to predict the hyperfine structure of the $^7F_0$ ground state of $Eu^{3+}:Y_2SiO_5$ (Site 1)

The experiment and prediction are for a magnetic field in the particula direction that gives the ZEFOZ point used in Zhong et al. Nature paper demonstrating six-hour coherence.

Contributions from:

1. Electronic effects due to mixing of $^7F_2$ with $^7F_0$ by crystal field.
2. Direct interaction of lattice and magnetic field with nucleus.

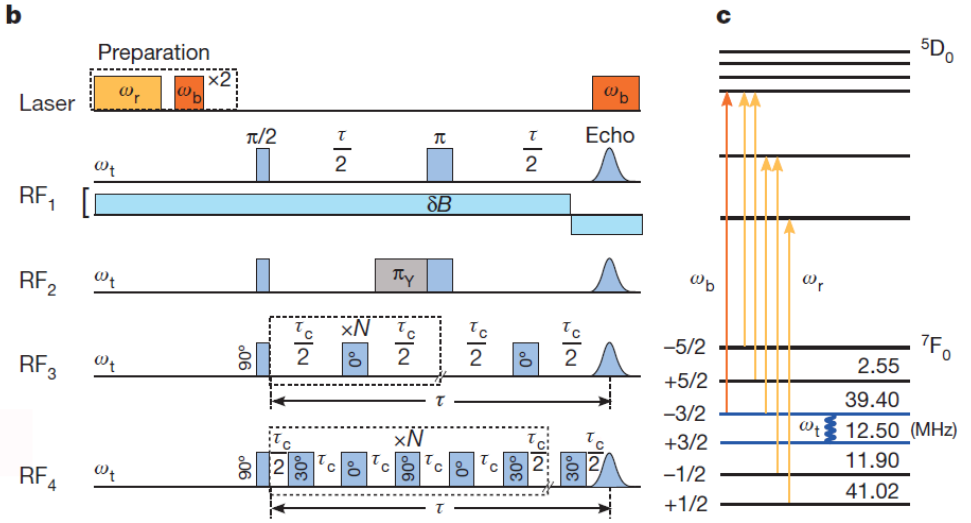

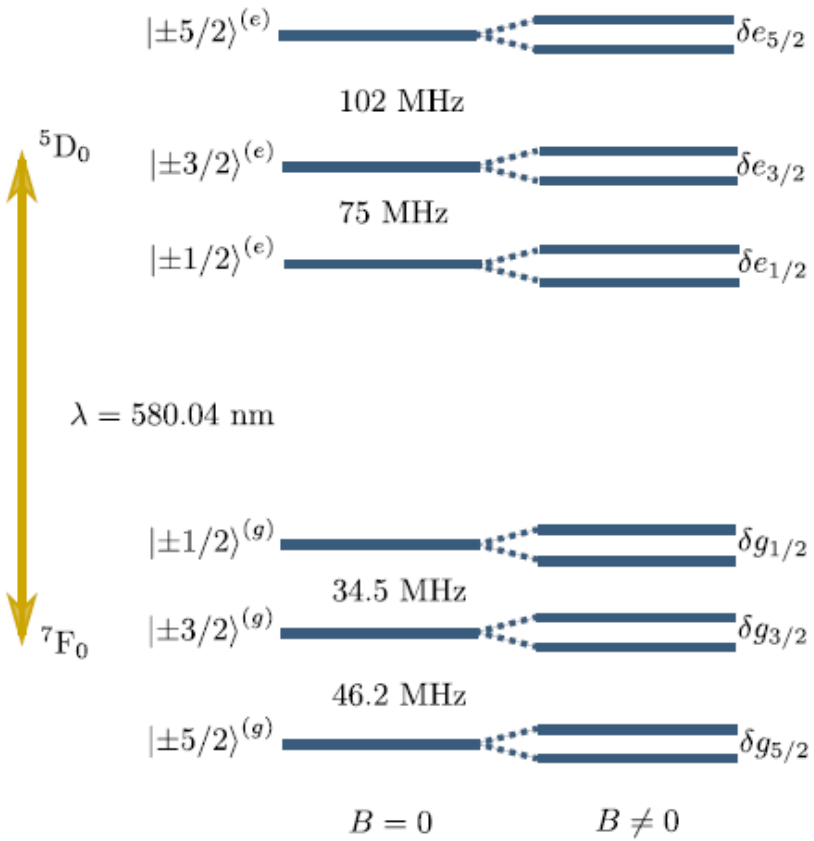

FIG. 1. The energy level structure of $^{151}Eu^{3+}$:Y_2SiO_5, without (left) and with (right) an external magnetic field B. The inhomogeneous broadening of the optical transition $^7F_0 \longleftrightarrow {}^5D_0$ resonant at 580 nm contains hyperfine $m_I = -5/2 \cdots + 5/2$ sublevels both for the ground $^7F_0$ and the excited $^5D_0$ states. The ground state hyperfine splittings were characterized in [31].

spin Hamiltonian [29,30]

$$\mathcal{H} = \hat{I} \cdot \mathbf{Q} \cdot \hat{I} + \vec{B} \cdot \mathbf{M} \cdot \hat{I} + (\vec{B} \cdot \mathbf{Z} \cdot \vec{B})\mathbb{1}. \qquad (2)$$

In this expression, the first term corresponds to the quadrupole interaction and is responsible for a partial lifting of the nuclear-spin states degeneracy in both the ground and the excited states for the $I = 5/2$ nuclear spin of europium (see Fig. 1, left). In general, this term includes pure quadrupolar and pseudoquadrupolar contributions [29]. The second term describes the Zeeman interaction and results in nondegenerate hyperfine levels in the presence of a magnetic field (see Fig. 1, right). The third term is the quadratic Zeeman interaction, which we neglect since it does not contribute to the admixtures of the eigenstates. The labels used for the hyperfine levels in Fig. 1 are only approximate, since m_I is not a good quantum number.

As the energy splittings due to $\mathcal{H}$ are very small compared to the optical transition, this term can be seen as a perturbation of the whole Hamiltonian. Two hyperfine Hamiltonians can be defined: one for the ground state $\mathcal{H}^{(g)}$ and one for the excited state $\mathcal{H}^{(e)}$. The hyperfine ground state Hamiltonian has already been determined in a previous work [31]. We are thus interested in the present work in characterizing the Hamiltonian of the excited state and its orientation with respect to the ground state Hamiltonian. This is done by determining experimentally $\mathbf{Q}^{(e)}$ and $\mathbf{M}^{(e)}$, that is, the quadrupole and Zeeman tensors of the excited state hyperfine Hamiltonian.

B. Symmetry considerations in Y_2SiO_5

$^5D_0$

Almost purely quadrupole from lattice.

Same principal axes for all doublets.

$^7F_0$

Quadrupole from lattice + CF mixing from $^7F_2 + {}^7F_4$

Different principal axes for the doublets.

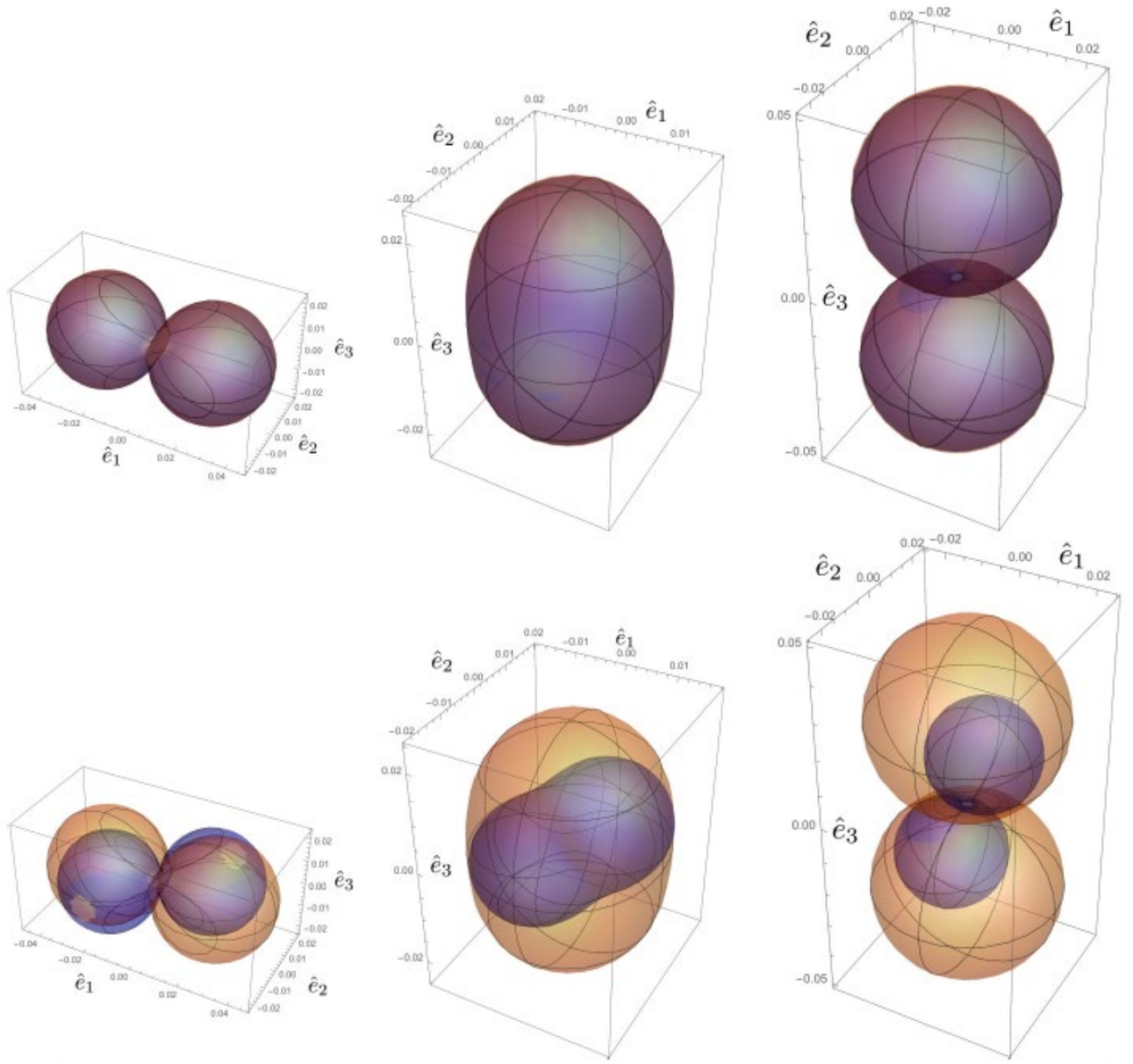

FIG. 7. Spherical plot (violet) of the energy splitting for the ground (three figures below) and excited (three figures above) states, $\delta_k/(2|\vec{B}|)$, in natural units for $k = 1/2$, $3/2$, and $5/2$ (from left to right) as a function of $\vec{n}(\theta,\phi) = \vec{B}/|\vec{B}|$). The orange plot is the hypothetical energy splitting if M were isotropic (i.e., $M \propto \mathbb{1}$), which is almost the case for excited state (and, hence, there the orange plot is basically covered by the violet one). The coordinate system is the eigenbasis of $\mathbf{Q}^{(e)}$ or $\mathbf{Q}^{(g)}$, respectively.

SH $^5D_0$,1: 1.39e-05

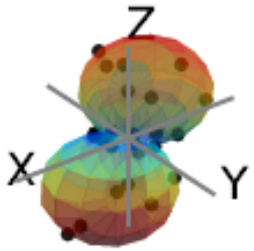

CF $^5D_0$,1: 1.46e-05

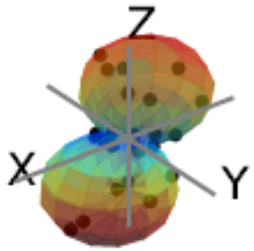

SH $^7F_0$, 1: 1.05e-05

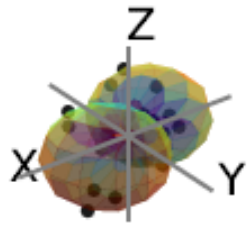

CF $^7F_0$,1: 9.20e-06

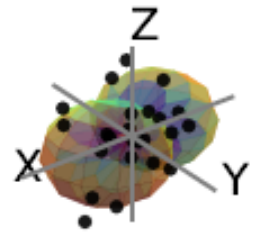

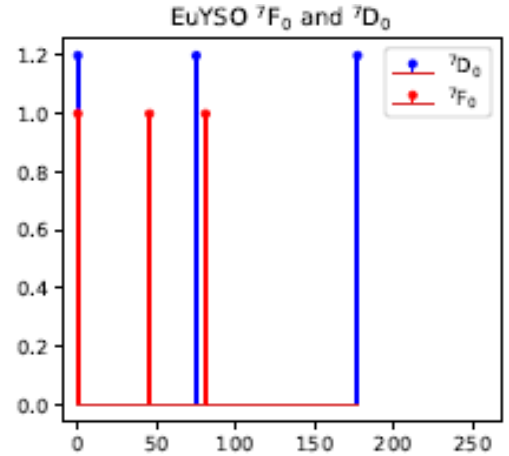

SH $^5D_0$,2: 7.54e-06

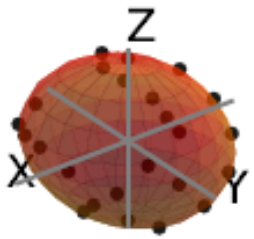

CF $^5D_0$,2: 7.85e-06

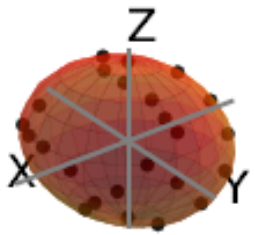

SH $^7F_0$, 2: 7.02e-06

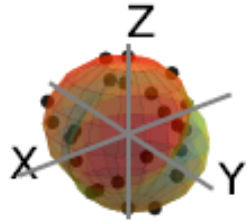

CF $^7F_0$,2: 7.22e-06

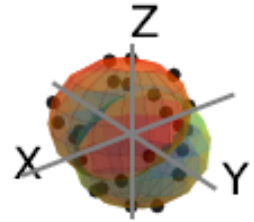

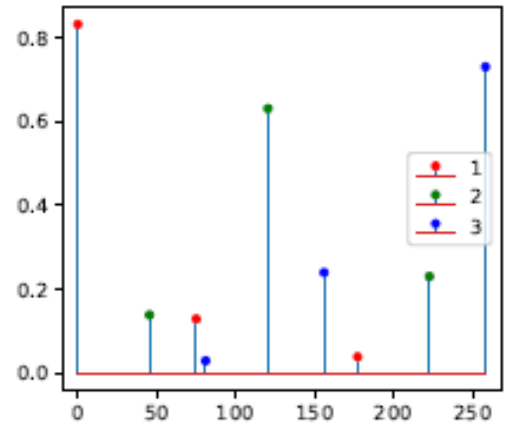

SH $^5D_0$,3: 1.50e-05

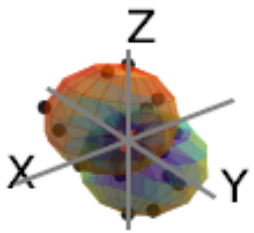

CF $^5D_0$,3: 1.56e-05

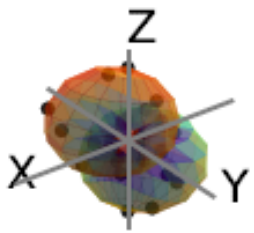

SH $^7F_0$, 3: 1.44e-05

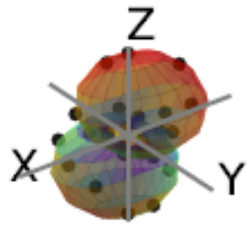

CF $^7F_0$,3: 1.39e-05

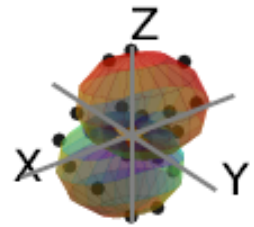

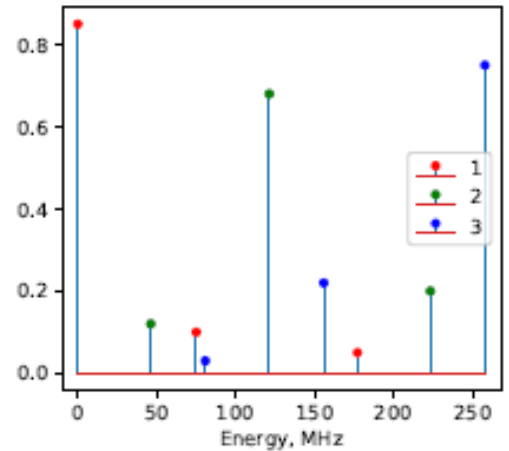

Conclusions

- Crystal-field modelling for several rare-earth ions: Ce^{3+}, Nd^{3+}, Sm^{3+}, Ho^{3+}, Er^{3+} in Y_2SiO_5 (YSO).
- Other groups include Yb^{3+}: Zhou et al. Inorganic Chemistry 59:13144 (2020).
- Due to the C_1 symmetry, directional magnetic data is required to determine unique sets of parameters. [May still not be unique!]
- Parameters can be scaled between ions.
- Prediction of polarization and high-field hyperfine structure for Er^{3+}:Y_2SiO_5.
- In progress:
  - Comparison with ab-initio calculations.
  - Micro and nanocrystals.
  - Prediction of magnetic-hyperfine structure for Eu^{3+}:Y_2SiO_5.
  - Work on other ions.

DODD-WALLS CENTRE
for Photonic and Quantum Technologies

UNIVERSITY OF CANTERBURY
Te Whare Wānanga o Waitaha
CHRISTCHURCH NEW ZEALAND